New Jersey Institute of Technology
Digital Commons @ NJIT

Dissertations | Theses and Dissertations

Fall 2002

Deposition and characterization of magnetron sputtered BCC tantalum

Anamika Patel
New Jersey Institute of Technology

Follow this and additional works at: https://digitalcommons.njit.edu/dissertations

Part of the Electrical and Electronics Commons

Recommended Citation

Patel, Anamika, "Deposition and characterization of magnetron sputtered BCC tantalum" (2002). *Dissertations*. 564.
https://digitalcommons.njit.edu/dissertations/564

This Dissertation is brought to you for free and open access by the Theses and Dissertations at Digital Commons @ NJIT. It has been accepted for inclusion in Dissertations by an authorized administrator of Digital Commons @ NJIT. For more information, please contact digitalcommons@njit.edu.

Copyright Warning & Restrictions

The copyright law of the United States (Title 17, United States Code) governs the making of photocopies or other reproductions of copyrighted material.

Under certain conditions specified in the law, libraries and archives are authorized to furnish a photocopy or other reproduction. One of these specified conditions is that the photocopy or reproduction is not to be "used for any purpose other than private study, scholarship, or research." If a, user makes a request for, or later uses, a photocopy or reproduction for purposes in excess of "fair use" that user may be liable for copyright infringement,

This institution reserves the right to refuse to accept a copying order if, in its judgment, fulfillment of the order would involve violation of copyright law.

Please Note: The author retains the copyright while the New Jersey Institute of Technology reserves the right to distribute this thesis or dissertation

Printing note: If you do not wish to print this page, then select "Pages from: first page # to: last page #" on the print dialog screen

NJIT
New Jersey's Science &
Technology University

The Van Houten library has removed some of the personal information and all signatures from the approval page and biographical sketches of theses and dissertations in order to protect the identity of NJIT graduates and faculty.

ABSTRACT

DEPOSITION AND CHARACTERIZATION OF MAGNETRON SPUTTERED BCC TANTALUM

by
Anamika Patel

The goal of this thesis was to provide scientific and technical research results for developing and characterizing tantalum (Ta) coatings on steel substrates deposited by DC magnetron sputtering. Deposition of tantalum on steel is of special interest for the protection it offers to surfaces, e.g. the surfaces of gun barrels against the erosive wear of hot propellant gases and the mechanical damage caused by the motion of launching projectiles. Electro-plated chromium is presently most commonly used for this purpose; however, it is considered to be carcinogenic in its hexavalent form. Tantalum is being investigated as non-toxic alternative to chromium and also because of its superior protective properties in these extreme environments.

DC magnetron sputtering was chosen for this investigation of tantalum coatings on steel substrates because it is a versatile industrial proven process for deposition of metals. Sputter deposited Ta films can have two crystallographic structures: 1) body center cubic (bcc) phase, characterized by high toughness and high ductility and 2) a tetragonal beta phase characterized by brittleness and a tendency to fail under stress. It was found in this work that the bcc Ta coatings on steel can be obtained reliably by either of two methods: 1) depositing Ta on a submicron, stoichiometric TaN seed layer reactively sputtered on unheated steel and 2) depositing Ta directly on steel heated above a critical temperature. For argon sputtering gas this critical temperature was found to be

400 °C at a pressure of 5 mtorr. With the heavier krypton gas, this critical temperature is reduced to 350 °C.

X-ray diffraction (XRD) was used to investigate the structure of tantalum and nitride films, and the composition of the nitride films was measured by nuclear reaction analyses (NRA), which were used to study in detail the enhancement of the bcc phase of Ta on steel. The scratch adhesion tests performed with a diamond hemispherical tip of radius 200 μm under increasing loads revealed high critical load values for failure (>15 N) for the bcc coatings versus the low load values (< 9 N) for the beta coatings. The coating deposited on TaN interlayers on sputter-etched steel had better adhesion than those on steel surface without sputter etching.

The results for this work have demonstrated that by controlling the various process parameters of dc magnetron sputtering, high quality bcc Ta coatings of multi-micron thickness with excellent adhesion to steel can be made. An important contribution of this dissertation is in the enhancing an understanding of this process. The impact of this research will be in a number of fields where superior protective castings are needed. These include military applications, electronic components, chemical processing, and others.

DEPOSITION AND CHARACTERIZATION OF MAGNETRON SPUTTERED BCC TANTALUM

by
Anamika Patel

A Dissertation
Submitted to the Faculty of
New Jersey Institute of Technology
in Partial Fulfillment of the Requirements for the Degree of
Doctor of Philosophy in Electrical Engineering

Department of Electrical and Computer Engineering

January 2003

Copyright© 2003 by Anamika Patel

ALL RIGHTS RESERVED

APPROVAL PAGE

DEPOSITION AND CHARACTERIZATION OF MAGNETRON SPUTTERED BCC TANTALUM

Anamika Patel

Dr. Marek Sosnowski, Dissertation Advisor — Date
Associate Professor of Electrical and Computer Engineering, NJIT

Dr. Roy Cornely, Committee Member — Date
Professor of Electrical and Computer Engineering, NJIT

Dr. Haim Grebel, Committee Member — Date
Professor of Electrical and Computer Engineering, NJIT

Dr. Zafar Iqbal, Committee Member — Date
Professor of Chemistry, NJIT

Dr. James Hirvonen, Committee Member — Date
Army Research Laboratory, Aberdeen, MD

BIOGRAPHICAL SKETCH

Author: Anamika Patel

Degree: Doctor of Philosophy

Date: January 2003

Undergraduate and Graduate Education:

- Doctor of Philosophy in Electrical Engineering,
  New Jersey Institute of Technology, Newark, NJ, 2003

- Master of Science in Electrical Engineering,
  New Jersey Institute of Technology, Newark, NJ, 1998

- Bachelor of Science in Electronics Engineering,
  University of Nagpur, Maharastra, India, 1995

Major: Electrical Engineering

Presentation and Publications:

Anamika Patel, Leszek Gladczuk, Charanjeet Singh Paur, Marek Sosnowski
"Tantalum nitride seed layers for bcc tantalum coatings deposited on steel by magnetron sputtering" submitted to *Materials Research Society proceedings*, Dec. 2002.

Leszek Gladczuk, Chirag Joshi, Anamika Patel, Zafar Iqbal, Marek Sosnowski and Jim Giuheen, "Corrosion-Resistant tantalum coatings for PEM fuel cell bipolar plates" submitted to *Materials Research Society proceedings*, Dec. 2002

Anamika Patel, Charanjeet Singh Paur, Leszek Gladczuk and Marek Sosnowski,
"Control of crystalline phase of tantalum deposited on steel by magnetron sputtering" 201st *Electro Chemical Society Meeting*, Philadelphia, PA, May 2002.

Anamika Patel, Leszek Gladczuk, Charanjeet Singh Paur and Marek Sosnowski,
"Sputter-deposited bcc tantalum on steel with the interfacial tantalum nitride layer" MRS Proceeding, Volume 697, pp. 5.6.1-5.6.6, November 2001.

Anamika Patel, "Tantalum coatings on gun steel" *IEEE North Jersey student presentation contest*, 2nd position, February 2002.

To the lotus feet of Guruhari Hariprasad Swamiji

ACKNOWLEDGEMENT

The author wishes to extend her sincere gratitude to her supervisor, Dr. Marek Sosnowski, for his guidance, moral support, and encouragement and for the opportunity to conduct research in the fascinating field of processing and characterization.

Special thanks are due towards Dr. James Hirvonen who not only served as a committee member and mentor, but also provided with Nuclear Reaction Analysis and Rutherford Backscattering Spectroscopy measurements. Furthermore, author wishes to thank Dr. Roy Cornely, Dr. Haim Grebel and Dr. Zafar Iqbal for serving as committee members and taking time to review the work.

I would like to express special thanks to all my colleagues at Ion Beam and Thin Film Research Laboratory for their support and help: Leszek Gladczuk, Charnjeet Singh Paur, Chirag Joshi, Cheng Li, Bhavin Shah and Younes Abassi. Special thanks to Maria Albano for her friendship and support. I would like to thank P. Ben, P. Serveshvar for their constant guidance plus encouragement and last, but not least my family at Aatam for their support, understanding and friendship throughout my research work.

TABLE OF CONTENTS

Chapter | Page

1 INTRODUCTION 1

1.1 Objective and Scope of Work 1

1.2 Synopsis 3

2 BACKGROUND 5

2.1 Properties of Tantalum 5

2.2 Deposition Methods for Tantalum Films 5

2.2.1 Chemical Vapor Deposition 6

2.2.2 Electrochemical Deposition 6

2.2.3 Physical Vapor Deposition 7

2.3 Overview of Sputtering Processes 9

2.3.1 DC Diode Sputtering 9

2.3.2 Radio Frequency Sputtering 10

2.3.3 Magnetron Sputtering 10

2.3.4 Reactive Sputtering 14

2.4 Prior Work on Ta Films and Coatings 14

2.4.1 Early Work on Ta Films 14

2.4.2 Tantalum Films as a Barrier Layer for Cu Interconnects in ICs 17

2.4.3 Work Reported on Ta Coatings 18

3 EXPERIMENTAL METHODOLOGY 19

3.1 DC Magnetron Sputtering System 19

3.2 Gas Flow and Pumping System 24

TABLE OF CONTENTS
(Continued)

Chapter **Page**

3.3 Substrate Preparation 26

3.4 Deposition Parameters 32

4 CHARACTERIZATION TECHNIQUES 35

4.1 Surface Profilometry 35

4.2 Four Point Probe Measurement 36

4.2.1 Resistivity Measurements on Deposited Ta 38

4.3 Optical Microscopy 38

4.4 Scanning Electron Microscopy 40

4.5 Atomic Force Microscopy 43

4.5.1 Principle of Atomic Force Microscopy 43

4.5.2 Equipment 46

4.6 X-ray Diffraction 48

4.7 Nuclear Reaction Analysis 53

4.8 Adhesion test 59

5 RESULTS 61

5.1 Ta Deposited on Tantalum Nitride seed layer 61

5.2 Tantalum Nitride Structure Promoting Bcc Tantalum 71

5.3 Tantalum deposited on Heated Substrate 84

5.4 Adhesion of Ta Coatings 89

6 DISCUSSION 94

TABLE OF CONTENTS
(Continued)

Chapter **Page**

6.1 Effect of Tantalum Nitride Interlayer on the Phase of Deposited Ta 94

6.2 Characteristics of Tantalum Nitride Film 96

6.3 Effect of Temperature on Deposited Ta 98

7 CONCLUSION 100

APPENDIX Details of Deposition Conditions 103

REFERENCES 105

LIST OF TABLES

Table		Page
3.1	Steps Followed for Grinding Steel Substrates	27
3.2	Sequential Steps Followed for Polishing Steel Substrates	28
5.1	Tantalum Phase Dependence on the Thickness of Tantalum Nitride Seed Layer on Steel	63
5.2	Comparison of Ta Grown on Tantalum Nitride Seed Layer Deposited on Steel Substrate with and without Sputter Etching	66
5.3	Summary of AFM Measurements Performed on Tantalum Nitride Films Deposited with Different Nitrogen Flow	76
5.4	Summary of XRD Results on the Tantalum Nitride Film on SiO_2	80
5.5	Result Showing the Change in Crystallographic Orientation with Change in the Film Thickness	87

LIST OF FIGURES

Figure		Page
2.1	Sputtering yield of Ta vs. the incident energy of the argon ion, plotted from the measurements reported by Straut and Wehner	8
2.2	Motion of the electron ejected from surface with the velocity v; a) with no electric field b) with a linearly decreasing electric field	12
2.3	Arrangement of target and magnets for circular magnetron source	13
2.4	Cross section of circular magnetron source, showing magnetic field, racetrack and electron orbits	13
3.1	Planar magnetron sputtering system built at New Jersey Institute of Technology in the Ion Beam and Thin Film Research Laboratory	19
3.2	Schematic diagram of the vacuum chamber of the planar magnetron deposition system	20
3.3	Inner view of the chamber showing the Torus 2 magnetron source	22
3.4	A view of the deposition chamber with the top lid lifted, showing the platter with the substrate holders	23
3.5	Design of the rotary platter with the slots for the substrate holder	23
3.6	Schematic of vacuum and gas flow control of the deposition system	25
3.7	Chart summarizing the surface preparation process	30
3.8	Steel substrates mounted on the holder	31
3.9	Steel, silicon and silicon dioxide substrates on the holder	31
3.10	Chart summarizing steps followed during deposition process	34
4.1	Example of an output of the film thickness measured by Dektak	36
4.2	Four-point probe resistivity measurement set up	37
4.3	Optical micrograph of the Ta coating (~50 μm) deposited on steel	40
4.4	Schematic of primary components of typical SEM	41

LIST OF FIGURES
(Continued)

Figure **Page**

4.5 Example of scanning electron micrograph of the Ta film deposited on steel during preliminary experiments 42

4.6 Schematic of a generalized scanning probe microscopy 43

4.7 Schematic arrangements of AFM showing the feedback loop for tapping mode operation 45

4.8 Atomic force micrograph of the tantalum nitride film on silicon dioxide substrate deposited by the reactive sputtering of Ta in argon and nitrogen plasma 47

4.9 Reflection of x-rays from two planes 48

4.10 Schematic showing the typical XRD set up 50

4.11 The standard powder diffraction spectra for bcc Ta 51

4.12 The standard powder diffraction pattern of beta Ta 51

4.13 XRD spectrum of bcc Ta deposited at room temperature on steel substrate with tantalum nitride interlayer 52

4.14 XRD spectrum of beta Ta deposited directly on steel substrate at room temperature 52

4.15 Incident beam energy vs. depth of resonance reaction (at 898 keV), in Ta-N target, of different composition 55

4.16 Principle of depth profile analysis using the resonance reaction $^{15}N(p,\alpha\gamma)^{12}C$ 56

4.17 Energy straggle vs. percentage of tantalum in 1 m thick Ta-N film calculated by TRIM code for the proton beam energies of 900 and 1000 keV 58

4.18 Energy straggle as a function of depth t which resonance reaction occurs (Er=898 keV) for a range of proton energies of 900-1050 keV, in TaN sample using TRIM code 58

LIST OF FIGURES
(Continued)

Figure **Page**

5.1 XRD spectrum of Ta coating deposited on steel substrate with and without the tantalum nitride interlayer 62

5.2 XRD pattern of the Ta film (~ 2 μm thick) deposited on sputter etched steel substrate with a 20 nm thick tantalum nitride interlayer 65

5.3 XRD spectrum of Ta film (~ 1 μm) deposited on sputter etched steel substrate with a 5 nm thick tantalum nitride interlayer 65

5.4 XRD spectrum of Ta deposited on steel substrate (after sputter etching) with an interlayer of (15 nm thick) tantalum nitride 67

5.5 Photomicrograph of the cross section of steel sample with Ta coating on an interlayer of 15 nm thick tantalum nitride deposited after sputter etching of the substrate 67

5.6 XRD spectrum of bcc Ta coating deposited on steel substrate (and no prior sputter etching) with 15 nm thick tantalum nitride interlayer 68

5.7 Photomicrograph of the cross section of steel sample with the Ta coating and tantalum nitride interlayer (15 nm thick) deposited without sputter etching 65

5.8 Photomicrograph of polished surface of mixed phase Ta coating deposited on steel with argon as a sputtering gas 69

5.9 Cross section of the steel sample with bcc Ta coating deposited on tantalum nitride seed layer with beta inclusions clearly visible as light needles 68

5.10 Deposition rate vs. the percentage of nitrogen concentration in the sputtering gas 72

5.11 Resistivity of tantalum nitride film on SiO_2 substrate vs. the percentage of nitrogen flow in the sputtering gas 73

5.12 AFM image of 2 μm x 2 μm area (Z= 20 nm/div) of the tantalum nitride film deposited with nitrogen concentration a) 5% b) 14% c) 18%, in a mixture of argon and nitrogen, on silicon dioxide substrate 74

LIST OF FIGURES
(Continued)

Figure **Page**

5.13 AFM image of 2 μm x 2 μm area (Z = 20 nm/div) of tantalum nitride film deposited, with nitrogen flow of a) 21% b) 28% c) 33% in a mixture of argon and nitrogen, on silicon dioxide substrate 74

5.14 X-ray diffraction spectra of tantalum nitride film deposited, on SiO_2 substrate, with nitrogen flow of a) 5% b)14% c) 18% nitrogen concentration in the sputtering gas 78

5.15 X-ray diffraction spectra of tantalum nitride film deposited, on SiO_2 substrate, with nitrogen flow of a) 21% b) 28% c) 33% nitrogen concentration in the sputtering gas 79

5.16 Comparison of XRD pattern from tantalum nitride film deposited on steel substrate with different nitrogen concentration in the sputtering gas mixture of argon and nitrogen.. 81

5.17 The nitrogen contents of tantalum nitride films deposited with different nitrogen concentration of 5% and 14% (flow of 1/18 and 3/18 respectively), measured by NRA. Film thickness was 1.0 μm and 0.8 μm respectively 82

5.18 Scanning electron micrograph of tantalum nitride film of thickness 10 nm deposited on a sputter etched steel substrate.. 83

5.19 XRD pattern of Ta deposited on steel substrate heated to 400 °C in argon, all peaks correspond to the bcc Ta phase.. 84

5.20 XRD spectrum of Ta deposited on heated steel substrate (350 °C) with krypton as the sputtering gas, all peaks correspond to the bcc Ta phase....... 85

5.21 XRD spectrum of mixed phase Ta film deposited on steel substrate at 200 °C with argon and 250 °C with krypton 86

5.22 XRD pattern of Ta film (4 μm) deposited on steel maintained at 400 °C during deposition 86

5.23 XRD spectrum of Ta deposited on heated steel substrate (400 C) showing the bcc structure with the crystallographic texture changing with the grow -ing thickness of the coating 87

LIST OF FIGURES
(Continued)

Figure		Page
5.24	XRD spectra from front and back of bcc Ta (2 μm thick) detached film deposited on heated steel substrate	88
5.25	Photomicrograph of the bcc Ta coating deposited on heated steel substrate with no trace of beta phase in the coating	88
5.26	SEM image, showing the Ta coatings deposited on sputter etched steel sample with an interlayer of tantalum nitride, after the groove test (performed at Benet Laboratories)	90
5.27	Scanning electron micrograph of Ta coatings deposited on steel substrate without sputter etching and with an interlayer of tantalum nitride	90
5.28	Coating failure pattern observed in beta Ta deposited on sputter etched steel substrate	91
5.29	Typical scratch pattern obtained on mixed phase tantalum coating deposited on 10 nm thick tantalum nitride interlayer	92
5.30	Coating failure pattern observed in beta –Ta coating deposited on sputter etched steel substrate	92
5.31	Failure observed in beta Ta coatings deposited on steel without tantalum nitride interlayer	93
6.1	Cross section of steel sample with bcc Ta coating grown on tantalum nitride interlayer and beta Ta inclusions are clearly observed as light needles in grey background of bcc	95

CHAPTER 1

INTRODUCTION

1.1 Objective and Scope of Work

The main goals of this research, presented in the following dissertation were:

1) To control the process of DC magnetron sputtering for the growth of high quality bcc tantalum (Ta) coatings on steel

2) To understand the effects of various parameters of DC magnetron sputtering on the resultant crystallographic phase and other properties of Ta coatings.

Sputtered Ta coating has two main phases: alpha phase, which has a bcc crystal structure (also found in bulk Ta) and beta phase, which has a tetragonal structure and is a meta-stable state. The bcc (α) phase is preferred over the beta phase for most applications, as it is characterized by high toughness and ductility whereas, the beta phase is brittle and hard and prone to failure under stress. One application of bcc Ta coatings is the protection of steel from erosive and corrosive wear. Crystallographic phase is an important factor controlling the coating performance. Sputtering parameters control the structure and the morphology in sputtered coatings. The mixed phase (bcc + beta) of Ta can be easily deposited but to grow a pure bcc phase requires a careful selection and control of the process parameters. Deposition of Ta has been extensively studied on substrates like silicon and glass, but the process of deposition of Ta on steel has not well documented.

This research was driven by a very specific application for the US Army, which funded the project. A problem of concern to the army is the damage of the gun tubes

caused by erosive and corrosive wear during firing [1]. Electroplated chromium has long been used as a protective coating in gun barrels. Protective coatings of chromium however are found not to be sufficient in extreme conditions created by new, advanced propellants. Additionally chromium, which is deposited by electro-plating in the hexavalent (VI) form, is carcinogenic. A major environmental hazard is created by chromium in the production, use and disposal of weapons. Increased restrictions and industrial hygiene requirements make it difficult to continue with electro-deposited chromium coatings. Tantalum was chosen as an alternate metal for the protective coatings and sputtering as a method of deposition of Ta, over CVD and electro chemical deposition, by the Army researchers. A CVD and electro-chemical deposition requires high deposition temperature, as discussed in Section 2.2. The gun barrel cannot be exposed to the high temperature (which is more than the tempering temperature of steel), as it will undergo undesirable changes in its mechanical properties.

This work involved design, assembly and testing of a planar DC magnetron sputtering system. The vacuum chamber housing the system and the sputtering source were manufactured by Kurt J. Lesker Company, PA while, other components were obtained from various manufacturers or were made at NJIT's machine shop. A series of depositions were carried out in this system with various sputtering process parameters. The influence of pressure (1-150 mT), gas flow (1-30 mT) and source power (100-1000 watts) or film properties, was investigated. Argon was mostly used as the sputtering gas for deposition of Ta and krypton was tested in some experiments. Tantalum was also deposited on a tantalum nitride interlayer on steel. During the reactive deposition of the tantalum nitride interlayer, a mixture of nitrogen and argon was used. Ta films and

coatings with thickness ranging from 1 to 50 μm were deposited on steel and control substrates of Si and SiO_2.

Thin films and coating of bcc tantalum were successfully obtained by two methods:

1) Deposition of Ta on a thin interlayer of tantalum nitride on steel,
2) Deposition of Ta on heated steel substrates.

This research was based on analysis of many experiments for deposition of Ta films and coatings and their characterization. Characterization techniques included x-ray diffraction (XRD), four point probe resistivity measurements, scratch (adhesion) tests, scanning electron microscopy (SEM), nuclear reaction analysis (NRA), optical microscopy, Rutherford backscattering (RBS) and atomic force microscopy (AFM).

An effort was made to better understand the Ta deposition process and to clarify often-contradictory information on this subject found in literature. This effort was also aimed to support work at the Army Research Laboratory and Benet laboratory. Thin films and coatings of pure bcc structure, with excellent adhesion to steel substrates, were successfully deposited by the DC magnetron process. These findings will also have potential application in other fields of technology and industry

1.2 Synopsis

This dissertation presents the results on bcc Ta deposition by DC magnetron sputtering system undertaken at the Ion Beam and Thin Film Research Laboratory at NJIT. The presentation of this thesis begins with a general description of the properties of Ta.

Deposition methods of Ta are discussed later followed by the literature review on Ta thin films and coatings in Chapter 2.

The details of the system with sample preparation method, substrate mounting and experimental parameters are discussed in Chapter 3.

Characterization of Ta films and coatings was performed subsequent to deposition. The film thickness was measured with a profilometer on control samples of Si and SiO_2. A crystallographic phase determination is based on x-ray diffraction (XRD) measurements. Electrical resistivity measurements were also performed on control sample of SiO_2 by the four-point probe method. Morphology of the films was determined by, optical microscopy and scanning electron microscopy (SEM) and Atomic Force Microscopy (AFM). Scratch tests to determine the adhesion of the coating were performed. Rutherford backscattering (RBS) data on Ta films was also studied. The structure of the interlayer of tantalum nitride was studied by nuclear reaction analysis (NRA). Chapter 4 addresses the working principles of these characterization techniques.

Results are focused on two methods of obtaining the bcc Ta coatings: i) deposition on a thin tantalum nitride interlayer and ii) deposition on a heated substrate. These results are reviewed in Chapter 5, discussed in Chapter 6 and the conclusions of this dissertation are summarized in Chapter 7.

CHAPTER 2

BACKGROUND

2.1 Properties of Tantalum

The element tantalum (Ta) was discovered in 1802 by Swedish chemist A.G. Ekenberg in Uppsala, Sweden. He named the new element after the figure of Geek mythology, Tantalus, to describe its resistance to acids. C. W. Balke first produced tantalum in United States in 1922 and commercial production has continued from that time.

Tantalum is earth's 49th most abundant element [2] but it is uncommon as it is found in earth's crust in a concentration of only 2.5 ppm. It has a strong affinity to oxygen and so it occurs mostly as oxide in association with niobium. Tantalum is produced as a byproduct of tin smelting.

Bulk Ta is shiny, grey colored metal. It has a high boiling point (5425 °C) and melting point (2996 °C). Its density is 16.6 gm/cc at 293K. Its atomic number is 73 and atomic weight is 180.95 gm/mole. In its bulk equilibrium form it has a bcc (body centered cubic) structure with a lattice constant of 3.30 Å. Its electrical resistivity is 13.5 μΩcm. Tantalum is also one of the most corrosion resistant metals known. It has good resistance to brittle fracture and failure due to vibration and shock.

2.2 Deposition Methods for Tantalum Films and Coatings

Main methods for Ta deposition can be classified as:

- Chemical vapor deposition
- Electrochemical deposition
- Physical vapor deposition.

2.2.1 Chemical Vapor Deposition

Chemical vapor deposition (CVD) creates a vapor phase dispersion of the material to be deposited by using a precursor molecule containing the atom to be deposited. The metal can be released by allowing a chemical reaction to take place in either the vapor phase very near to the substrate or on the substrate itself. Advantages of this process are the relative low cost of the equipment and its low operation expenses. One drawback of CVD is that the crystalline structure, thickness and adhesion of the film are very sensitive to the substrate temperature and gaseous stream. In the work reported by Brossa [3] CVD coatings of Ta were produced by thermal reduction of $TaCl_5$ with hydrogen or zinc.

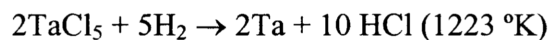
$2TaCl_5 + 5H_2 \rightarrow 2Ta + 10\ HCl$ (1223 °K)

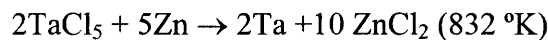
$2TaCl_5 + 5Zn \rightarrow 2Ta + 10\ ZnCl_2$ (832 °K)

However, it was found that CVD-Ta has poor metallurgical properties and a high resistivity as compared to PVD-Ta [4].

2.2.2 Electrochemical Deposition

Electrochemical deposition of tantalum is also reported in the literature [5]. The electrolyte used was a eutectic mixture of LiF-NaF-KF (FLINAK), which was prepared from reagent grade fluoride salts. To this mixture K_2TaF_7 was added. The intermediate reversible process produced insoluble TaF_2, which grows by providing additional nucleation sites to give dense coatings:

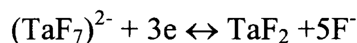
$(TaF_7)^{2-} + 3e \leftrightarrow TaF_2 + 5F^-$

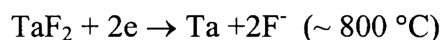
$TaF_2 + 2e \rightarrow Ta + 2F^-$ (~ 800 °C)

The final irreversible process produces tantalum. This process of electro deposition was carried out at temperatures ranging from 700 to 800 °C. Tantalum coatings obtained by this method had the bcc structure, as reported by Lee et al. [6]. The main drawback of this process was that liner technology had to be used for deposition of Ta on gun barrels, as the steel substrate could not be exposed to high temperatures of the molten salt.

2.2.3 Physical Vapor Deposition

Main categories of physical vapor deposition (PVD) are vacuum evaporation and sputter deposition. Vacuum evaporation is a process in which atoms or molecules, emitted from a thermal evaporation source, deposit on the substrate with little or no collision with gas molecules in space between the source and the substrate so that their trajectory is a line of sight. One of the advantages of evaporation can be, the high deposition rates [7]. Vacuum deposition of Ta however requires heating to a very high temperature above 3350 °C in order to get vapor pressure of 0.1 torr at the source. This technique is not very popular for Ta deposition.

When a solid surface is bombarded by energetic particles (accelerated ions), atoms of the solid near the surface can be knocked out due to collisions between the surface atoms and energetic particles. This phenomenon is known as sputtering. In general, the sputtering process consists of four steps: 1) the ions are generated and accelerated towards the target, 2) the ions sputter target atoms, 3) the ejected (sputtered) atoms are transported to the substrate, where 4) they condense and form a film. The number of sputtered atoms per incident ion is known as sputtering yield of the target material. Sputtering yields of metals with argon ions with energy below 1 keV are of the order of unity [8]. Figure 2.1 shows the dependency of sputtering yield of tantalum on the

energy of argon ions [9]. There could be some complications also associated with this type of old data such as presence of surface oxide may dominate the result i.e. instead of measuring on Ta it could be performed on Ta_2O_5.

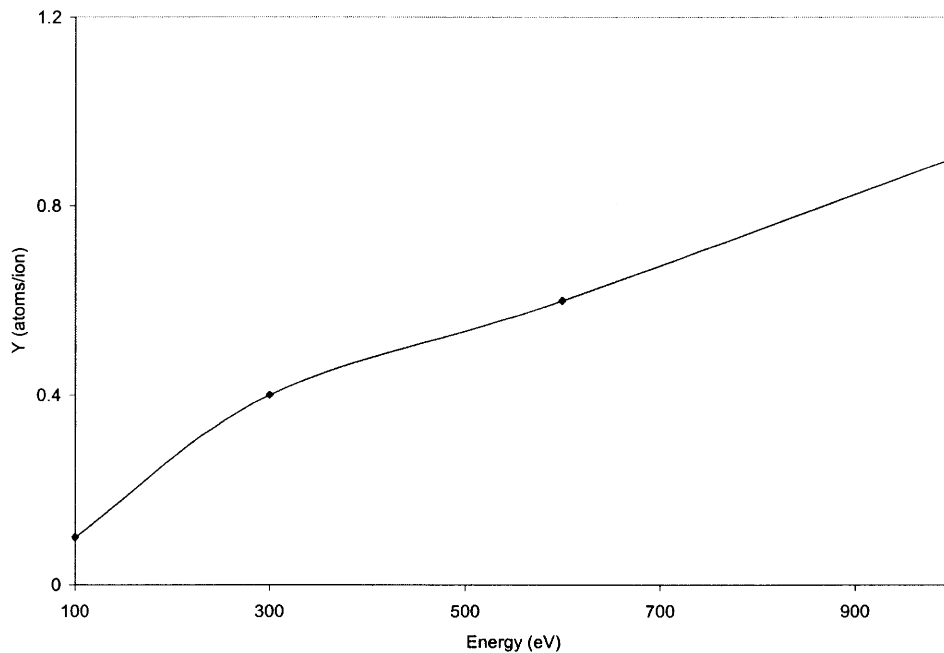

Figure 2.1 Sputtering yield of Ta vs. the incident energy of the argon ion, plotted from the measurements reported by Straut and Wehner [9].

One of the important characteristics of sputtering is its universality. As a cathode target atoms are ejected by physical momentum-exchange process, practically most any solid material can be sputtered [10]. There are different types of sputter deposition in use today, such as direct current (DC) sputtering, radio frequency (RF) diode sputtering, ion beam deposition and magnetron sputtering. DC magnetron sputtering was used for this research work because it is the most effective and versatile technique for the deposition of metals.

2.3 Overview of Sputtering Processes

2.3.1 DC Diode Sputtering

This technique takes its roots from the work by W.R. Groove on glow discharge almost 150 years ago [11]. Grove sputtered from the tip of a wire held very close to a highly polished silver surface, at a pressure of about 0.5 torr. In diode sputtering the material, which needs to be sputtered, is the cathode of an electrical circuit and hence this method is also known as cathode sputtering. The substrate is placed on an electrically grounded anode. These electrodes are housed in a chamber, which is pumped to low base pressure ($\leq 10^{-5}$ torr). Argon is commonly introduced into the chamber to maintain a specific pressure of a few hundred millitorr. An electric field accelerates the electrons, which collide with argon atoms and ionizes them. This process of electron collision is known as the electron impact ionization. In this collision the primary electron removes an electron from the atom, producing a positive ion and an additional electrons. For example,

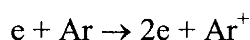

$$e + Ar \rightarrow 2e + Ar^{+}$$

The two electrons released in this process can then be accelerated by an electric field until they can produce ionization too. This continuous process of ionization results in the glow discharge.

The minimum energy required for the ionization process to occur is the energy required to remove the weakly bound electron from the atom and is known as ionization potential. In case of argon it is 15.75 eV. The electric field accelerates the charged particles in the glow discharge and the electrons move toward the anode, and the ions towards the cathode. When the ions strike the cathode, they may sputter some of the target atoms off, predominantly electrically neutral particles. The sputtered atoms, from

the target fly off in random directions and some of them land on the substrate, condense there and form the film. The rate of film formation depends on the amount of material sputtered from the target; this in turn depends on the ion flux at the target, which is proportional to the current. The amount of sputtering also depends on the sputtering yield and thus on the ion energy.

2.3.2 Radio Frequency Sputtering (RF)

To sputter insulators (dielectrics), DC diode sputtering process cannot be used because the glow discharge cannot be maintained with a dc voltage if the cathode is not electrically conductive. This can be explained by the fact that when the cathode is bombarded by a positive ion, which is neutralized, an electron is stripped from the cathode surface. Such electrons can be replaced by electrical conduction, if the cathode is a conductor, but in case of an insulator this is not possible. Hence the front surface of the cathode (insulator) accumulates the positive charge and the potential difference (between cathode surface and anode surface) decreases. When this value decreases below the value required to sustain the plasma, the plasma extinguishes. To replenish the lost electrons in insulator surfaces a technique was developed which involves the application of an ac voltage instead of dc to the electrode. The applied power has the oscillations in radio frequency range hence the technique is known as radio frequency (RF) sputtering [10].

2.3.3 Magnetron Sputtering

The beginning of the magnetron sputtering technique dates back to 1936 when Penning [12] proposed the application of perpendicular magnetic field in order to increase the plasma concentration of glow discharge. DC and RF sputtering processes normally

exhibit low deposition rates, as most secondary electrons emitted from the target move away from it before ionizing sputtering gas atoms. If a magnetic field is applied parallel to the surface of a target of a dc sputtering system (perpendicular to the electric field), due to Lorentz forces, the secondary electrons that are accelerated from the target to the substrate are forced into a spiral path in the vicinity of the target surface. To understand this effect, consider an electron normally emitted from a surface with velocity v into a region of magnetic field B and zero electric field. The electron will describe a semicircle of radius r, provided it does not collide and will return to the surface with velocity v. Hence the effect of magnetic field is to trap the emitted electron near the surface. To examine a situation, which is closer to the magnetic sputtering application, consider a strong electric field, which exists in the space above the surface of the sputtering target and also the magnetic field, which is parallel to the surface. Let the electric field E decrease linearly with the distance from the target through the dark space (L). The electric field is thus given by,

$$E = E_o(1 - \frac{y}{L}) \tag{2.1}$$

Here, y is the dimension perpendicular to the target with y = 0 at the target surface, the electric field is E_o. The electron emitted from the target will be rapidly accelerated vertically, initially away from the target by the strong normal electric field at the surface but simultaneously it experiences an increasing force due to magnetic field, F = q(v x B). The presence of an electric field along with the magnetic field changes the electron path from circular to cycloidal (hopping) as shown in Figure 2.2, provided the electron stays in the dark space [13]. This increases the electron path length in the plasma and hence increases the probability of collision with sputtering gas atoms near the target surface.

The increase in the production rate of ions that strike the target increases the sputtering rate. The deposition rate enhancement is commonly a factor of 10 over the diode sputtering method. It is also possible to sputter at a lower pressure as compared to DC diode sputtering process. The system geometry for a simple planar magnetron sputtering system is similar to DC and RF sputtering system but the applied magnetic field makes the system more effective. Magnetron sputtering is presently the most commonly used sputtering method [14].

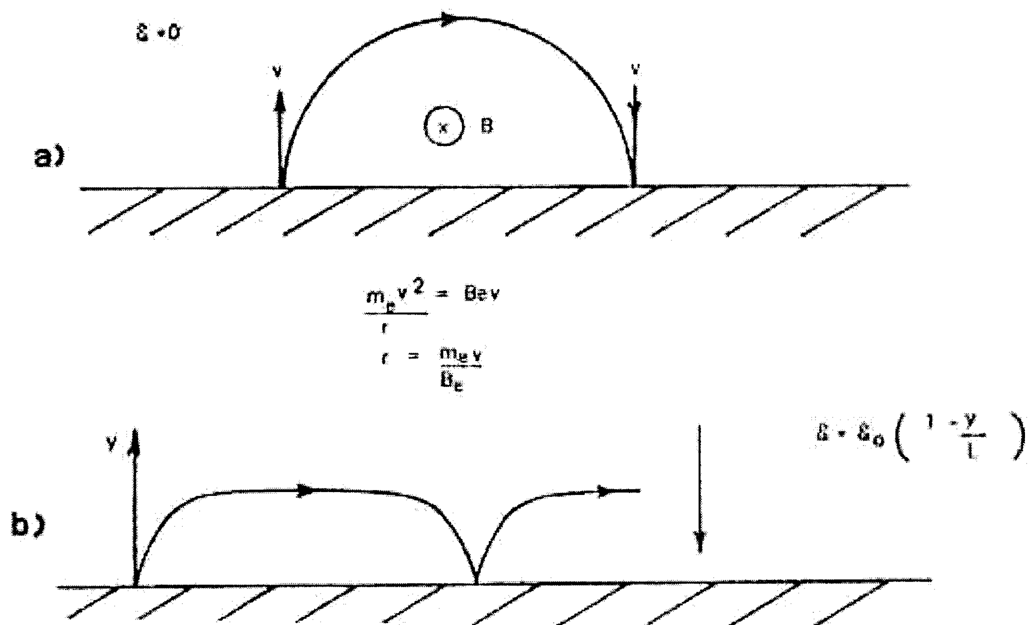

Figure 2.2 Motion of the electron ejected from the surface with a velocity v a) with no electric field, b) with a linearly decreasing electric field [9].

There are many types of magnetrons in practical sputtering systems. The most widely used magnetron electrode configuration in sputtering system is the circular magnetron [8]. In circular magnetrons the target surface is planar, and the B-field is created by permanent magnet behind the target. A schematic of target arrangement and magnets for a circular magnetron is shown in Figure 2.3.

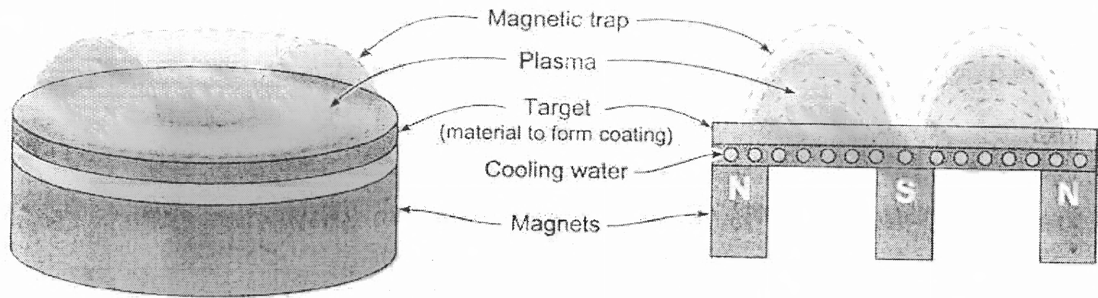

Figure 2.3 Arrangement of target and magnets for circular magnetron source [10].

The plasma is most intense where the magnetic field is parallel to the target surface and this is where maximum ejection of target atoms is expected. This results in the target erosion pattern called the racetrack. A more detailed cross section view of a circular magnetron sputtering source is shown in Figure 2.4.

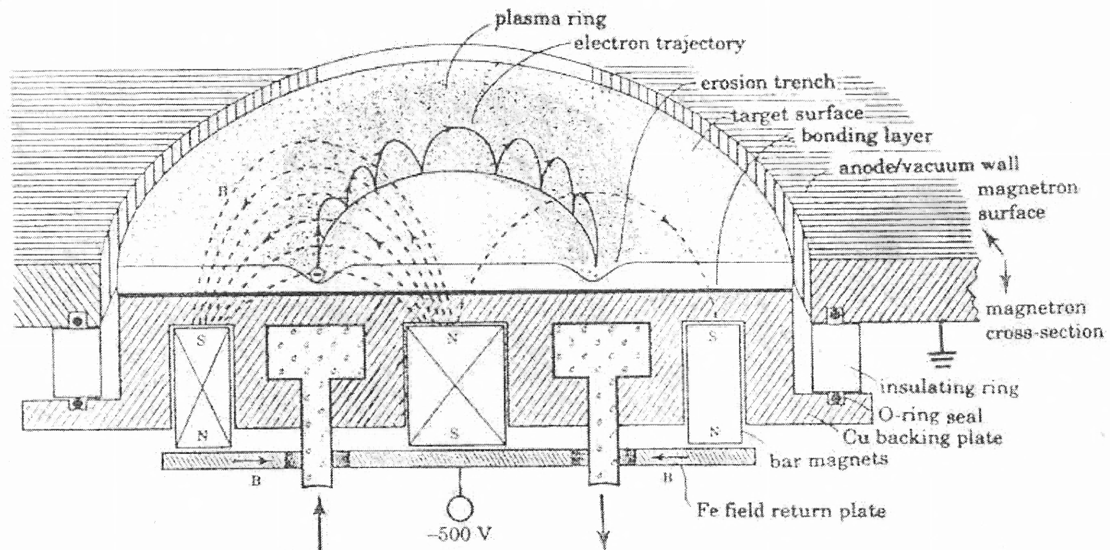

Figure 2.4 Cross section of circular magnetron source, showing magnetic field, racetrack, and electron orbits [8].

The disadvantage of magnetron sputtering is the localized erosion of the target, which gives low target material utilization, non-uniform deposition pattern and requires frequent replacement of the target. Uniformity improves as the target to wafer spacing is

increased but this causes a decrease in the deposition rate. Thus a tradeoff is often made between deposition rate and thickness uniformity

Sputter deposition can also be performed by ion beam sputtering with energetic ion bombardment of target in vacuum using an ion gun. Ensinger [15] has reported on wear and corrosion protection Ta coating deposited by ion beam sputter deposition.

2.3.4 Reactive Sputtering

Reactive sputtering is the process where at least one of the coating species enters the system in the gas phase. The advantage of reactive sputtering is that complex compounds can be formed using relatively easy to fabricate metallic targets. The difficulty in reactive sputtering is the complexity, which accompanies its versatility. Reactions can occur on the target surface, following which the reacted material is sputtered. They also occur at the substrate, and in cases of high working pressure, in the gas phase. When sputtering with a reactive gas and argon mixture, the relationship between film properties and the reactive gas injection rate is generally non-linear. The condensing film could be considered as an additional pump for the reactive gas. Examples of reactive sputtered films include Al sputtered in O_2 to form Al_2O_3; Nb, Ti and Ta sputtered in N_2 to form NbN, TiN, TaN all in presence of argon.

2.4 Prior Work on Ta Films and Coatings

2.4.1 Early Work on Ta Thin Films

Tantalum films have been investigated since 1970. Sputtered Ta films have mainly two crystallographic principle phases known as the alpha and the beta phase. Alpha has the

bcc structure (3.31 – 3.33 Å), while beta has a tetragonal structure (a = 5.34 Å and c = 9.94 Å). The electrical resistivity of the two phases also differs by a factor of ten. The high resistivity (180-300 μΩcm) beta phase is preferred for thin film resistors while; the low resistivity bcc phase is preferred for thin film interconnects. The bcc phase is also characterized by high toughness and ductility and hence is desired in the protective coatings whereas the beta phase is hard and brittle and prone to failure under stress. The beta phase transforms to the bcc phase above 750 °C [16,17]. A new phase with a fcc lattice was reported in the films deposited on the MgO substrate by using electron beam evaporation. This fcc phase in a 100 Å film transformed into a bcc phase with the growing film thickness [7,18]. The fcc phase has not been seen in films deposited by dc sputtering.

Typically, thin sputtered films are nucleated in the tetragonal β phase while the bcc α phase is found in bulk. Most of the literature is inconsistent regarding the conditions that promote a particular phase of tantalum. The first report on the β phase of tantalum in sputtered films (for a varying thicknesses of 100 – 20,000 Å) was published in 1965 [19]. It was concluded that the β phase was formed when the concentration of the various impurities were below a critical level in the vacuum chamber, while the residual gas impurities and the gas contamination promoted the formation of bcc tantalum. Impurity levels in films will be controlled by; 1) deposition rate and 2) arrival rate of "impurities" in vacuum. L. Maissel and R. Glang also observed the dependence of particular phase formation on the base pressure of the chamber, with a base pressure in the range 10^{-5} torr promoting the formation of the bcc phase [20]. Some other studies could not confirm the dependence of phase formation on the residual gas and proposed

the existence of an "X" impurity on the substrate, which resulted in the formation of alpha tantalum [21]. In the work of Westwood, which was published in 1970, it was demonstrated that a 1000 Å thick interfacial layer of carbon or gold on glass and alumina substrate promoted the bcc phase of tantalum [22]. Further, D. Mills reported the β phase in tantalum sputtered onto an oxide-coated surface while the bcc phase formed on non-oxide surface [23]. Feinstein et. al, reported that β phase is meta-stable and their work also showed that the presence of O or OH on the surface of the substrate was necessary for the nucleation of β tantalum [24]. The substrates that do not readily form surface oxides (e.g. Au, Pt, W etc) were shown to nucleate the bcc phase of tantalum.

In later years, these results were contradicted. Hieber and Mayer reported that the thin film of carbon (non-oxide surface) does not affect the structure of tantalum film [25]. Sato observed β tantalum on all the substrates (including Au and Pt) except titanium, which has the crystal structure very close to bcc tantalum [26]. Contradictory views of researchers were explained to some extent by misinterpretation of X-Ray Diffraction (XRD) data. Some of the peaks in the XRD spectra of the two phases almost coincide [27]. There has been strong evidence, however that the structure of tantalum thin films may be influenced by the structure of the substrate or the interfacial layer deposited on the substrate prior to the deposition of the film. Face and Prober found that the thin (>3 Å) Nb (niobium) interfacial layer favors the formation of bcc phase of tantalum on silicon substrate [28] and also a thin titanium layer on silicon promoted the bcc phase of tantalum [29]. It was also shown that it is not possible to obtain β -Ta on bcc-Ta while the opposite is possible [30]. Schauer described a method for producing thin films of tantalum in the bcc phase by heating the glass substrate to 300 °C during deposition [31].

Studies on the transformation of the beta phase Ta to the bcc phase, as a function of annealing temperature is also reported in literature [16,17,32].

2.4.2 Tantalum Film as a Barrier Layer for Cu Interconnects in ICs

The interest in Ta films increased recently with the trend of replacement of aluminum with copper metallization in semiconductor integrated circuits [33]. The introduction of Cu in microelectronic devices made it necessary to deposit a barrier layer between SiO_2 and Cu, to avoid Cu diffusion into SiO_2, which is very strong and deteriorates the electrical performance of device even at temperatures as low as 200 °C [34]. Tantalum has proved to be one of the most promising barrier metals. As reported by P. Catania et al., the phase of Ta deposited on Si is sensitive to the pre-cleaning and also to the ion bombardment energies at the substrate [35]. Lower ion bombardment energies (~10eV) produced bcc Ta film while increasing the ion bombardment energy (>40eV) resulted in the increase of β phase in the film. Colgan and Fryer [36] described the method of making bcc Ta thin films by introducing an intermediate layer as thin as 20 Å of Ta(N) on the silicon substrate. This seed layer of Ta (N) was RF sputtered with nitrogen and argon as the sputtering gas. IBM implemented a liner which was the bi-layer of Ta/TaN in the process of manufacturing the first CMOS chips with Cu interconnects [37]. This liner was deposited from a pure Ta target, using Ar and N_2 sputtering gases.

2.4.3 Work Reported on Ta Coatings

Very little work has been done to investigate the phase characteristics of the thicker (i.e., >1 μm) sputtered Ta films. In the last decade, after tantalum was chosen as a promising material for protective coating in gun barrels, a new research area has been opened for

obtaining thick Ta films. The β phase of Ta, which was previously observed in thin films, was also produced in thick coatings [38]. Matson et al. reported on the thick (>25 μm) tantalum coatings deposited on niobium interfacial layers and also on heated steel substrates [39]. The coatings consisted mostly of the bcc phase with a few % of the β phase, which was observed at the interface between the steel substrate and tantalum coating on all their samples. As demonstrated by Lee and Windover, a niobium layer can promote the growth of bcc tantalum, irrespective to the impurity contents. Adhesion was a problem in these coatings, often with mixed phases [6,40,41]. Excellent behavior in soft and ductile bcc Ta area and cracking and delamination in the β Ta area of the coatings was reported [6]. Hence, minimizing or elimination of the β phase Ta was suggested for the superior coating performance. Effects of sputtering gas species and the substrate biasing was also reported on the thick sputtered Ta film [39]. Koski et al. [42] has reported on the improvement in the adhesion of the film grown on steel substrate, by sputter etching used along with the appropriate chemical cleaning method.

In conclusion, many process parameters have been identified that influence the structure of sputtered Ta. A specific effect of each of these variables is still being debated primarily because it is difficult to fully isolate each variable from the effect of the others. Much work has been done to understand this complex dependency in the area of thin films but unfortunately extrapolations of thin film deposition conditions to the thick coatings are not easy and straightforward. This research work addresses this issue.

CHAPTER 3

EXPERIMENTAL METHODOLOGY

3.1 DC Magnetron Sputtering System

A planar DC magnetron sputtering system was designed and assembled at the Ion Beam and Thin Film Research Laboratory at NJIT. Kurt J. Lesker Company, PA, manufactured the vacuum chamber and the key components (pumps, gauges etc.) of the system, came from various manufacturers. Shields, substrate holders and the other internal chamber components were made at the NJIT machine shop. The assembly and testing of this system was a part of this thesis work. A photograph of the magnetron system is shown in Figure 3.1. A schematic diagram with more details of the planar magnetron system is shown in Figure 3.2.

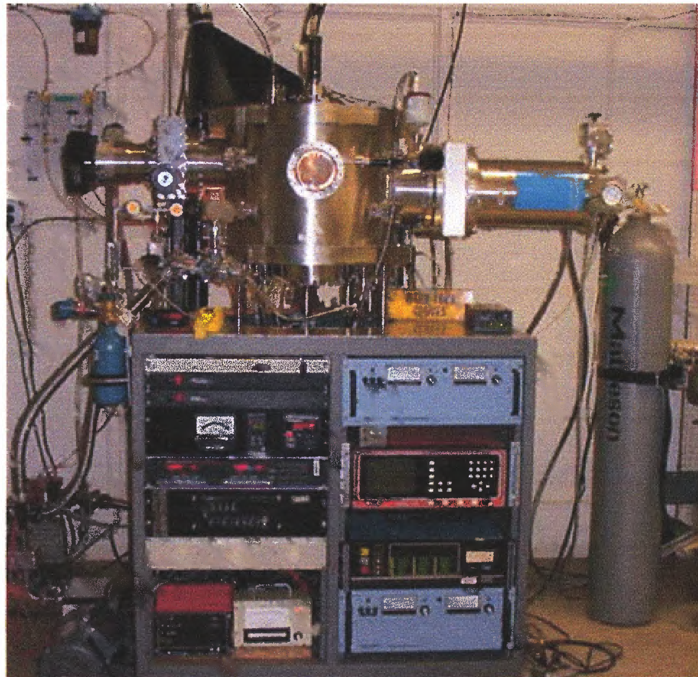

Figure 3.1 Planar magnetron sputtering system built at New Jersey Institute of Technology in the Ion Beam and Thin Film Research Laboratory.

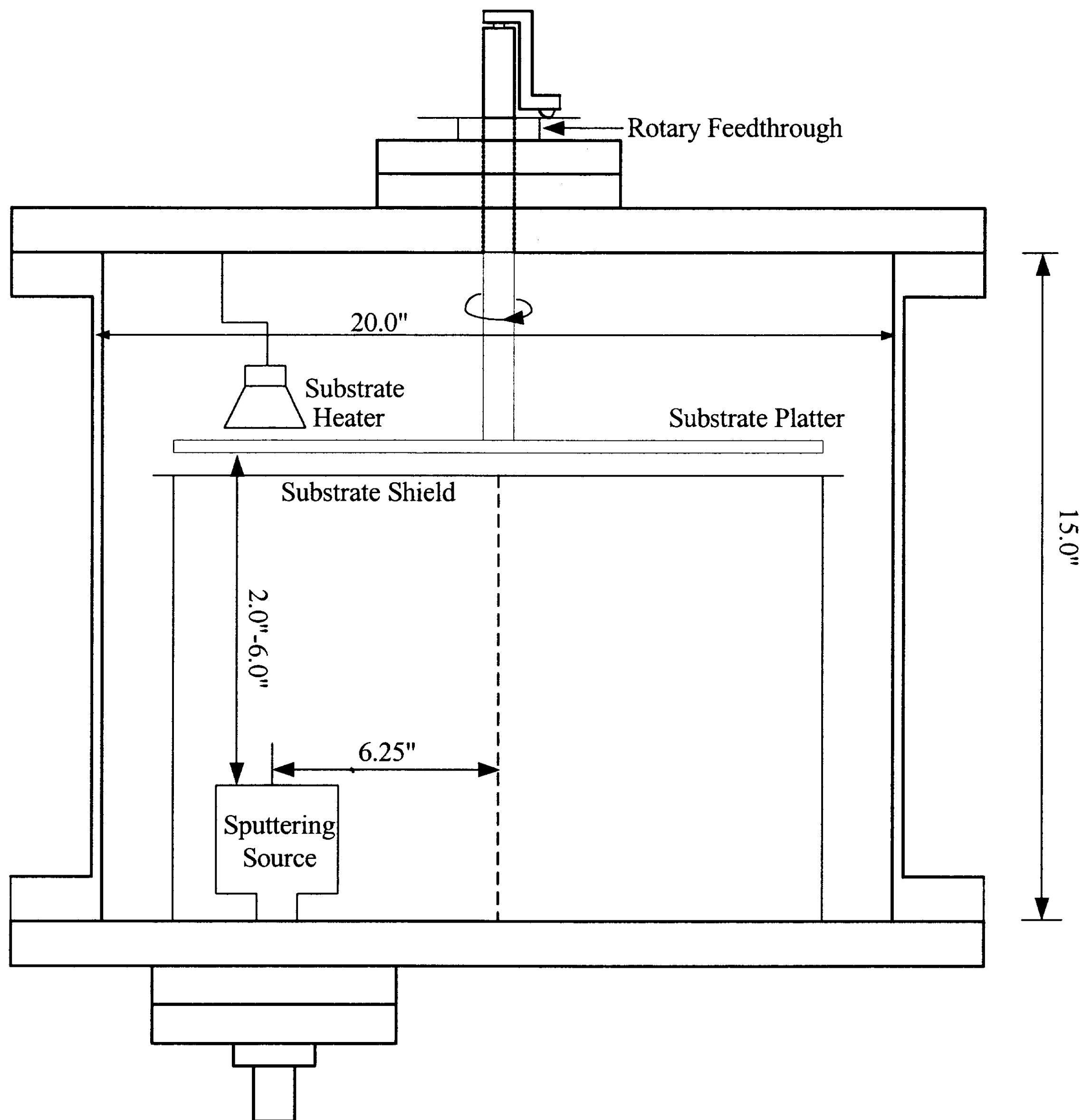

Figure 3.2 Schematic diagram of the vacuum chamber of the planar magnetron deposition system.

The system chamber is cylindrical in shape with a volume of approximately 80 l, inside diameter is 20 inches and an inside height of 15 inches. The chamber has numerous ports and these ports allow flexibility in attaching various accessories, vacuum feed-through and gages. A cryogenic vacuum pump (CTI-Cryotorr-8) with motorized control gate valve is attached to the pumping port of the chamber. A turbo molecular pump, which pumps the system during deposition, throttled by the gate valve is attached to a 4.5 inch Con-Flat (CF) flange on the opposite side of the chamber. In the sidewall on the front of the chamber is the view port, which allows for viewing the process. Other chamber ports were used for sensors like as ionization gauge and a capacitance pressure gauge (0-1 torr). Initially a residual gas analyzer (RGA) sensor was mounted to monitor the partial pressure of the residual gases in the chamber before sputtering. Later the system was modified to measure the partial pressure of the residual gases during sputtering. Two mass flow controllers (0-100 sccm) are attached to a read out which reads the gas flows. The bottom flange of the chamber has four 8 inch CF flanges to which, up to four deposition sources could be attached. For this research work a sputtering source (Torus 2) with the target diameter of 2 inches is attached to the bottom flange with a compression vacuum seal. The seal allowed the vertical movement of the source and thus the adjustment of the distance between the target and the substrate mounted above the source. The source is fitted with a Ta target (2 inch in diameter and 0.125 inch thick) and is clamped to water-cooled copper base plate. Figure 3.3 shows the inner view of the chamber with the source. A motorized hoist lifts the heavy top lid of the chamber. Top lid has CF ports, one of which has the carrousel substrate platter attached

to it. Other ports on top have feedthroughs for thermocouples, a high voltage cable (for pre-sputtering) and the cables for heating lamps.

Figure 3.3 Inner view of the chamber showing the Torus 2 magnetron source.

The chamber has a rotary feedthrough that supports a platter with eight circular slots and it holds one substrate holder in each slot. 45-degree rotation of the platter changes the position of the holder above the target. Figures 3.4 and 3.5 show the picture and the schematic of the platter respectively. A stainless steel shield (0.062 inches thick) is mounted 0.25 inches below the substrate platter by four posts attached on the bottom flange of the chamber. This shield limits the deposition to, one substrate holder and prevents deposition on the chamber top lid and walls.

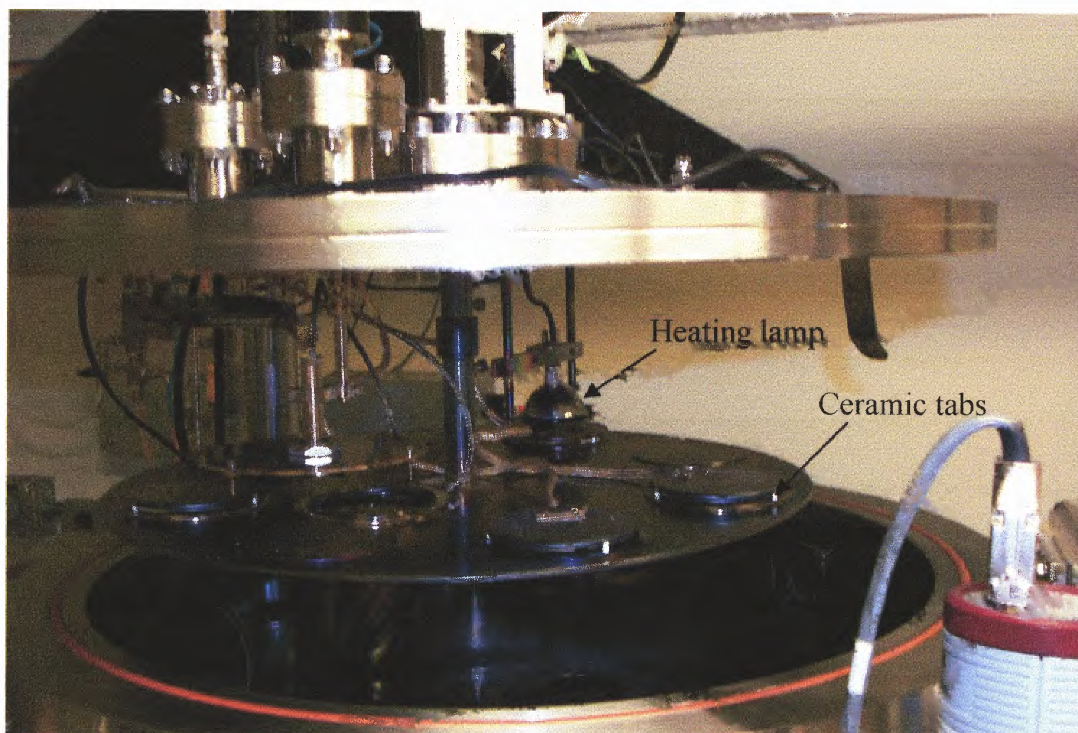

Figure 3.4 A view of the deposition chamber with the top lid lifted, showing the platter with the substrate holders.

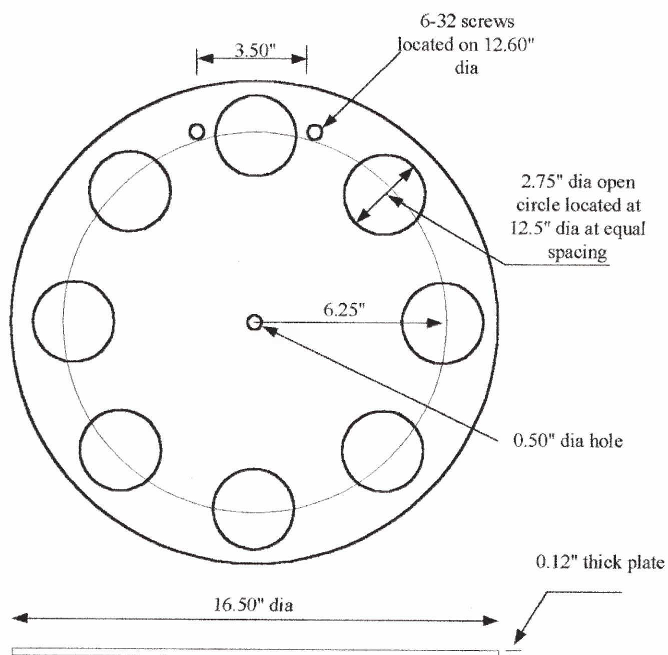

Figure 3.5 Design of the rotary platter with the slots for the substrate holder.

3.2 Gas Flow and Pumping System

A mechanical pump (Leybold D8B) pumps the chamber to a fore vacuum of 200 mtorr. A micro maze filter attached between the chamber and the pump prevents any back streaming of the oil pump vapors into the chamber. A cryo-pump pumps the system to a base pressure of 8×10^{-8} torr and the turbo pump pumps the system during the deposition. A thermocouple gauge measures the fore vacuum and the ionization gauge measures the high vacuum. A pressure transducer (MKS Baratron) measures the working pressure of the chamber, with a range from 0.1 mtorr to 1 torr. Two different gases can be admitted to the chamber through the mass flow controllers (MFC). Four-channel read out, to which the flow controllers were attached, was calibrated for each gas used in the sputtering process. A RGA measures the partial pressure of the gases during sputtering too as it is differentially pumped by a small turbo pump. The schematic diagram of the vacuum and gas flow system is shown in Figure 3.6.

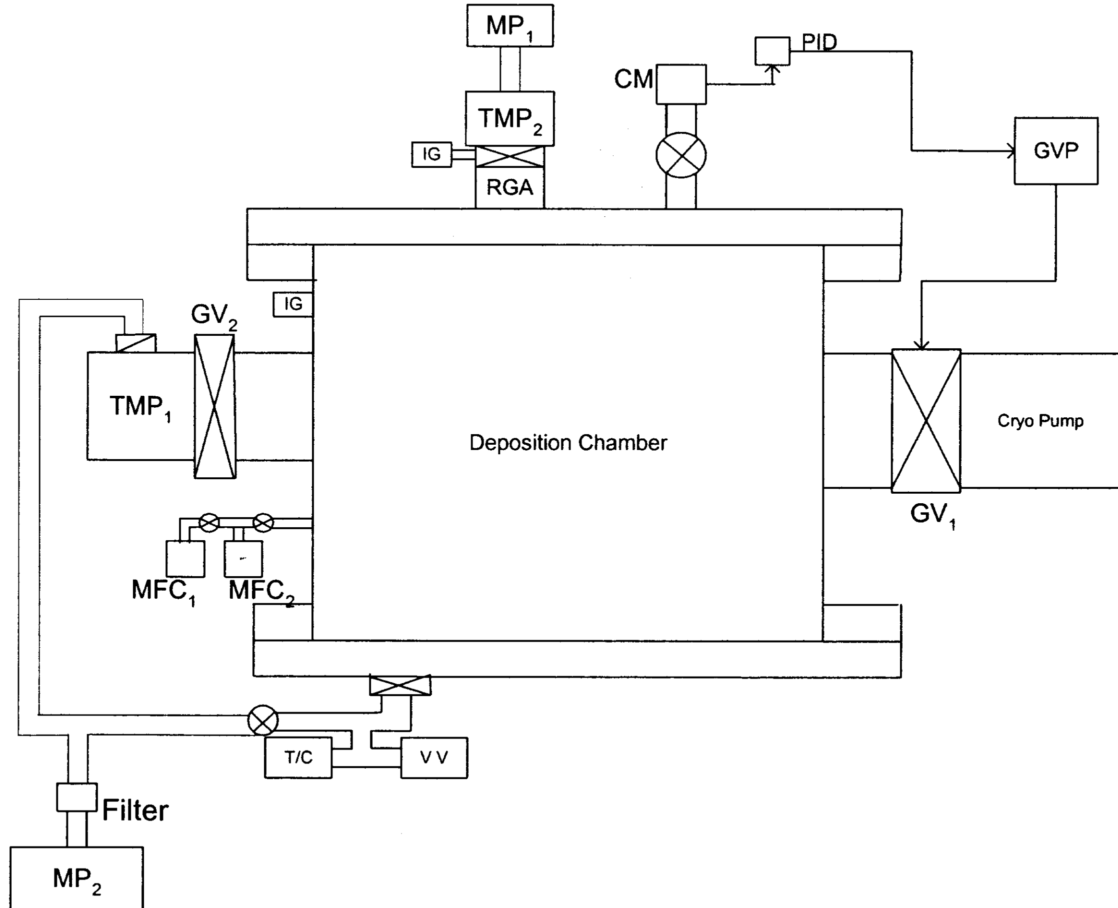

TMP-Turbo-molecular pump; CM-Capacitance manometer; RGA-Residual gas analyzer; MFC-Mass flow controller; GVP-Gate valve positioner; MP-Mechanical pump; IG-Ionization Gauge; vv- Venting valve; T/C- Thermocouple gauge

Figure 3.6 Schematic of vacuum and gas flow control of the deposition system.

3.3 Substrate Preparation

Substrate surface preparation is considered an important step in coating technology, as it is important for a good bonding, between the coating and the substrate. Substrate preparation can also influence some other characteristics of the films and coatings. In the present study, square substrates of 0.5 inch x 0.5 inch and 0.2 inch thick were machined from gun steel and 4340 steel.

The substrate surface was subjected to grinding, abrasion and polishing. The manner in which abrasives are supported on the backing material and the speed at which the particles are removed decides whether the process is grinding, abrasion or polishing. During grinding the abrasives are cemented together to a rigid block. After cutting the steel samples, initial grinding was done on 60-grit size grinding wheel at NJIT's machine shop.

Abrasion generally employs a layer of abrasive particles cemented onto a cloth or paper backing. Surface speed is another parameter that distinguishes between abrasion and grinding process. Grinding is done at high surface speeds and significant heating of the surface layers take place due to friction between the two surfaces. Unlike grinding, abrasion employs lower speeds and liquid coolant and so heating of the specimen surface is avoided. Polishing uses abrasive particles that are not firmly fixed but suspended in liquid. Metallographic preparation procedure actually has a sequence of grinding stages with increasing fineness, which is followed by the abrasion process of increasing fineness and the final step involves the polishing process of increasing fineness until the desired surface finish is achieved.

MINIMET 1000 polisher/grinder manufactured by the Buehler Company was used for steel substrates surface preparation. Being a highly automated machine it provides control of rotating speed (from 3.5 – 35 cm/s), pressure applied to the specimen (from 5-50 N) and polishing time (up to 99 minutes at a time). Adhesive backed silicon carbide abrasive papers applied to glass plate were used to grind the surface of steel surface. To grind the steel substrate, SiC abrasive paper of abrasive sizes from 240 grit to 600 grit was used sequentially. The steps of grinding steel substrates are summarized in Table 3.1.

Table 3.1 Steps Followed for Grinding Steel Substrates

Step	Abrasive, size	Lubricant	Speed (cm/s)
#1	SiC, 240 grit	DI water	17.5-24.5
#2	SiC, 320 grit	DI water	17.5-24.5
#3	SiC, 400 grit	DI water	17.5-24.5
#4	SiC, 600 grit	DI water	17.5-24.5

Polishing of the steel substrates was performed using diamond paste of descending sizes from 15 μm to 0.5 μm. An alumina suspension of size 0.05 μm was used to achieve the final scratch free steel surface. The sequence of polishing established for steel substrates are summarized in the Table 3.2. The controlled samples of silicon and silicon dioxide did not need polishing as they were cut from highly polished wafers. More details on sample preparation are reported in the thesis work of Y. Abassi [43].

Table 3.2 Sequential Steps Followed for Polishing Steel Substrates

Step	Abrasive, size	Lubricant	Speed (cm/s)
#1	Diamond, 15μm	**	21-28
#2	Diamond, 10μm	**	21-28
#3	Diamond, 6μm	**	21-28
#4	Diamond, 3μm	**	21-28
#5	Diamond, 1μm	**	21-28
#6	Diamond, 0.5μm	**	21-28
#7	Alumina-suspension, 0.05 μm	DI water	17.5-35

*** paste provided by the supplier of the abrasive*

The surface cleaning was achieved by electro cleaning followed by ultrasonic cleaning. The electro-cleaner solution used was "59 special" made by North West Company. The details of the composition of "59 special" is not known but is described as highly alkaline. This process removes the oil and grease left on the steel surface from machining operations and polishing but does not remove the metal from the sample. In this process the sample was connected to the positive terminal while the negative terminal was connected to a copper electrode. After electro-cleaning process was completed, the samples were rinsed in DI water, to remove the residual alkaline cleaner. Usually the final polishing was done after electro cleaning.

Finally, steel, Si, and SiO_2 samples were subjected to ultrasound cleaning. In ultra sonic cleaning, substrates are treated with high intensity sound waves, which generate the pressure fluctuations that produce microscopic bubbles in the liquid medium. These bubbles produce the shockwaves, which impinges on the sample surface and

removes the dirt from the surface. These cleaning processes involved three steps. During the first step the samples were ultrasonically cleaned with methanol for 10 minutes and during the second step with acetone for 5 minutes. In the final step samples were cleaned with methanol again for 10 minutes. The samples were then kept in desiccators to prevent any contamination before loading them in the chamber.

The surface oxides on the substrate can be removed by chemical or sputter etching. In the sputtering process an in-situ method of cleaning such as, sputter etching is one of the most effective methods for improving the adhesion of the growing film. Sputter etching is the name given to the process of removal of material from a surface by sputtering. In this process of cleaning, the material being cleaned is made the target (cathode) of the sputtering system. This cleaning method is also known to have negative effects on substrates, which includes re-deposition, cone formation on the surface and some surface contamination due to impacts of sputtering gas ions [44]. In this research work, the substrates holders with the substrates were sputtered etched in argon plasma. The DC voltage used for sputter etching was in the range of 300-400 V at a working pressure of 180-230 mtorr when argon was flowed into the chamber at 18 sccm. The sputter etching current density was 10-100 $\mu A/cm^2$. The sputter etching time was typically 20 minutes. To avoid re-deposition on the substrates from the mounting screws and the holders, a ceramic substrate holder was used in some cases.

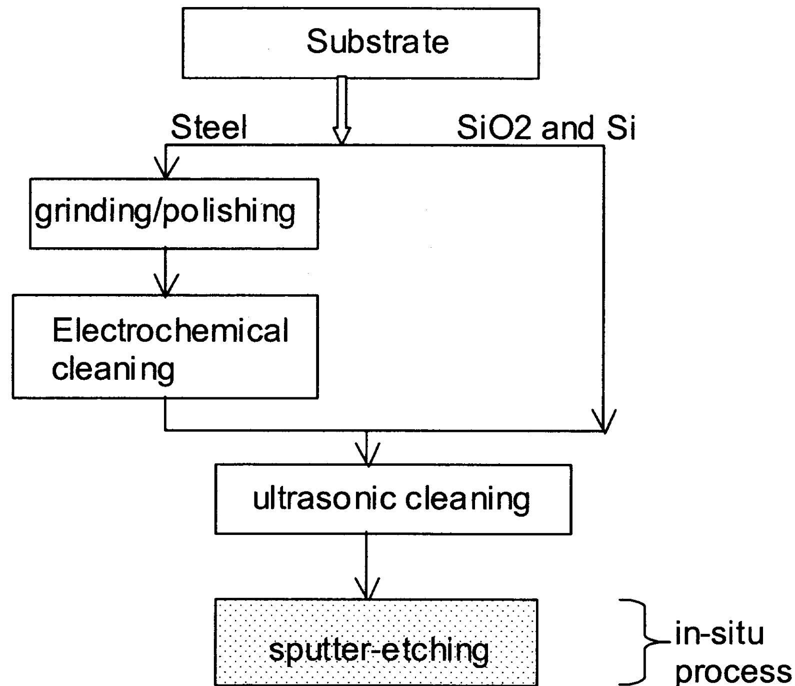

Figure 3.7 Chart summarizing the surface preparation process.

Substrates of steel and SiO_2 are mounted on steel holders and a maximum of 7 holders could be loaded for one process cycle. Figure 3.8 shows the picture of the mounted steel substrates. As seen, there are two sets of substrates one with a size of 0.8 inch x 0.8 inch and second with a size of 0.5 inch x 0.5 inch. Together with steel substrates, a control sample of SiO2 substrates was also mounted as shown in Figure 3.9. Substrates are mounted in the holders outside the chamber and then the holders are inserted into the slots in the platter. The substrate holders are insulated from the platter by ceramic tabs (Figure 3.4) so that the voltage can be supplied to them during sputter etching. The holders are grounded during sputter deposition.

Figure 3.8 Steel substrates mounted on the holder.

Figure 3.9 Steel, silicon and silicon dioxide substrates on the holder.

3.4 Deposition Parameters

A series of depositions were carried out on various substrates including steel, silicon and silicon dioxide, by changing the sputtering parameters. The magnetron source was energized by a DC power supply from Electronic Measurement Inc. (model TCR 1600S1.5) for depositions. In some experiments, which required the higher deposition current, anther DC power supply from Electronic Measurement Inc. (model TCR 600S5) was used. A maximum power of one kilowatt could be delivered to the source. During depositions typically 350 V and 0.5 A were supplied to the source during Ta deposition. A tantalum target (with 99.95% purity), of 2 inches diameter and 0.125 inches thickness was used for all depositions. The distance between target and substrate was maintained at 2 inch in most of the experiments. This distance was chosen in order to generate the conditions in the large deposition system used for gun barrel coatings. Sputtering was carried out between 1- 100 mtorr and the gas flow rates of 2-10 mtorr. Argon (99.999 %) was used as the sputtering gas and krypton (99.998 %) was also tested for few experiments. During the deposition of the nitride interfacial layer, tantalum was reactively sputtered with an argon and nitrogen (99.999 %) mixture. During experiments in which substrate heating was required, the substrate holder was heated from the back by a halogen lamp (300 W, 120 V), shown in Figure 3.4. This can increase the temperature of the substrate up to 400 °C. The procedure (Figure 3.10) that was followed for the process was:

1. Samples were prepared (as explained in previous Section 3.3) and loaded into the chamber.
2. The chamber was baked for 7-8 hours in high vacuum (300 °C measured on the substrate platter), to reduce the background gas contamination.
3. After the pre-run bake-out, the system was cooled overnight. The base pressure obtained after this run was about 8×10^{-8} torr.
4. On the following day, if the target was new it was cleaned before deposition, by sputtering for an hour with the shutter of the source closed.
5. The substrates were sputter etched in argon plasma.
6. A tantalum nitride interlayer was deposited on these sputter-etched substrates or, depending on the experiment, the substrate is heated till temperature stabilizes.
7. Ta was deposited and steps 5, 6 and 7 are repeated for each holder.

At the completion of the deposition run, the system was allowed to cool overnight before venting with nitrogen for substrate removal.

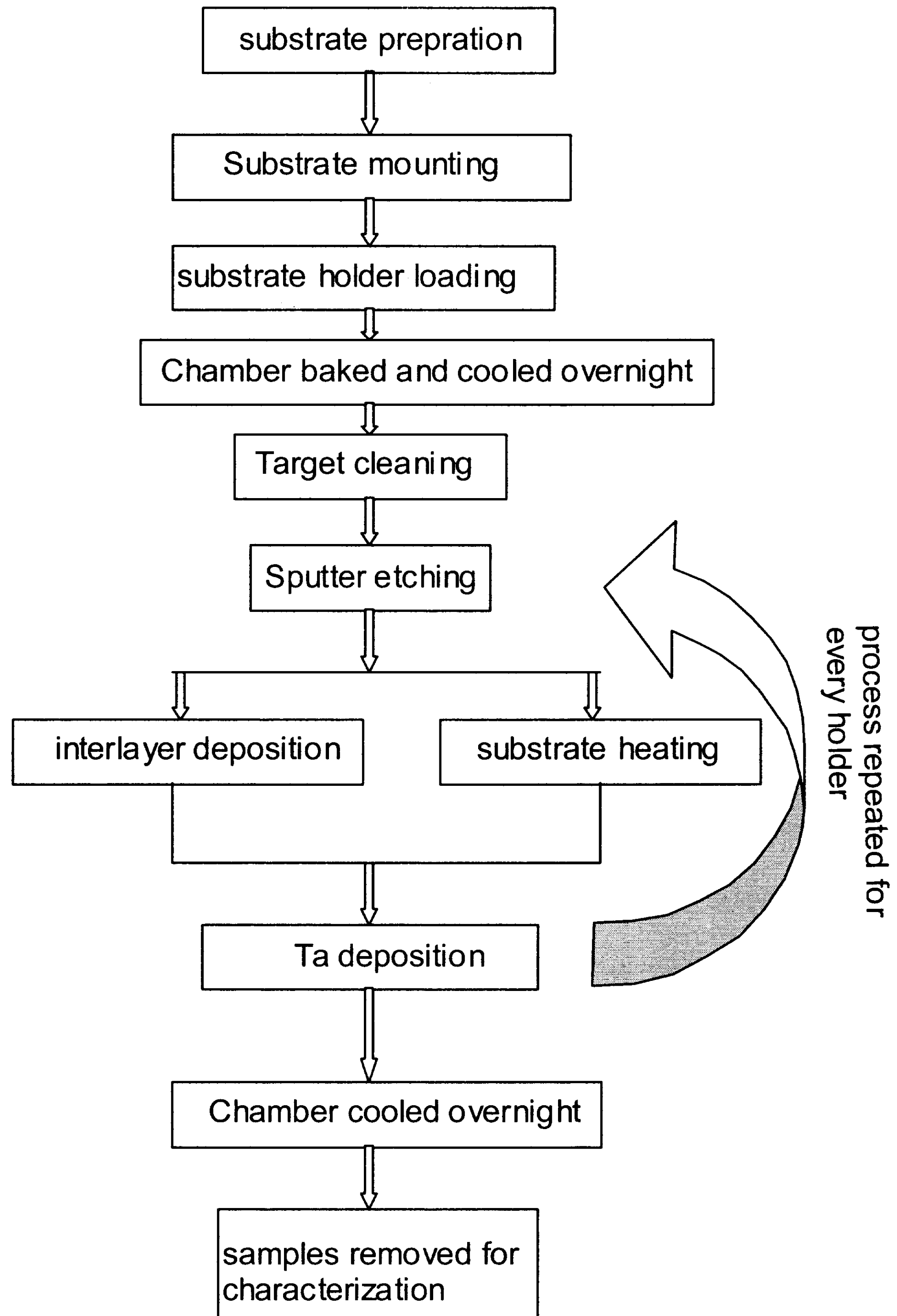

Figure 3.10 Chart summarizing steps followed during deposition process.

CHAPTER 4

CHARACTERIZATION TECHNIQUES

4.1 Surface Profilometry

Surface profilometry technique is used to determine the thickness of deposited films. In this work, masking a portion of the SiO_2 substrate, with a steel foil at an edge, created a step in the film. The step height was measured by electro-mechanically tracking the motion of mechanical stylus as it sweeps across the step. A Sloan Dektak IIA surface profilometer from Veeco Instruments Inc. at Microelectronics Research Center (NJIT) was used for all the measurements. The measurement functions and the leveling are computer controlled in this equipment. The height of the step contour trace gives the thickness of the film. The deposition rate was calculated, by dividing the total thickness of the film, by the total time of deposition.

The thickness of films and coatings was measured on the control substrate of SiO_2. Steel substrates, were masked by a holding screw but due to a shadowing effect the step was not clearly defined. Hence, the thickness was not measured on the steel substrates with this technique; rather an estimate was made from the thickness measurement results on SiO_2 substrates mounted on the same holder.

The minimum thickness, that the available profilometer could measure, was 100 nm. This limitation did not hamper the thickness measurement of Ta films and coatings but it precluded the thickness measurement of thinner (5-70 nm) interlayers. To determine the thickness of tantalum nitride interlayer, thicker (400-900 nm) films were deposited and from the deposition rate the thickness of thinner interlayer was estimated.

Thicknesses of some Ta coatings were also measured using optical microscopy, which will be discussed in Section 4.3. Figure 4.1 shows an output from the profilometer. The vertical scale is in Angstroms and the horizontal scale is in microns. As seen from the graph, the step in the profile corresponds to a Ta coating of 26.2 μm on SiO_2 substrate.

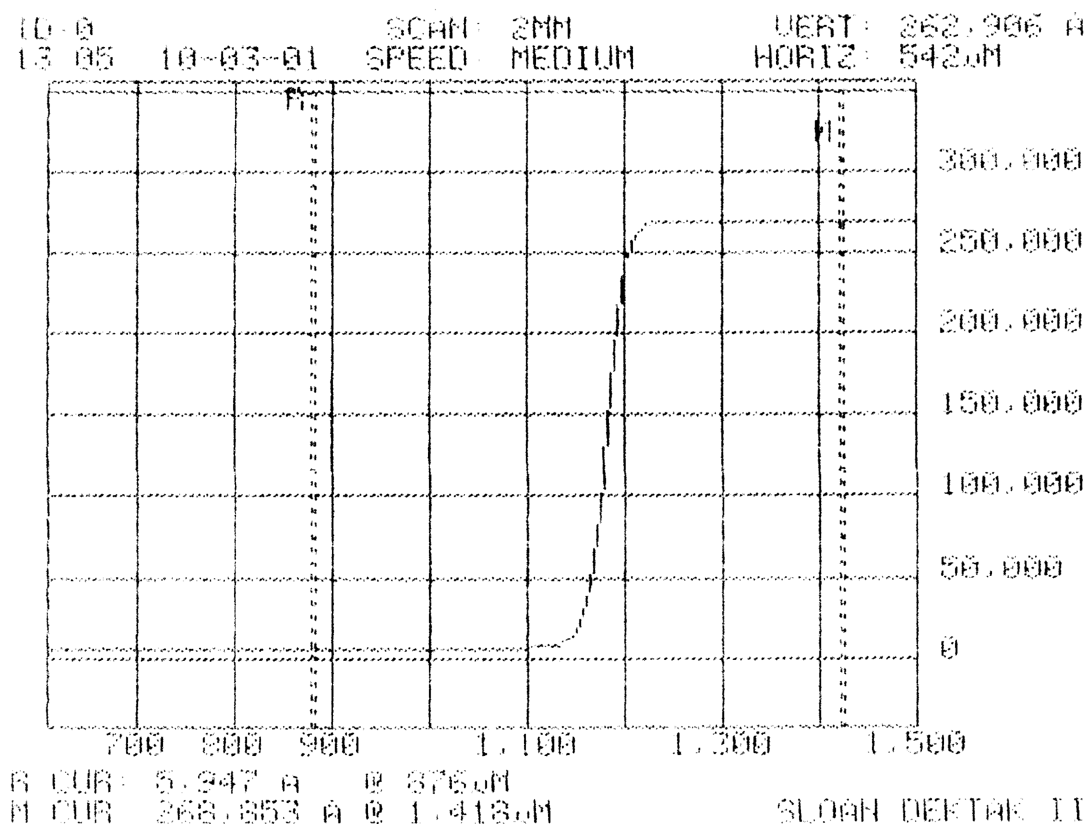

Figure 4.1 Example of an output of the Ta film thickness measured by Dektak.

4.2 Four-Point Probe Resistivity Measurements

Four-point probe measurement reveals the resistivity of the specimen under test. This method is one of the common methods used to measure the resistivity of films. Four probes are used, in which the outer two probes supply a constant current and the inner two measures the voltage drop across a portion of the sample. Probes used for resistivity

measurements are usually made of hard metals such as tungsten, and are ground to a sharp point. A current source forces current (I) through the sample, while a voltmeter measures the voltage (V), as shown in Figure 4.2.

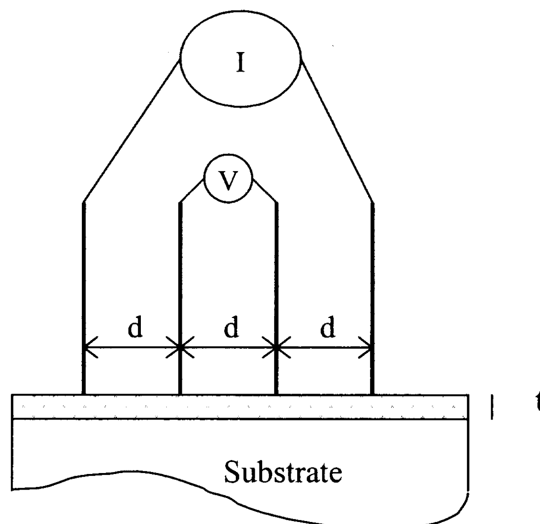

Figure 4.2 Four-point probe resistivity measurement set up.

Independent measurements of voltage and current yield the film resistivity if the film dimensions are known. Electrostatic analysis of the electric potential distribution within the film yields,

$$R_s = kV/I \tag{4.1}$$

where, R_s is the sheet resistance, k is a constant that depends on the configuration and spacing of the contacts. Multiplying the sheet resistance by the thickness of the film gives the resistivity of the film material.

4.2.1 Resistivity Measurement of Deposited Ta

The resistivity of Ta coatings and films deposited on SiO_2 substrate was measured using four-point probe at Microelectronics Research Center (NJIT). The resistivity values observed from various measurements are as follows,

- bcc Ta = 16 – 25 μΩ cm
- beta Ta = 160 – 200 μΩ cm
- Tantalum nitride interlayer = 240 – 4800 μΩ cm.

4.3 Optical Microscopy

The optical microscopy can examine the features on the sample by reflection of visible light from the surface. Optical microscope is one of the simplest tools that can be used to observe microscopic features in metallic specimen. Surface features like size of the grains, their distribution, surface defects, and distribution of phases can be revealed under the microscope, after careful surface preparation and chemical etching in some cases. An optical microscope consists essentially of three parts: 1) an illuminator, to illuminate the surface of the specimen, 2) an objective, and 3) an eyepiece, to form and enlarge the image. This microscope does-not reveal fine scale atomic details (existence of dislocations, structure of the crystal etc.), because of the limited resolving power. The smallest distance, which may be resolved, is given by,

$$\delta = \frac{0.5\lambda}{2\mu \sin\alpha} \qquad (4.1)$$

where, λ is the wavelength of the illumination. The denominator is the numerical aperture with μ the refractive index of the medium (μ=1 for air) and α the angle subtended by the maximum cone of rays entering the objective. Therefore, in an optical microscope the resolution increases with an increase in the numerical aperture. Having even the most favorable case, with α approaching 90°, the resolution cannot exceed 200 nm, as the wavelength of light is about 500 nm.

The author in this study was only interested in thickness measurement and phase distribution in Ta coatings, under optical microscope. The steel sample with thick Ta coating was cross-sectioned and after polishing, was observed under the microscope. Image was the then electronically stored through a Kodak Microscopy Documentation System (MDS 290). Figure 4.3 shows an image of cross-sectioned steel sample with thick (46 μm) Ta coating. Optical microscopy was also used for photomicrograph technique was used to reveal the difference in color and texture brought out by polishing. Beta phase being harder appears lighter and the bcc being softer appears darker under the optical microscope. Example of such image is presented in the next Chapter (# 5).

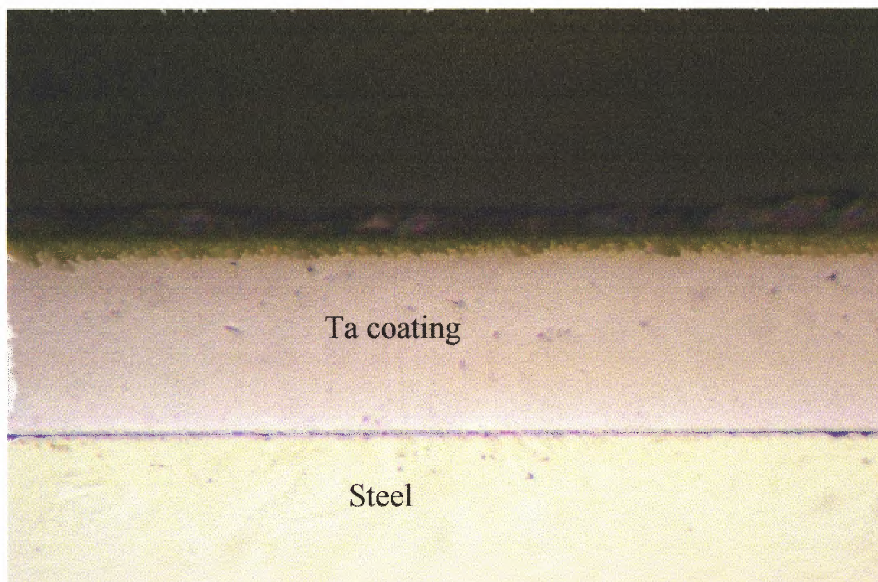

Figure 4.3 Optical micrograph of the Ta coating (~ 50 μm) deposited on steel.

4.4 Scanning Electron Microscopy

Scanning electron microscopy (SEM) is the widely used technique to characterize very small features of surfaces with a spatial resolution of a micrometer or even less resolution. The SEM provides information related to morphology, and topographical features. It is also capable of determining near surface elemental compositions of micro-volumes with the addition of an x-ray spectrometer.

A SEM consists of an electron accelerator that focuses as the electron beam from a tungsten or lanthanum hexaboride (LaB_6) cathode filament on to the specimen with the help of electromagnetic lenses. The beam is moved across an area of the specimen in a raster form. Upon impinging on the specimen, the primary electrons are scattered elastically, and some lose energy inelastically, to other atomic electrons or to the lattice. A detection system measures the intensity of electrons scattered by the specimen and is used to form the image. The schematic of the SEM setup is shown in

Figure 4.4. In SEM, insulating specimens cannot be analyzed directly, as it accumulates the absorbed electrons on the surface. Eventually, the accumulated electrons built up a charge region. This can cause to deflect the beam in an irregular manner, leading to severe image distortion. Such samples can often be coated with a thin conducting layer such as Al for subsequent examination.

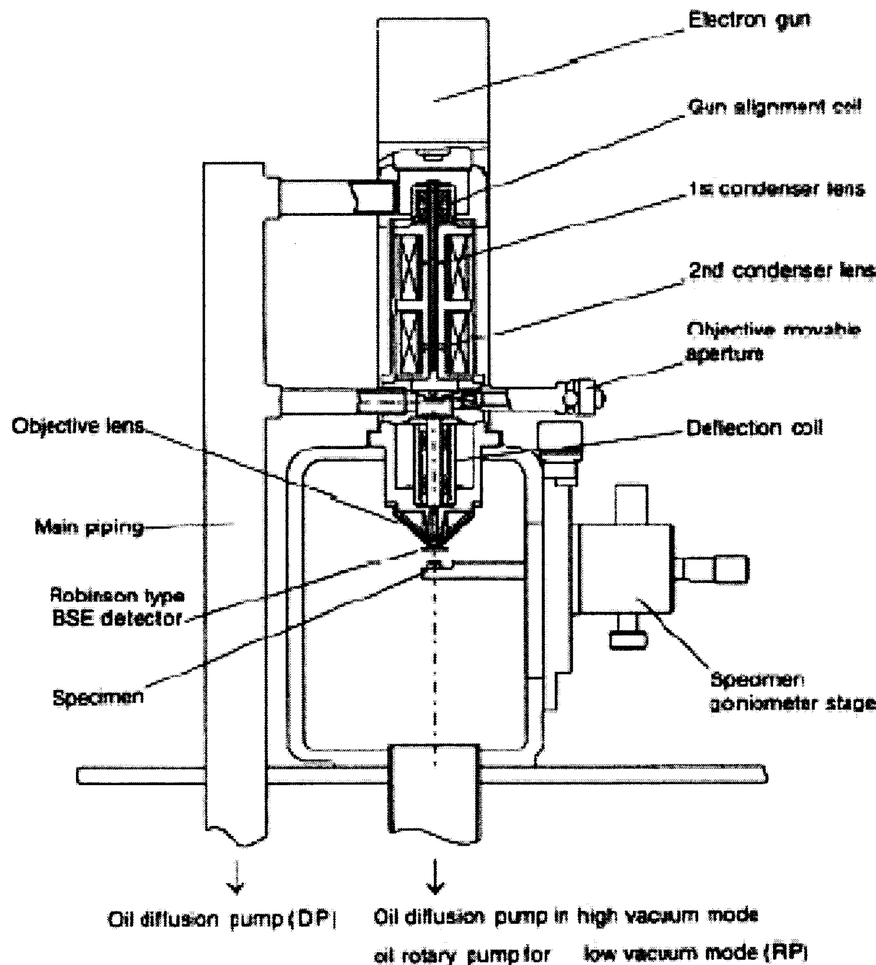

Figure 4.4 Schematic of primary components of typical SEM [45].

In this work, SEM was used to examine the surface topography of Ta and TaN films. The author used an Electroscan 2020 model, Environmental Scanning Electron Microscope (ESEM) at an accelerated voltage of 20 kV to study the surface morphology

of tantalum films deposited on steel and SiO_2 substrates. Water at a vapor pressure of 5 torr is used in the chamber as a conducting medium. Initial Ta film deposited on steel was found to be flaky and non-continuous as shown in Figure 4.5. Later, to improve the quality of the film, a proper cleaning procedure and baking was developed, which is described in Sections 3.3 and 3.4.

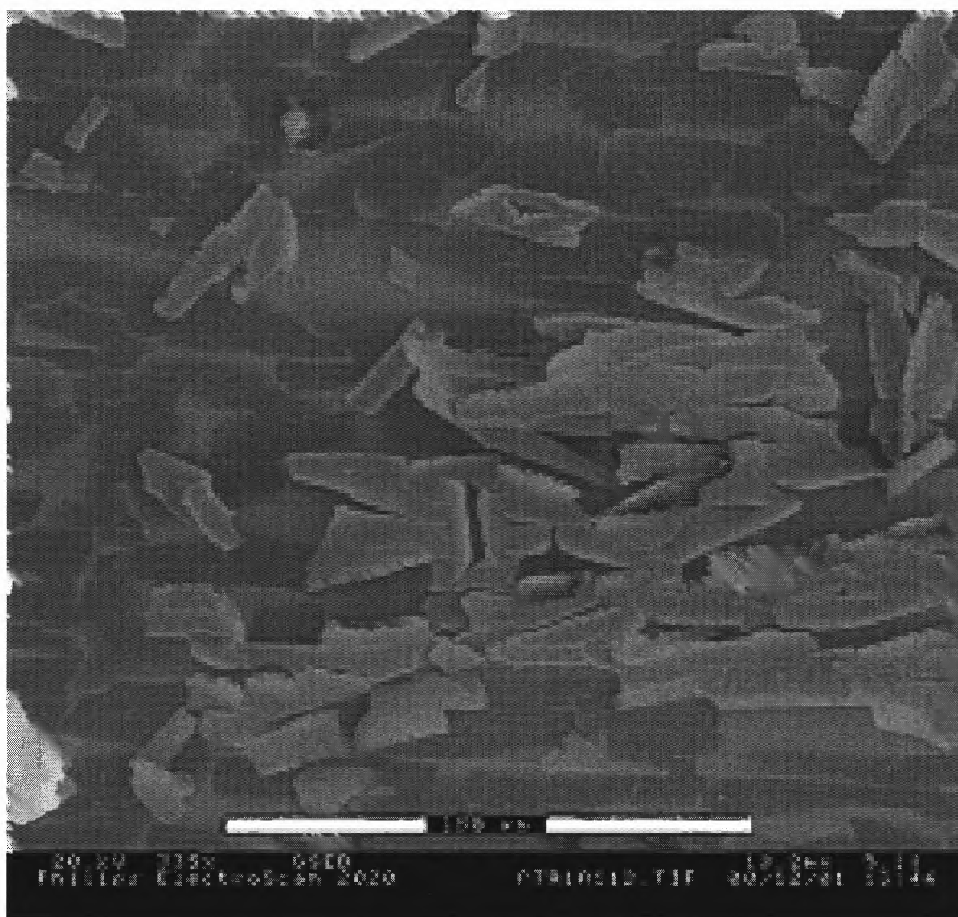

Figure 4.5 Example of scanning electron micrograph of the Ta film deposited on steel during preliminary experiments.

4.5 Atomic Force Microscopy

Atomic force microscopy (AFM) is one of characterization techniques commonly used for surface study. This technique is very attractive for surface imaging of various materials. It's a type of scanning probe microscopy (SPM). A schematic of generalized SPM is shown in Figure 4.6.

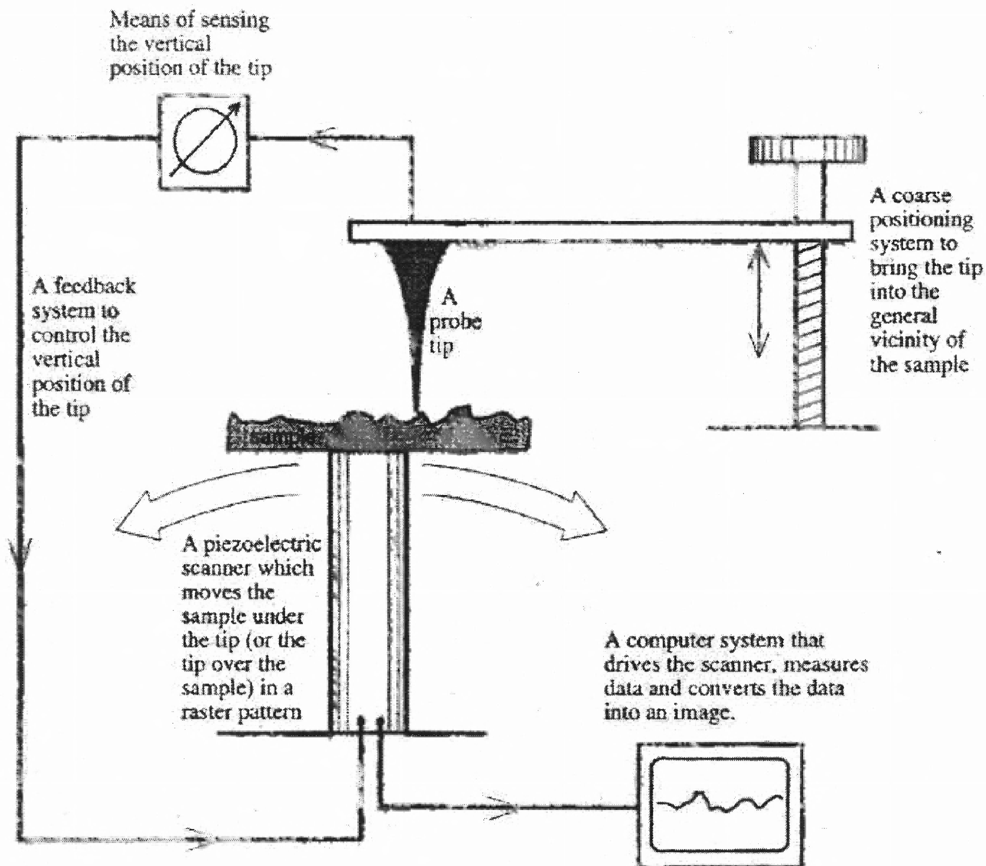

Figure 4.6 Schematic of a generalized scanning probe microscopy [46].

4.5.1 Principle of Atomic Force Microscopy

AFM measurement involves scanning of a sample surface with a sharp tip. The tip mounted on the end of a flexible cantilever is a few microns long and less than 10 nm in diameter. Forces between the tip and the sample surface cause the cantilever to bend, or

deflect. A detector measures the cantilever deflection as the tip is scanned over the sample, or the sample is scanned under the tip. The measured cantilever deflections allow a computer to generate a map of surface topography. Several forces typically contribute to the deflection of an AFM cantilever. The force most commonly associated with AFM is an inter-atomic force called the Van der Waals force. AFM can be operated in mainly two modes: 1) Contact mode and 2) Tapping mode. In the contact regime, the tip is held less than a few angstroms from the sample surface, and the inter-atomic force between the tip and the sample is repulsive. In the non-contact regime, the tip is held on the order of tens to hundreds of angstroms from the sample surface, and the inter-atomic force between the tip and sample is attractive (largely a result of the long-range Van der Waals interactions). Discussion will be limited to the tapping mode, as it was the only mode used for this study. A schematic arrangement of major components for tapping mode operation of AFM could be seen in Figure 4.7.

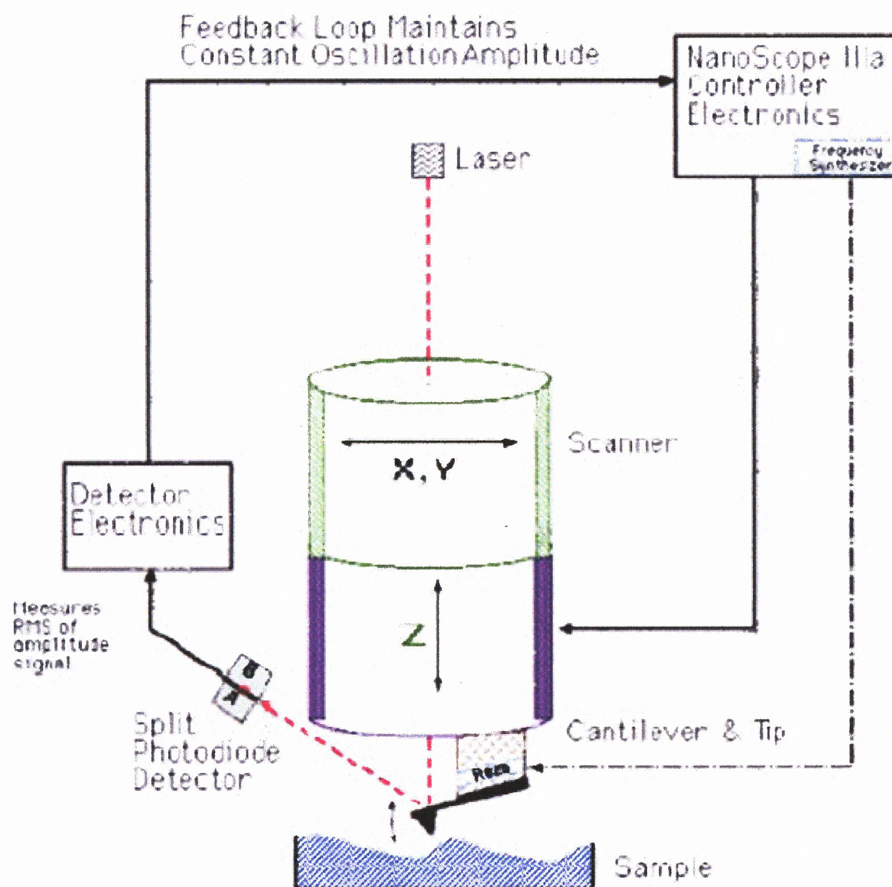

Figure 4.7 Schematic arrangements of AFM showing the feedback loop for tapping mode operation [46].

Tapping mode AFM operates by scanning a tip attached to the end of an oscillating cantilever across the sample. The cantilever is oscillating at or near its resonant frequency with amplitude ranging typically from 20 nm to 100 nm. The frequency of oscillation can be at or on either side of the resonant frequency. The tip lightly "taps" on the sample surface during scanning, contacting the surface at the bottom of the swing. The feedback loop maintains constant oscillation amplitude by adjusting the distance between the tip and the sample and maintains a constant RMS of the oscillation signal acquired by the split photodiode detector. The laser deflection detects the root-mean-square amplitude of the cantilever oscillation. Recording the vertical movement of

the cantilever at every x, y data point, forms the topographical image. The main advantage of the tapping mode over the contact mode is that lateral, shear forces are eliminated, which are present in the contact mode. This enables tapping mode to probe soft, fragile samples without damaging their surfaces.

4.5.2 Equipment

In this research, AFM instrument used was a Nano-Scope IIIa manufactured by Digital Instruments and was available at York Center of NJIT. This Nano-Scope is capable of scanning up to 152 μm x 152 μm horizontal areas and 5 μm vertical distances. The instrument was used to study the surface morphology of tantalum nitride interlayers deposited on SiO_2 substrates with various nitrogen flows. Example of a two dimensional image from AFM is shown in Figure 4.8. Three-dimensional images from this characterization technique are discussed in Chapter 5.

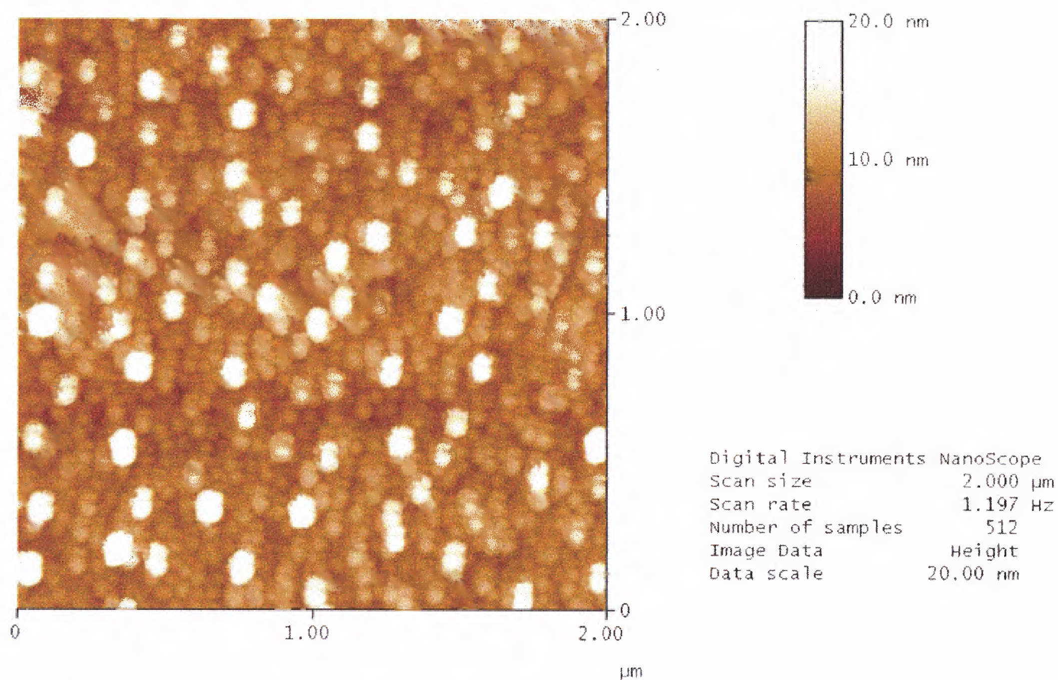

Figure 4.8 Atomic force micrograph of a tantalum nitride film on a silicon dioxide substrate deposited by the reactive sputtering of Ta in argon and nitrogen plasma.

4.6 X-ray Diffraction

The principle of diffraction is used in this technique to determine lattice constants, identification of crystalline materials, orientation of single crystals, preferred orientation of polycrystals etc. A diffraction beam may be defined as a beam composed of a large number of scattered rays mutually reinforcing one another [45]. Diffraction is therefore, a scattering phenomenon that involves interaction between ordered arrays of atoms lattice and x-rays. An x-ray diffraction pattern follows a basic principle of Bragg's law,

$$n\lambda = 2d \sin\theta \tag{4.2}$$

where, λ is the wavelength of the x-ray beam, d is the distance between each set of atomic planes of crystal lattice, θ is the angle of diffraction and n represents the order of diffraction. Figure 4.9 shows the reflection of X-ray beam from the planes of a specimen.

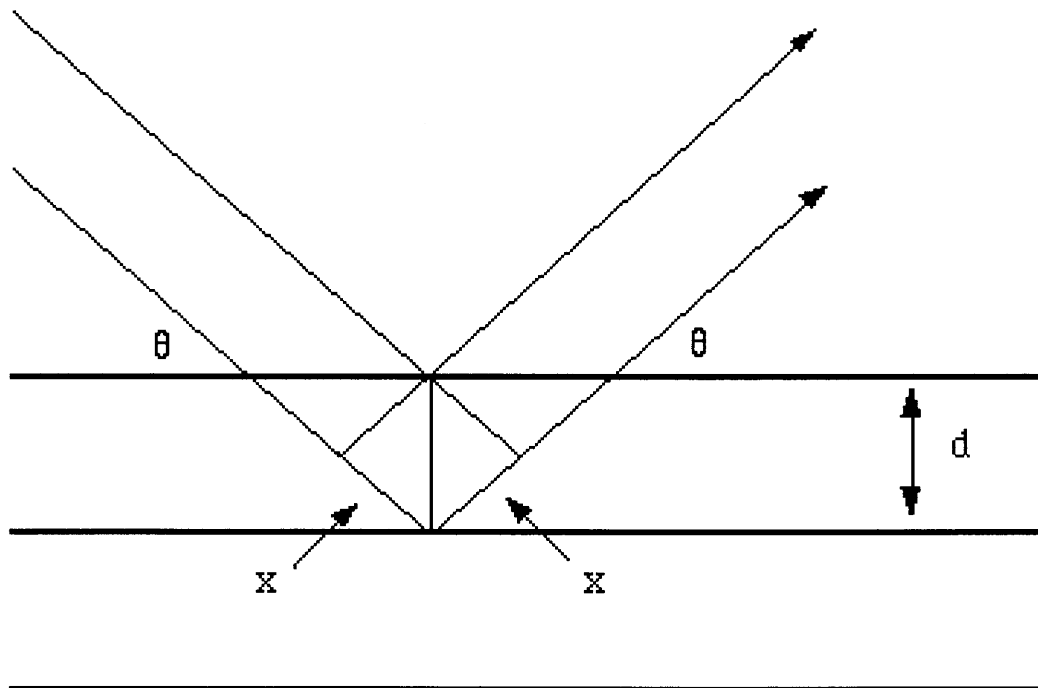

Figure 4.9 Reflection of x-rays from two planes.

X-ray diffraction is useful for studying crystals because the wavelength used is close to the spacing of atomic planes in a crystal. The X-ray diffraction instrument consists of: 1) a source of radiation (consisting of an X-ray tube and a high-voltage generator), 2) a detector, and 3) a diffractometer. A schematic of a XRD setup is shown in Figure 4.10. The inter-planar distances depend solely on the dimension of the crystal's unit cell, whereas the intensities of the diffracted rays are a function of the placement of the atoms in the unit cell. An unknown crystalline material can be identified by comparing intensities of its pattern to the patterns in powder diffraction reference files, compiled by the joint committee on powder diffraction standards (JCPDS). Advantages of XRD are that it is non-destructive and does not require any sample preparation or removal of the film from the substrate. The X-ray diffraction method has limitations for studying very thin films of light elements due to the fact that the great penetrating power of X-ray means that with typical incident angles, their path length through such films is too short to produce diffraction beams of sufficient intensity. Under such conditions the substrate, rather than the film, dominates the scattered X-ray signal. This limitation was only of concern in the case of very thin TaN film studied in this work.

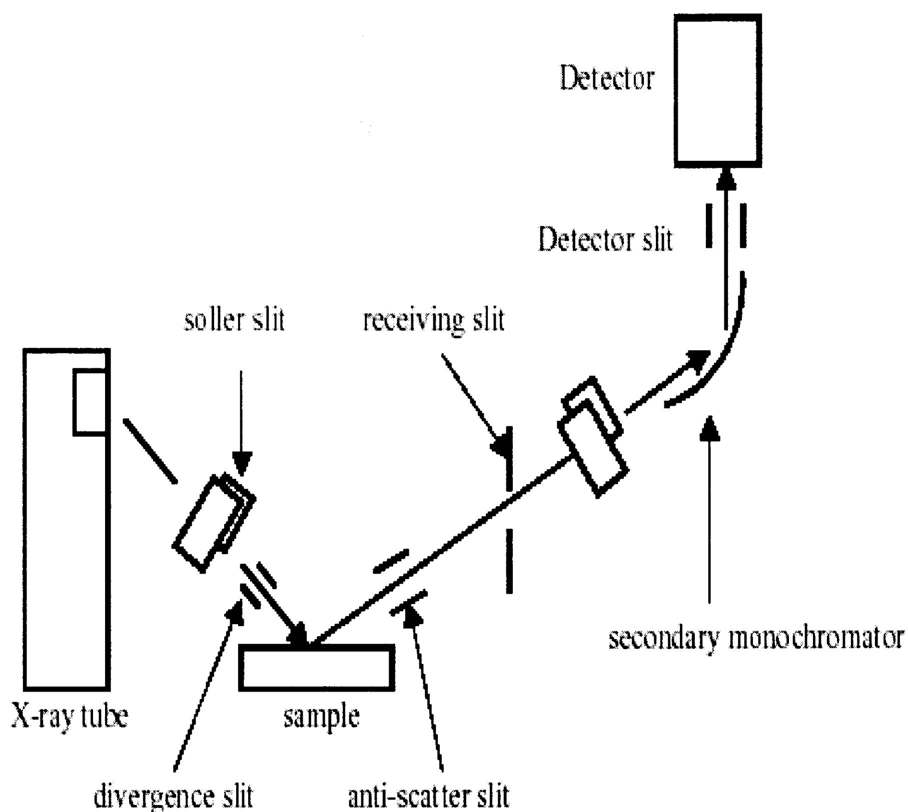

Figure 4.10 Schematic showing the typical XRD set up [45].

XRD measurements of the Ta and tantalum nitride films deposited on steel and control sample of SiO_2, was done using a Philips X'Pert MPD instrument with Cu Kα radiation. Measured spectra were compared with the standard powder spectra for bcc Ta [47] and beta Ta [48] as shown in Figures 4.11 and 4.12 respectively. Typical XRD spectra for films of bcc and beta Ta are shown in Figures 4.13 and 4.14 respectively.

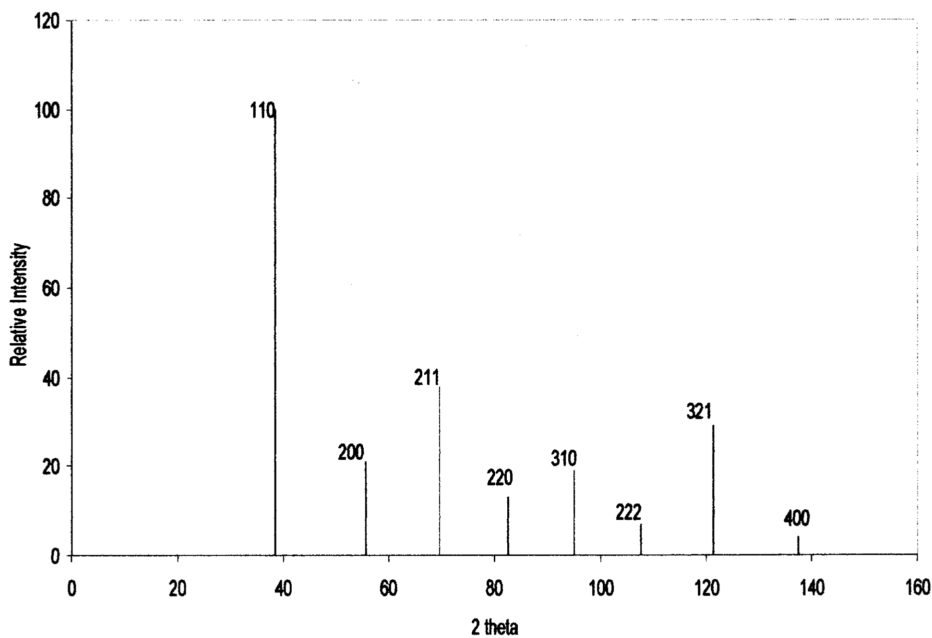

Figure 4.11 The standard powder diffraction spectra for bcc Ta [47].

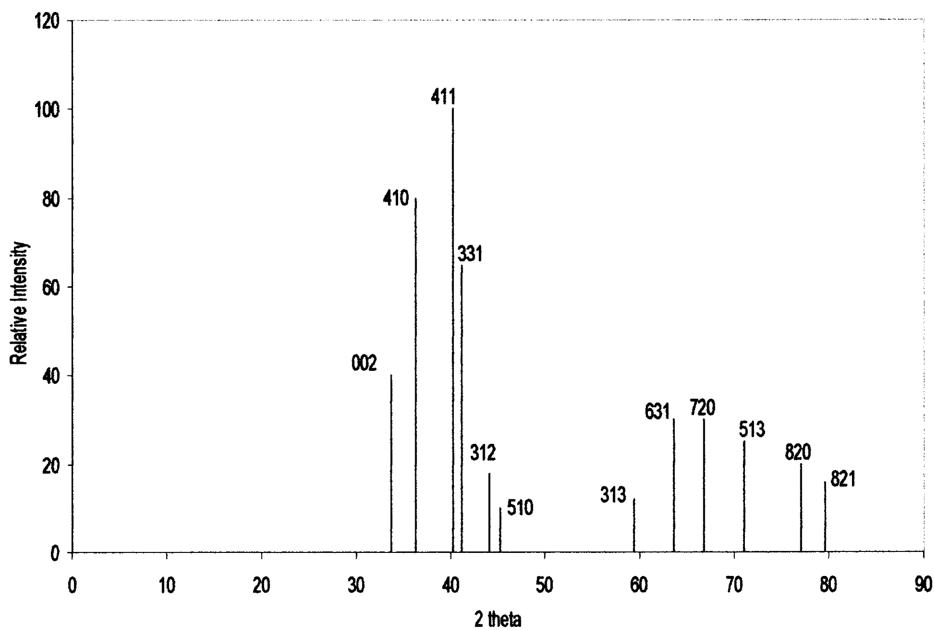

Figure 4.12 The standard powder diffraction pattern of beta Ta [48]

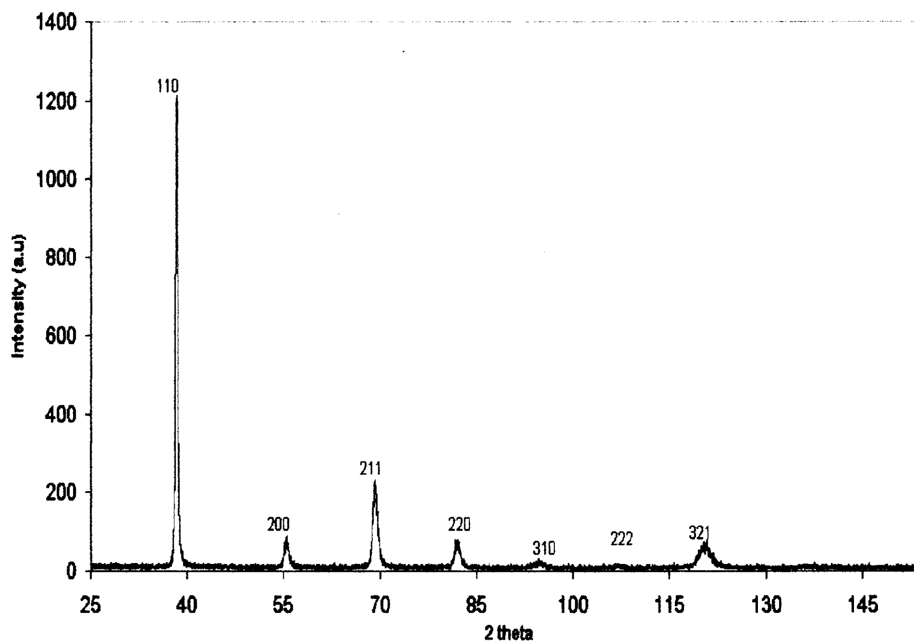

Figure 4.13 XRD spectrum of bcc Ta deposited at room temperature on steel substrate with tantalum nitride interlayer.

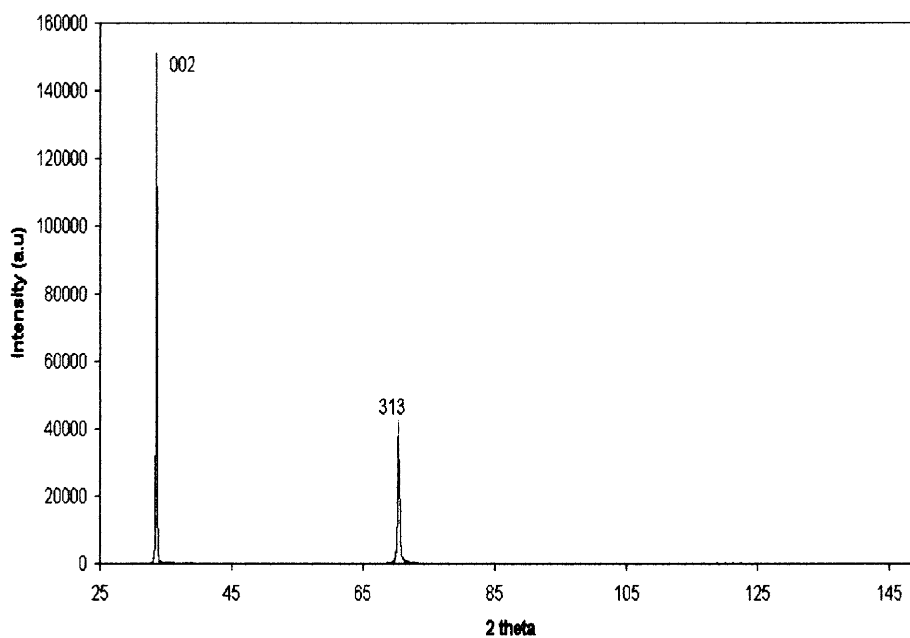

Figure 4.14 XRD spectrum of beta Ta deposited directly on steel substrate at room temperature.

4.7 Nuclear Reaction Analysis

Many isotopes of chemical elements can be detected using resonant nuclear reactions. When accelerated particles such as protons, deuterons or other light element ions interact with the target atom nuclei, gamma rays and secondary particles can be emitted. If the so called, coulomb barrier is overcome allowing the nuclei to form a compound nucleus and de-excite with the emission of gamma rays or emerging particles. Resonant reactions occur only if the incoming particles have the specific resonance energy for the two nuclei to interact. Nuclear reaction analysis (NRA) is a non-destructive method that can be used to analyze the concentration and depth distribution of specific light element isotopes in thin films. When a beam of charged particles produced in an accelerator, with energy from few hundred keV to several MeV, hits the low atomic number (Z) nuclei in the sample, nuclear reactions may be induced. When products of these reactions are detected, the spectrum of particle yield vs. incident energy can be obtained. In many cases of $(p,\alpha\gamma)$ reactions α particles have energies that are low for effective detection and the associated γ rays are detected instead.

Two important parameters in NRA are reaction's Q value and the cross sections. Q value is the energy released in a specific nuclear reaction, which determines the energy of particles resulting from the reaction. Reactions with high (positive) Q values are most suitable for NRA. The cross section relates to the rate at which particles are removed from the beam by a particular reaction. The cross section of a reaction is measured as a function of incident ion energy and detector angle with respect to incident beam. Secondary particle or gamma rays yields are directly proportional to the reaction cross section hence this information allows an experimenter to select the incident beam energy

and beam detector angle to maximize sensitivity. NRA complements other accelerator based ion beam techniques like Rutherford back scattering (RBS), which is less sensitive for light element detection. When a layer of a light element film is deposited on a heavy substrate, then the RBS spectrum of light element is superimposed on top of the spectrum of heavy element, or in other words, the light element signal is seen against a huge background thereby limiting its sensitivity. For NRA there is no natural background from high Z component because to interact with high Z nuclei the particles require high energies.

The NRA method was used to detect the nitrogen content of the interlayer of tantalum nitride on steel. The reaction on which these measurements were based is as follows:

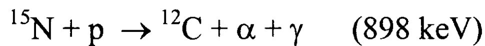

$$^{15}N + p \rightarrow {}^{12}C + \alpha + \gamma \quad (898\ \text{keV})$$

The Q value for the above reaction is 4.964 MeV [49] with a resonant energy of 898 keV. The proton with the resonance energy interacts with nitrogen on the surface of the sample and the gamma rays are emitted. To detect the nitrogen below the surface of the sample, the beam energy is increased to compensate for slowing down of protons in the sample. For calculating the content of nitrogen in a given sample, the detected gamma yield is compared to the yield measured on a standard reference sample, (e.g. TiN) containing a known fraction of nitrogen. The difference in the stopping cross sections in these two different media is also taken into account. The depth x at which a bombarding particle with an initial energy E_b will slow down to an energy E, is given by:

$$x = \int_{E}^{E_b} dE / S(E)$$

S(E) is the stopping power (dE/dx) of the sample [50].

The program SRIM (The Stopping and Range of Ions in Matter), developed by James Ziegler at IBM was used for calculating the stopping and range of ions into matter. The Monte Carlo program TRIM (the Transport of Ions in Matter) is the most comprehensive program included in SRIM [51]. The projected range, defined as the mean depth from the target surface at which the ion comes to a halt, can also be calculated using SRIM. Knowing the projected range as a function of energy, the depth corresponding to a resonance reaction occurring can be calculated. Figure 4.15 shows the resonance depth as a function of beam energy for different percentages of Ta in tantalum nitride films.

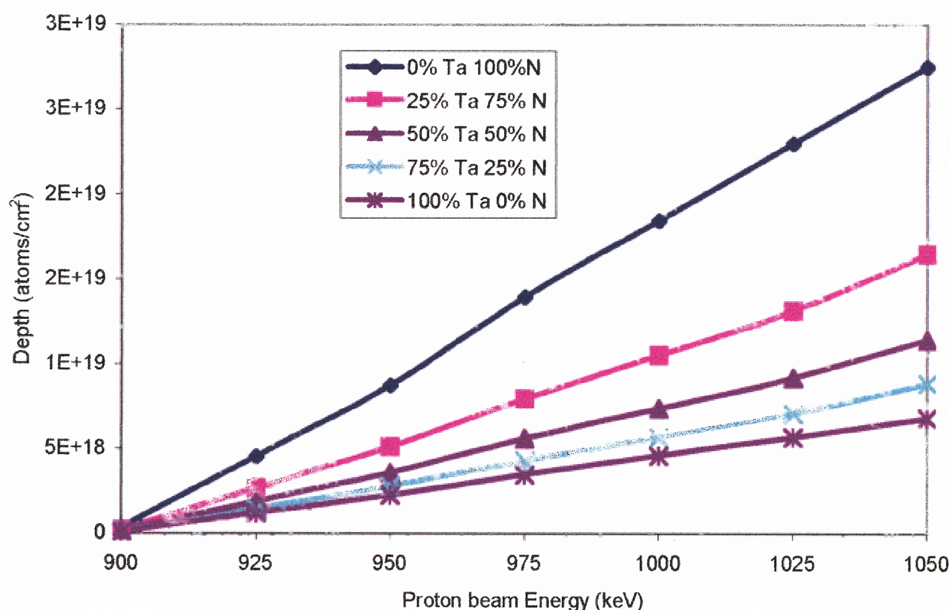

Figure 4.15 Incident beam energy vs. depth of the resonance reaction $^{15}N(p,\alpha\gamma)^{12}C$ (at 898 keV), in Ta-N target, of different composition.

As seen in Figure 4.15, a film containing more nitrogen has a lower stopping power for the protons and so the resonance reaction for proton with a given energy will occur deeper in the sample, as compared to the tantalum nitride film containing less nitrogen.

The gamma yield vs. bombarded energy curve can be converted to a concentration vs. depth plot. The principle of nitrogen depth profiling on the surface and inside the sample is shown in Figure 4.16.

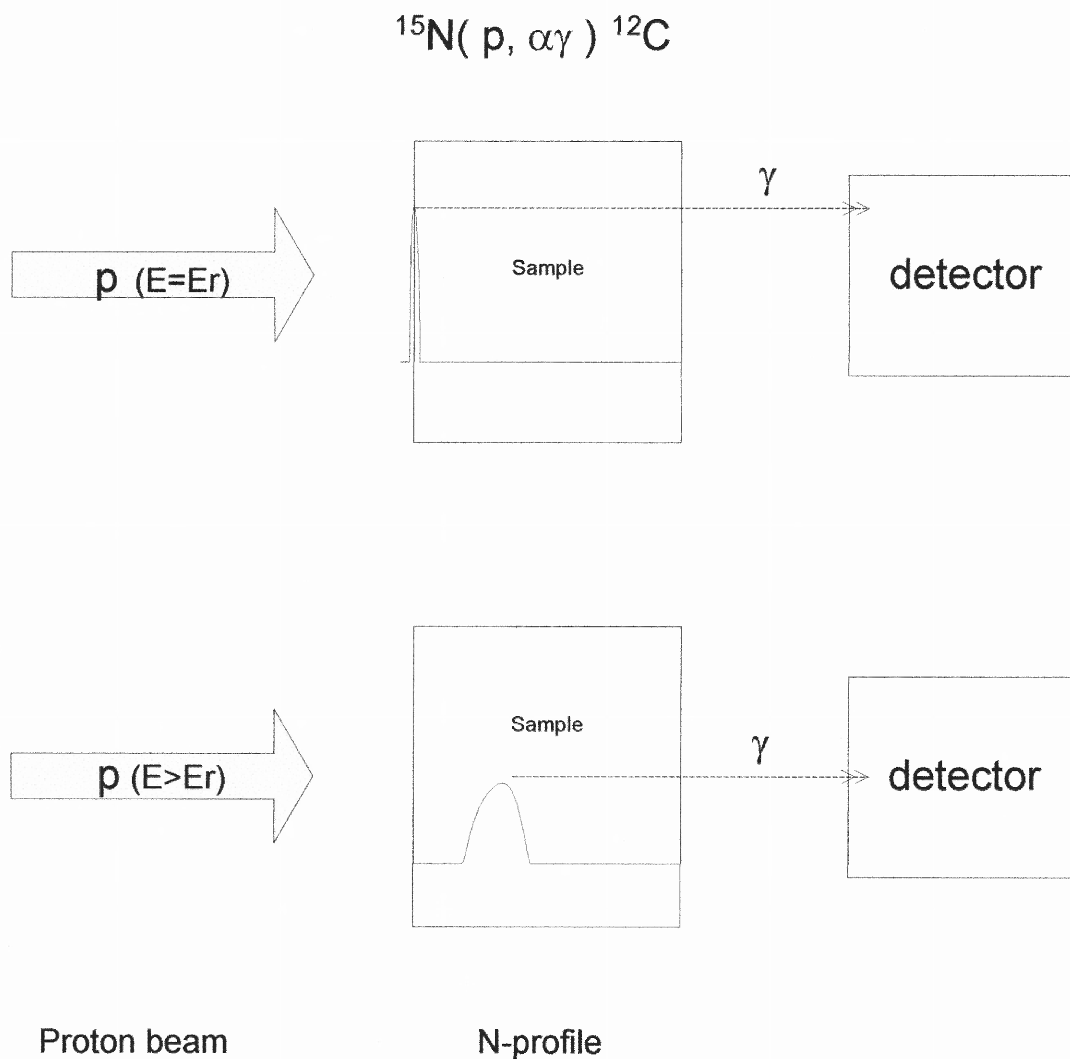

Figure 4.16 Principle of depth profile analysis using the resonance reaction $^{15}N(p,\alpha\gamma)^{12}C$.

As the beam of proton penetrates the film surface, the slowing down is accompanied by a spreading of their energy, which is called energy straggling. This is due to the statistical fluctuations in the number of collisions along the trajectory of the incident particles inside the sample. If the straggle is appreciable it will somewhat degrade the resolution of the depth profile (of nitrogen concentration) measurements.

Using the TRIM code, the energy straggling of protons passing through 1 μm films of in the stoichiometric TaN (density: 8.813 gms/cm^3) was calculated as 6.29 ± 0.04 keV for an incident proton energy range of 900-1050 keV. It was also found from the TRIM code that the energy loss occurs mainly through interactions with electrons. Energy straggle increases with the atomic number of the target element, as this number is equal to the number of electrons in an atom. In Figure 4.17 it is shown that the straggle increases with the increase in the tantalum content of tantalum nitride film as the Ta atom (Z=73) is heavier compared to nitrogen atom (Z=7). The figure also shows that energy straggle is essentially the same for two incident beam energies of 900 and 1000keV.

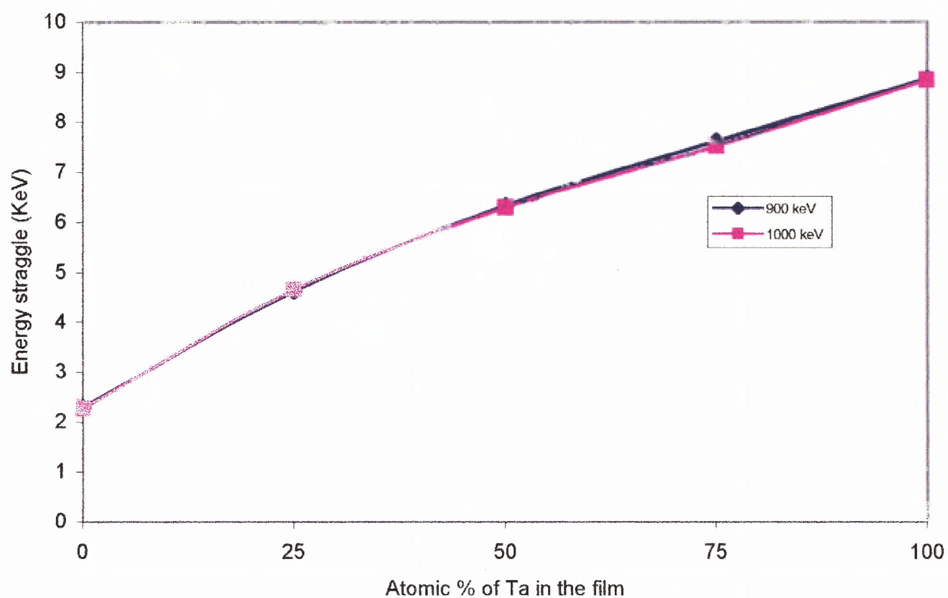

Figure 4.17 Energy straggle vs. percentage of tantalum in 1 μm thick Ta-N film calculated by TRIM code for the proton beam energies of 900 and 1000 keV.

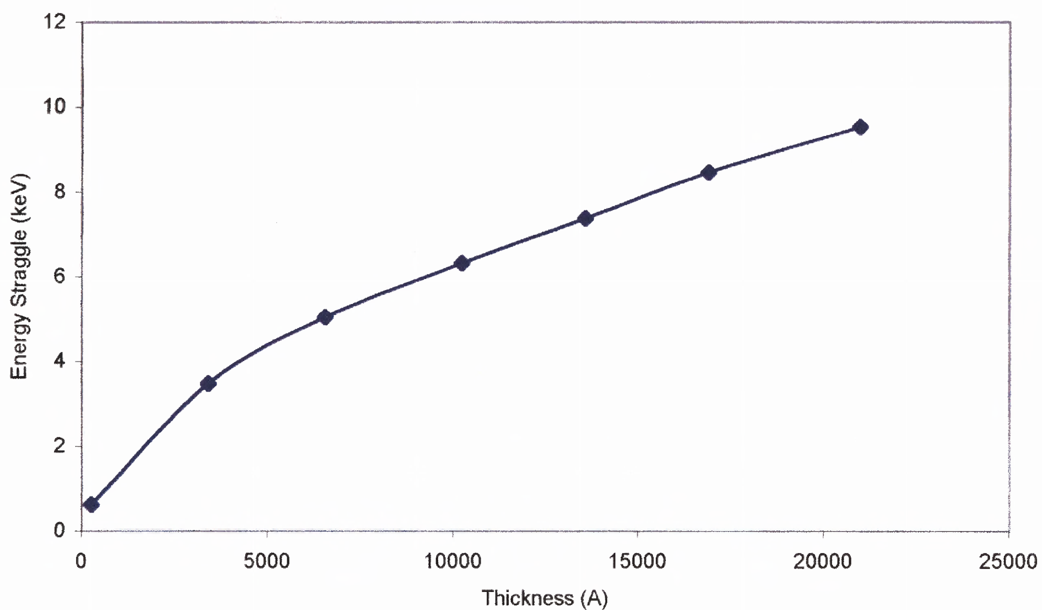

Figure 4.18 Energy straggle as a function of depth at which the resonance reaction occurs (E_r = 898 keV) for a range of proton energies of 900-1050 keV, in a TaN sample calculated using TRIM code.

Figure 4.18 shows the proton energy straggle calculated (using TRIM code) as a function of depth at which the resonance reaction (E_r = 898 keV) occurs, in TaN sample with the estimated film density of 8.813 gm/cm^3 or 5.448E +22 atoms/cm^3. Each point in the graph corresponds to, a different incident beam energy. It's clear from Figure 4.18 that energy straggle increases with the increase in the depth at which the resonance reaction occurs. The energy straggle exceeds the ion beam energy spread of 2 keV at the depth of approximately 170 nm and beyond this depth determines the resolution of the experiment.

4.8 Adhesion Test

Protective coating needs not only to be continuous and defect free but also needs to be strongly adhering to the substrate it intends to protect. One of the primitive ways to measure adhesion is to apply an adhesive tape to the surface of the coating and to subsequently examine the result of stripping. Those, which are weakly bond to the substrate comes off easily, while those, which are strongly bonded will remain on the substrate. However, the above method is highly qualitative and gives no indication of the relative magnitudes of adhesive forces.

A specific test, namely the scratch test was used in this study to determine the adhesion of the coating with the substrate. In this test, a critical load characterizes the mechanical resistance of the coating, which is the minimum load at which damage by separation of the coating from the substrate can be observed. More specifically tipped stylus with a given load or a gradually increasing load is drawn across the sample under test. A commercially available scratch tester, Revetest Automatic Scratch Tester with a Rockwell C diamond tip (conical angle, 120°; hemispherical tip of radius 200 μm) was

used for these studies. The applied load could either be kept constant or linearly increased while scratching. The tester was equipped with an integrated optical microscope, an acoustic emission detection system and a device to measure the tangential frictional force, giving the friction coefficient value during scratching. The critical load for a coating substrate system can be determined by optical, acoustical or mechanical methods. When a series of similar samples have to be tested for the critical load measurement, the acoustic emission and frictional force are used. These two do not replace the optical observation, which in turn gives the useful indications on the nature of the failures. In most cases, the three methods provide complementary information.

Some samples were subjected to a groove adhesion testing performed at Benet Laboratories. The test used is a modification of a standard groove test for soft coatings. The modification induces a plowing of coating rather than cutting. One major advantage is that when poor adhesion is present, the coating tends to fully delaminate. This gives ease of examination of the substrate.

CHAPTER 5

RESULTS

The research was aimed to produce a high quality, bcc Ta coatings on steel substrate by sputtering. Two methods of deposition of bcc Ta were successful:

1. Deposition of Ta at room temperature, on a seed layer (interlayer) of tantalum nitride formed by reactive sputtering of Ta in Ar and N_2 gases.
2. Deposition of Ta on heated steel substrate.

This chapter presents the results obtained by these two methods. Results obtained on Ta deposited on a seed layer of tantalum nitride are presented in Section 5.1. The result of the study of structure and morphology of tantalum nitride seed layer promoting the bcc phase of Ta are presented in Section 5.2, while Section 5.3 describes, the results of Ta deposition on heated steel substrates. Adhesion of coatings obtained by both methods was investigated and the results are presented in Section 5.4.

5.1 Tantalum Deposited on Tantalum Nitride Seed layer

In this part of the research, the influence of a tantalum nitride seed layer on the structure of Ta sputter deposited on steel was investigated. A seed layer of tantalum nitride was reactively sputtered in a nitrogen and argon gas mixture, followed by Ta deposition in argon. An example of the influence of this tantalum nitride interlayer on the crystallographic phase of Ta coatings is shown in Figure 5.1. All the peaks in the XRD spectrum of Ta deposited on steel without the interlayer, correspond to the Ta beta phase while all the peaks in the spectrum of Ta deposited with the tantalum nitride interlayer represent bcc structure. Details of the deposition parameters for these samples are given

in the appendix. In the XRD spectra of some Ta films deposited on steel without the seed layer, the peaks corresponding to both phases (mixed phase) were observed.

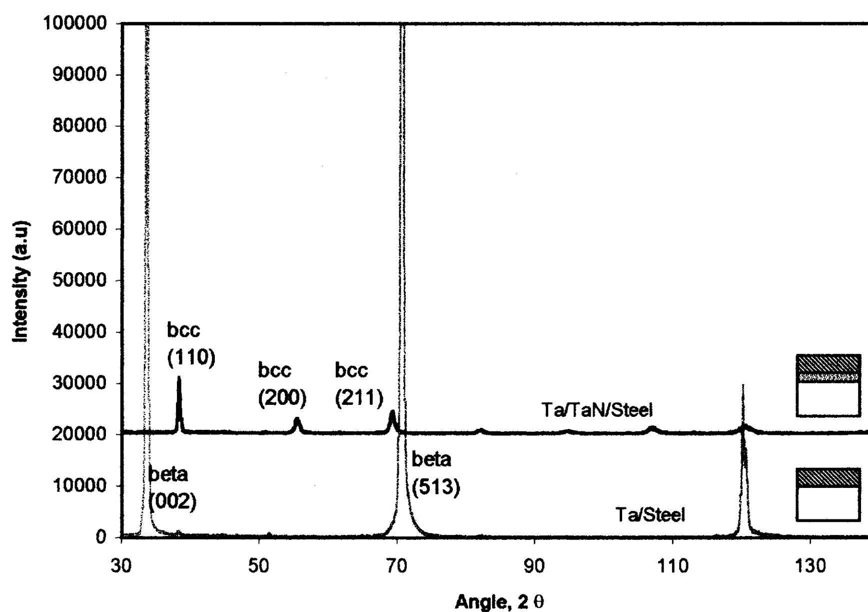

Figure 5.1 XRD spectra of Ta coatings deposited on steel substrates with and without the tantalum nitride interlayer.

Resistivity measurements were also performed on tantalum films and coatings deposited on the control substrates of SiO_2 with tantalum nitride seed layer. Ta deposited without an interlayer exhibit a resistivity of 160-200 μΩcm, which corresponds to literature values of tetragonal beta phase Ta. The resistivity of Ta films deposited with the tantalum nitride interlayer was measured as 20-25 μΩcm indicative of the bcc phase. This is further evidence that a tantalum nitride interlayer promotes the growth of bcc phase of Ta.

It was assumed that the thinnest possible interlayer is desired to minimize its effect on the Ta coating integrity. To find the minimum thickness of the interlayer required to produce a pure bcc phase of Ta, a wide range of interlayer thickness (4 nm to

3 μm) was investigated and the influence of interlayer thickness on the phase of deposited Ta was studied. This seed layer thickness was reduced sequentially from the maximum of 3 μm and the phase composition of subsequently deposited Ta films was measured by XRD. Results from this study are given in Table 5.1.

Table 5.1 Tantalum Phase Dependence on the Thickness of Tantalum Nitride Seed Layer on Steel.

Sample No.	Nitrogen concentration*	Seed layer thickness (nm)	Phase of Ta	Crystallographic orientation**
021902Ta06a_2	10%	120	bcc	110,211
042402Ta05a_1	10%	60	bcc	110,211,310
041502Ta04a_1	10%	40	bcc	110,220
022502Ta01a	10%	30	bcc	110,211,310
022502Ta02a	10%	20	bcc	110,211,220
082102Ta04a	12%	20	bcc	110,211,220
082102Ta04a	12%	20	bcc	110,211,220
080702Ta03a	14%	20	bcc	110,220
080702Ta04a	18%	20	bcc	110,211
072302Ta06a	21%	20	bcc	110,211,220
022502Ta03a	10%	10	bcc + β	bcc(110,211,220,310) β(002)
061102Ta03a2	10%	12	bcc + β	bcc(110) β(002,513)
040502Ta03a_1	14%	10	bcc + β	bcc(110,211,220) β(002)
041502Ta01a_1	10%	5	bcc + β	bcc(110,211) β(002)

* *Measured by the flow of nitrogen and argon during reactive sputtering*
** *Prominent peaks in XRD spectra*

Figure 5.2 shows an example of the XRD spectrum of Ta deposited on a 20 nm thick tantalum nitride seed layer, deposited with nitrogen and argon flow ratio of 2/18 (10% nitrogen concentration). Figure 5.3 shows the XRD spectrum of Ta deposited on a thinner (5 nm) seed layer of tantalum nitride deposited under the same condition.

As indicated by the peaks in the spectra, a pure bcc structure of Ta was obtained on the 20 nm thick seed layer (Figure 5.2) but a mixed phase, with prominent beta phase peaks was obtained with a 5 nm thick seed layer (Figure 5.3). The 20 nm thick seed layer, deposited with a 10% nitrogen concentration in the sputtering gas did not produce a pure bcc phase in some Ta films. However, tantalum nitride layers deposited at somewhat higher nitrogen concentrations of 14%, 18% and 21%, all with thickness of 20nm, produced bcc Ta in all films. Ta sputtered on nitride seed layers deposited with all the above gas compositions and thickness of more than 20 nm also grows exclusively with the bcc phase. Additionally, Ta deposited with a seed layer thickness of less than 20 nm grows with a mixed phase similar to one presented in the XRD spectrum of Figure 5.3. It was thus established that the minimum thickness of tantalum nitride seed layer to grow bcc Ta on steel (subjected to sputter etching before deposition), is 20 nm.

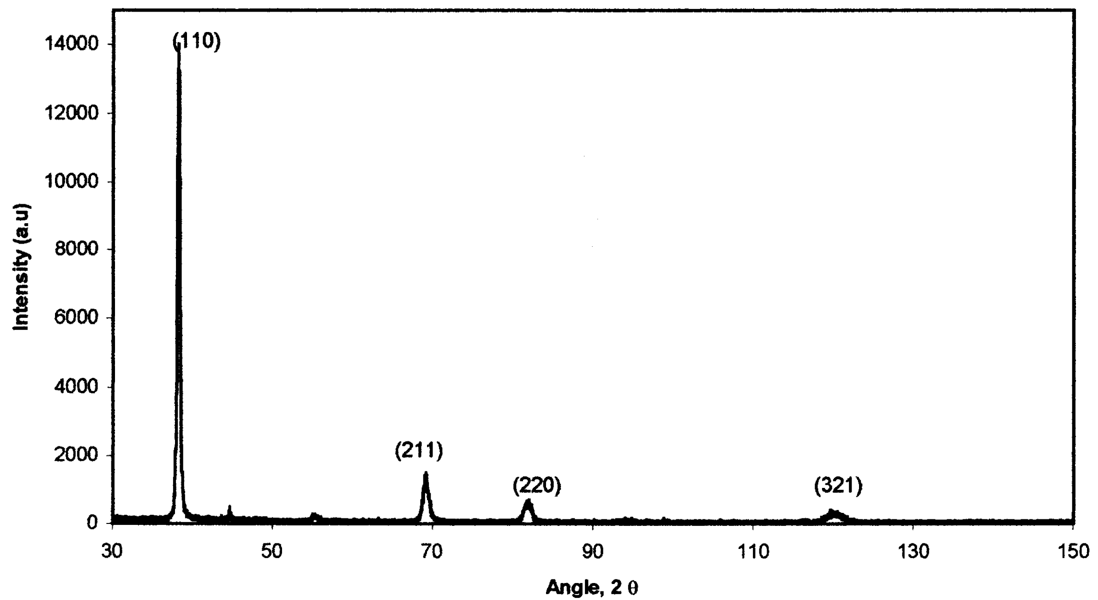

Figure 5.2 XRD pattern of the Ta film (~ 2 μm thick) deposited on a sputter etched steel substrate with a 20 nm thick tantalum nitride interlayer.

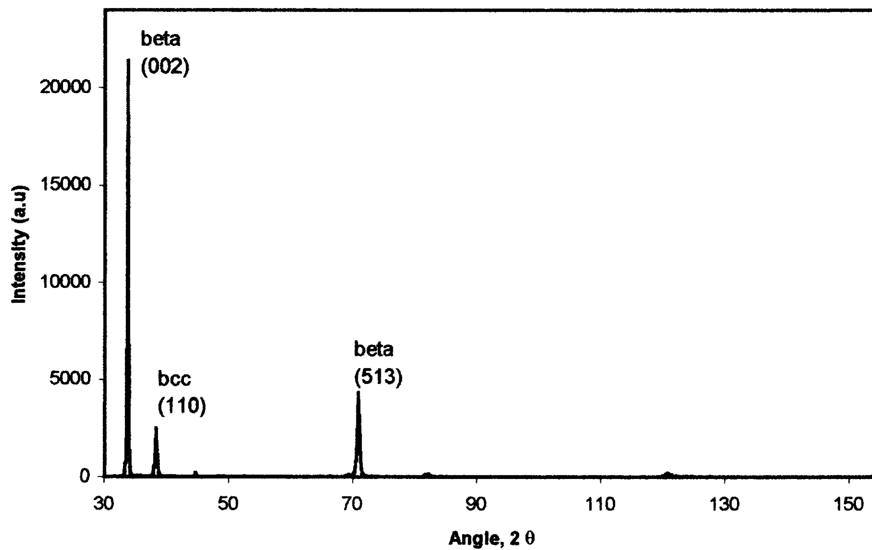

Figure 5.3 XRD spectrum of Ta film (~1 μm) deposited on a sputter etched steel substrate, with a 5 nm thick tantalum nitride interlayer.

The influence of substrate sputter etching on the critical thickness of the seed layer required for the growth of bcc Ta was also investigated. Table 5.2 shows the comparison of seed layer thicknesses required to produce bcc Ta on steel substrates with and without sputter etching prior to deposition. The bcc Ta films were observed on thinner (less than 20 nm) tantalum nitride seed layers that were deposited on steel substrates, which were not subjected to sputter etching prior to deposition.

Table 5.2 Comparison of Ta Grown on Tantalum Nitride Seed Layer Deposited on Steel Substrate with and without Sputter Etching

Sample No.	Nitrogen concentration*	Sputter etching	Seed layer thickness (nm)	Phase of tantalum	Crystallographic orientation**
011602Ta01a_2	10%	NO	15	bcc	110, 211
011602Ta05a_1	14%	NO	15	bcc	110,211
021102Ta01a_4	10%	YES	15	mixed	bcc(110,211) β (002)
040502Ta03a_1	14%	YES	10	mixed	bcc(110,211,220) β (002)
012902Ta02a_3	10%	NO	7	bcc	110,211
020502Ta03a	14%	NO	7	bcc	110,211
041502Ta01a_1	10%	YES	5	mixed	bcc(110,211) β (002)
020502Ta02a	10%	NO	4	bcc	110,211

* *Measured from the nitrogen and argon gas flow during reactive sputtering*
** *Peaks on the XRD spectra*

A special case of this study is presented in Figure 5.4 showing the XRD spectrum and Figure 5.5 showing the photomicrograph of the cross-sectioned thick (46 μm) Ta coating deposited with a tantalum nitride seed layer of ~15 nm on sputter etched

steel substrate. For comparison, XRD and photomicrography was performed on a Ta coating (47 μm) deposited on the steel substrate with the same seed layer of tantalum nitride (~15 nm) but with no prior sputter etching performed on the steel substrate.

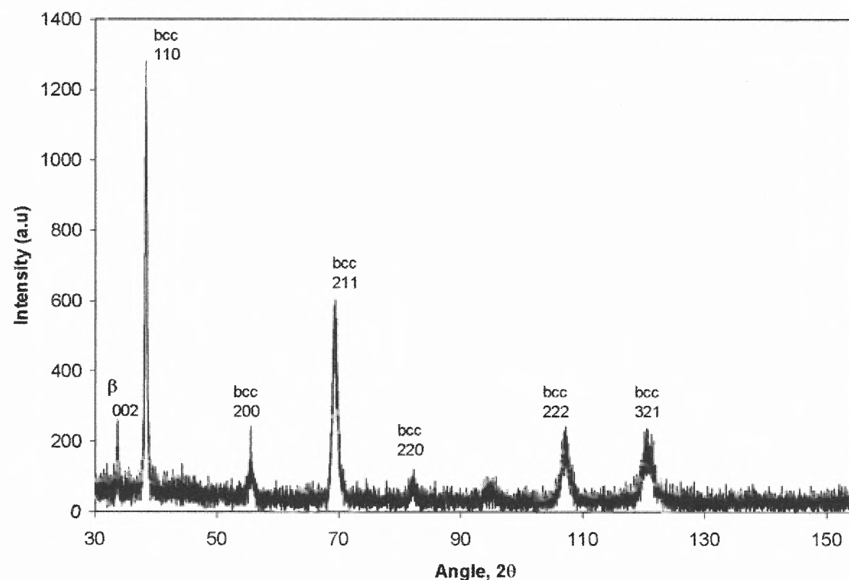

Figure 5.4 XRD spectrum of Ta deposited on steel substrate (after sputter etching) with an interlayer of (15 nm thick) tantalum nitride.

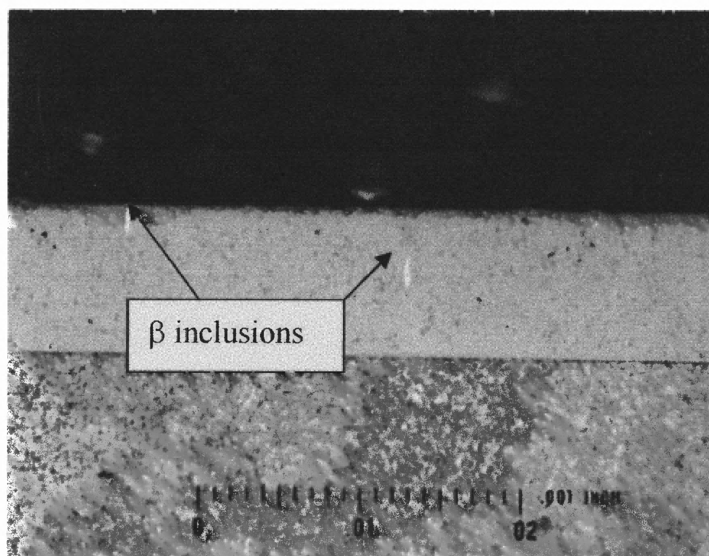

Figure 5.5 Photomicrograph of the cross section of steel sample with Ta coating on 15 nm thick tantalum nitride interlayer, deposited after sputter etching of the substrate.

As seen in the spectrum (Figure 5.4) there were some beta peak inclusions in the Ta coating deposited on sputter etched steel along with peaks of bcc phase. Such beta phase inclusions were also observed by photomicrography performed at Benet laboratories on the same sample. Beta inclusions could be clearly observed as light spots in a gray background of bcc matrix, in the photomicrograph (Figure 5.5). The XRD pattern (Figure 5.6) and the photomicrograph (Figure 5.7) reveals that Ta deposited with a tantalum nitride seed layer (~15 nm) on steel substrate, with no prior sputter etching, had the pure bcc phase, unlike the one deposited on the sputter etched steel. Results obtained from this study, indicate that sputter Ta coatings deposited on sputter etched steel substrates require a thicker tantalum nitride seed layer to grow in the bcc phase structure.

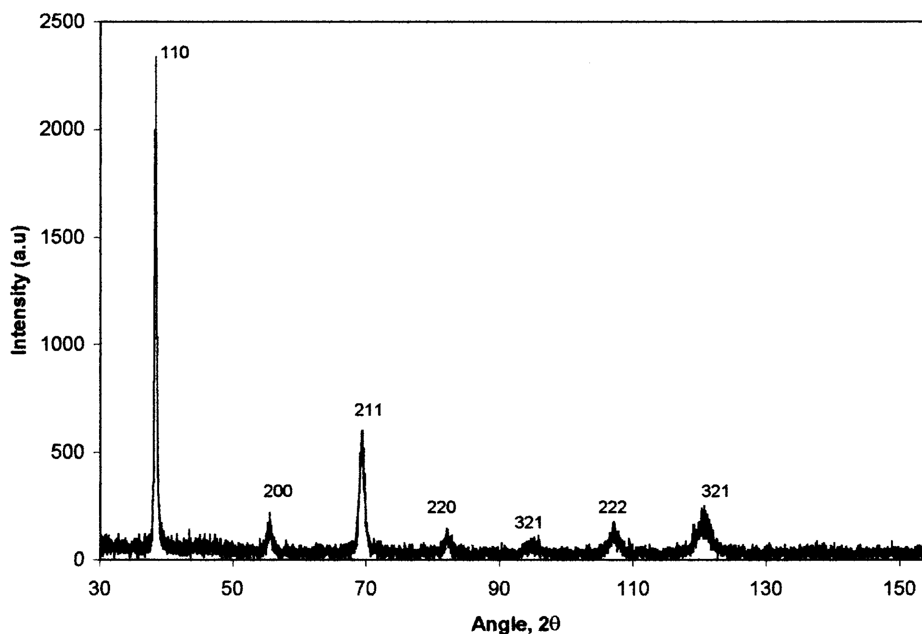

Figure 5.6 XRD spectrum of bcc Ta coating deposited on a 15 nm thick tantalum nitride interlayer steel substrate (without prior sputter etching).

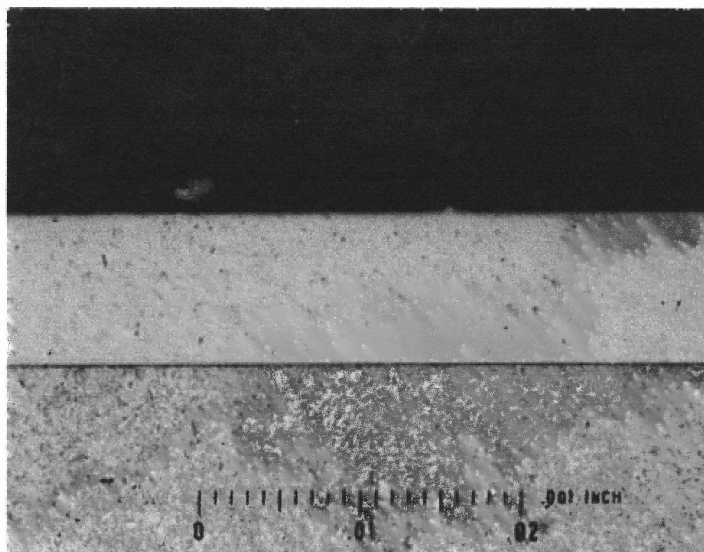

Figure 5.7 Photomicrograph of the cross section of steel sample (without sputter etching) with a Ta coating on top of tantalum nitride interlayer (15 nm thick).

The surface of the Ta coating was also studied by photomicrography performed at NJIT. An example is presented in Figure 5.8 showing a plane view of the polished coating surface of a 45 μm thick Ta deposited on steel, with a 15 nm thick tantalum nitride interlayer. As seen from the photomicrograph, the Ta coating has a mixed phase with numerous beta phase inclusions appearing in light color on the dark background of mostly bcc film. A cross section of the same film is shown in Figure 5.9, with needle shaped beta phase inclusions (light color) that were found to grow in a bcc phase (darker color).

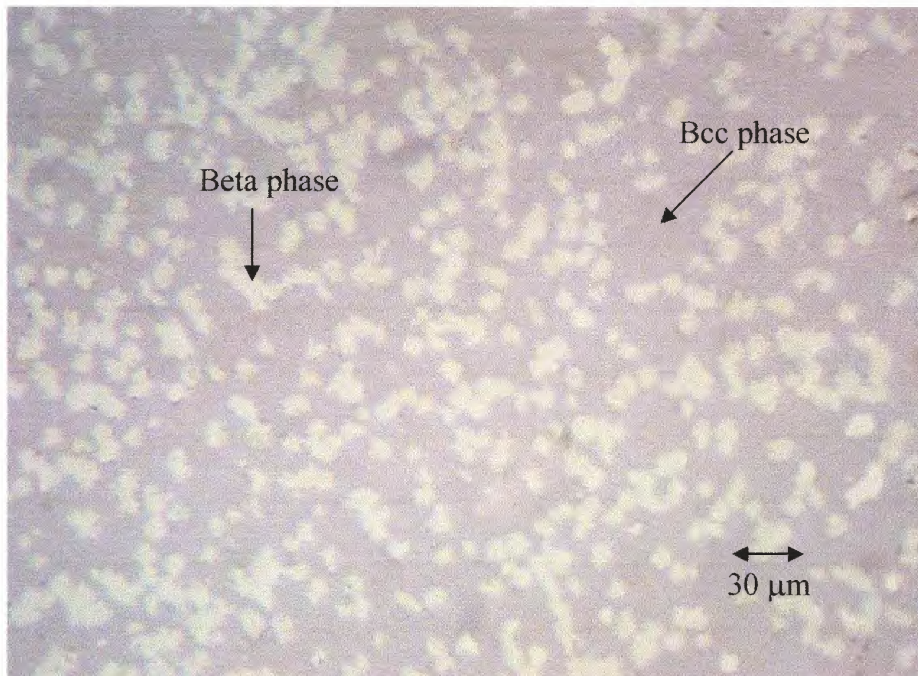

Figure 5.8 Photomicrograph of polished surface of mixed phase Ta coating deposited on steel with argon as a sputtering gas.

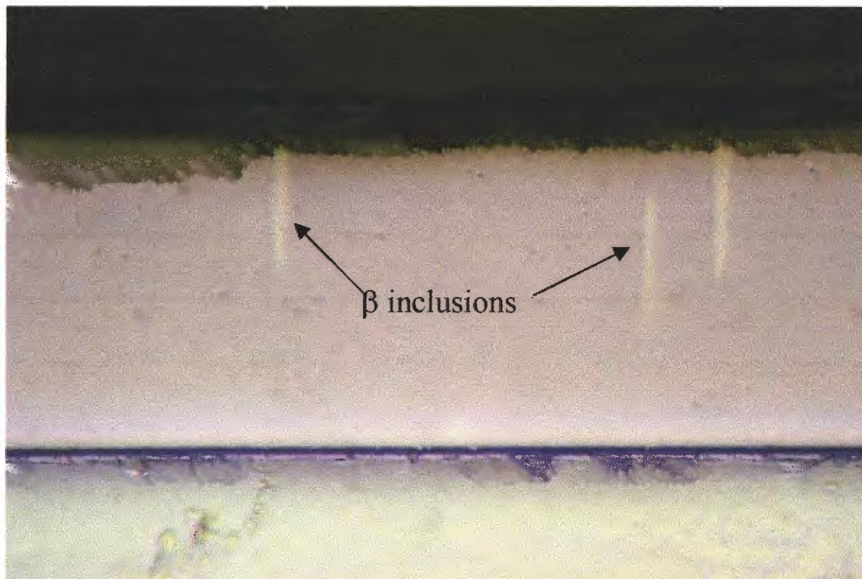

Figure 5.9 Cross section of the steel sample with bcc Ta coating deposited on tantalum nitride seed layer with beta inclusions clearly visible as light needles.

5.2 Tantalum Nitride Structure Promoting Bcc Tantalum

The results presented in Section 5.1 show that a tantalum nitride under layer plays an important role in the overgrowth of bcc Ta. As it was shown, there is a critical thickness of the nitride seed layer necessary to grow bcc Ta that depends on the flow of nitrogen during the reactive sputtering of Ta. The critical thickness also depends on the treatment of the steel surface by sputter etching prior to the nitride deposition. To understand these phenomena, properties of tantalum nitride films were studied as a function of varying nitrogen flow in a mixture of nitrogen and argon during reactive sputtering. Due to the limitation of the characterization equipment, thick tantalum nitride films (600-900 nm) were deposited for the study and the results were used to understand the properties of thin (20-50 nm) seed layer deposited under the same condition.

For the estimation of the deposition rates of reactively sputtered Ta, the film thicknesses were measured by a profilometer on control samples of SiO_2. The dependence of the deposition rate on the nitrogen concentration is presented in Figure 5.10. As seen in the plot, increasing the nitrogen concentration from 1.6 to 33% decreases the sputtering rate from 0.87 nm/s to 0.43 nm/s. Similar results are reported in the literature [52,53,54] on sputtered tantalum nitride films. The decrease in the deposition rate could be due to nitridation of the target also known as target poisoning, and also due to low ionization efficiency of nitrogen gas atom [55]. In the phenomenon of target poisoning, a compound layer is grown on the target, which decreases the amount of open sites for metal sputtering on the cathode surface. This effect was indicated in the observed increase in the value of applied voltage when the sputter power supply was working in a constant current mode.

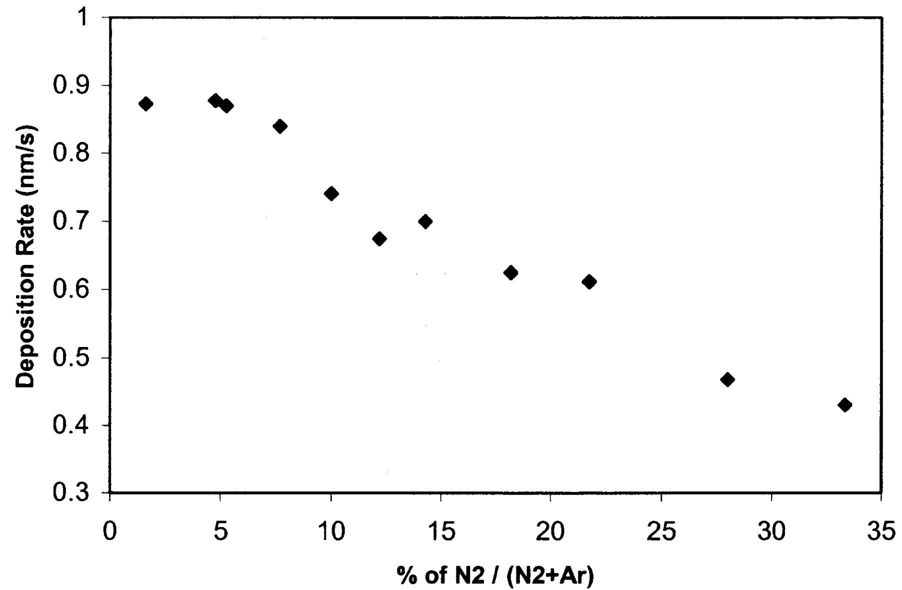

Figure 5.10 Deposition rate vs. the percentage of nitrogen concentration in the sputtering gas.

The electrical resistivity of tantalum nitride films, measured as a function of nitrogen concentration during reactive sputtering, is plotted in Figure 5.11. With 1.6% of nitrogen in the sputtering gas, the resistivity of the film was 240 μΩ cm. An increase in the nitrogen flow between 4 to 7% increased the resistivity values of the film to 300-330 μΩ cm. A yet higher nitrogen flow of 10% to 14% gave film resistivity values between 340-370 μΩ cm. A significant increase in the resistivity of the film was observed at nitrogen concentrations between 18 to 33 %, reaching a very high value of 4800 μΩ cm at a nitrogen concentration of 33%.

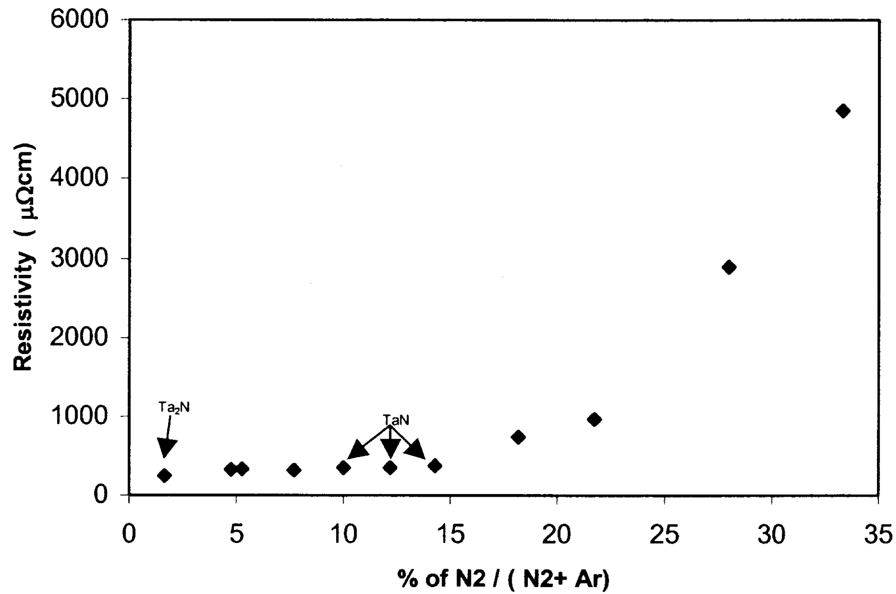

Figure 5.11 Resistivity of tantalum nitride films on SiO_2 substrate vs. the percentage of nitrogen concentration in the sputtering gas.

In order to understand their morphology and the crystallographic structure, tantalum nitride films were investigated by AFM and XRD. These measurements were made on the films that were deposited on SiO_2 substrates, because their flatness and smooth surface makes them suitable for characterization by AFM and four-point probe. Figures 5.12 and 5.13 shows 2 μm x 2 μm area AFM scans of the surface of tantalum nitride film deposited with nitrogen concentrations of 5%, 14%, 18%, 21%, 28% and 33%.

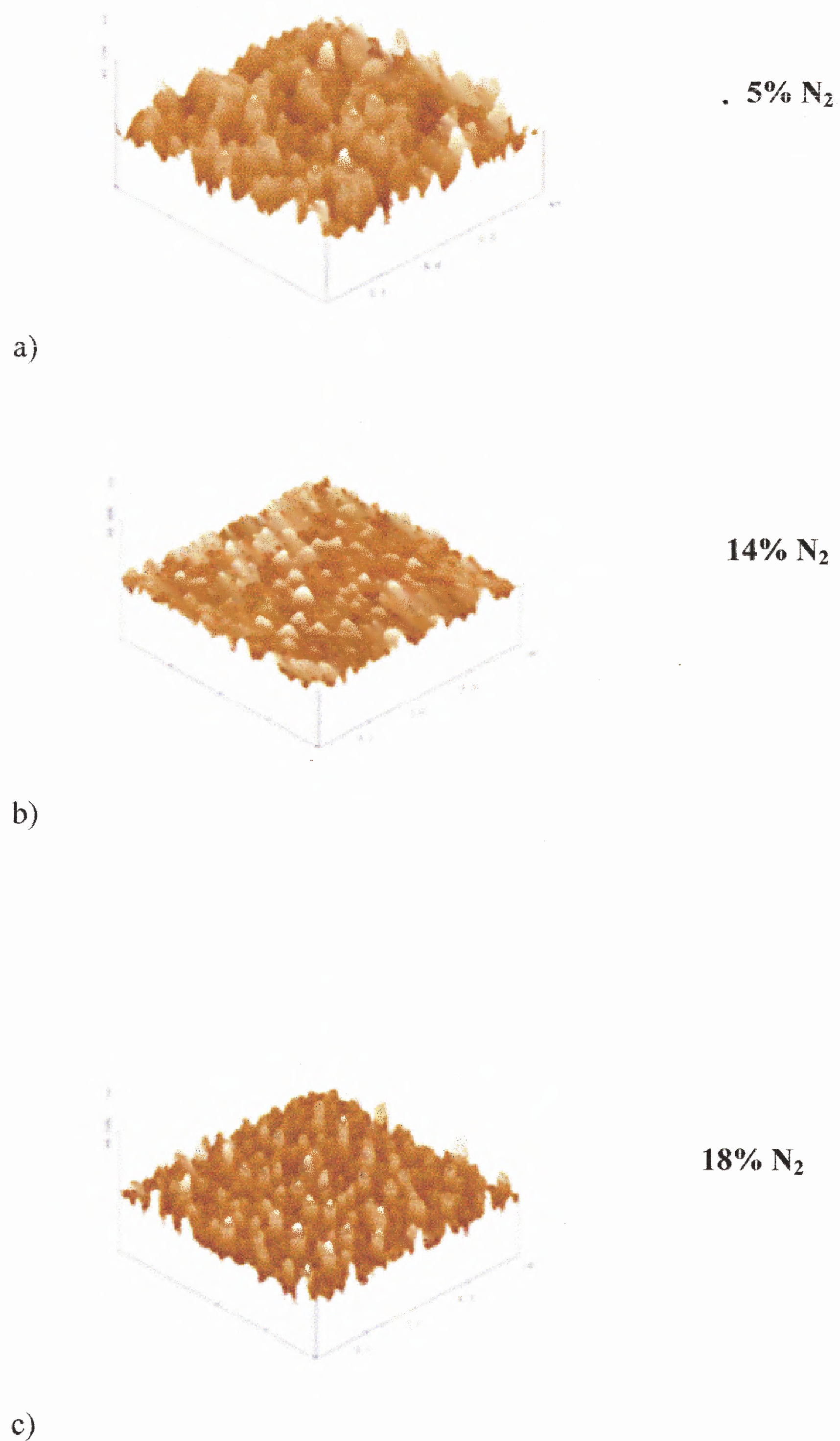

Figure 5.12 AFM image of 2 μm x 2 μm area (Z= 20 nm/div) of the tantalum nitride film deposited with nitrogen concentration of a) 5% b) 14% c) 18%, in a mixture of argon and nitrogen, on silicon dioxide substrate.

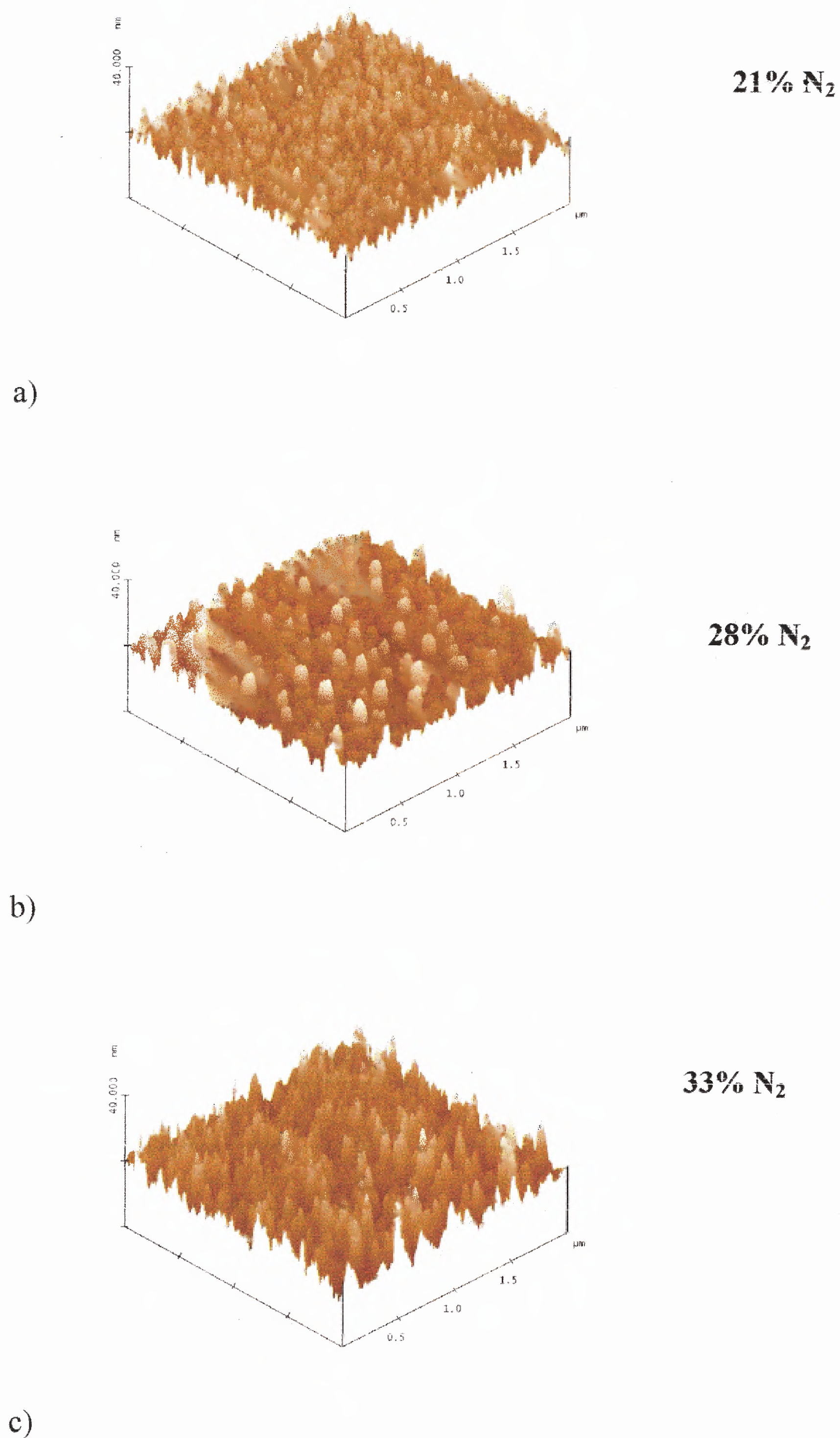

Figure 5.13 AFM image of 2 µm x 2 µm area(Z= 20 nm/div) of the tantalum nitride film deposited with nitrogen concentration a) 21% b) 28% c) 33%, in a mixture of argon and nitrogen, on silicon dioxide substrate.

The surface roughness of the surface of tantalum nitride film was determined as,

$$Ra = \frac{1}{n}\sum_{i=1}^{n}\left|z_i - z\right| \qquad \text{.................................. 5.1}$$

where, Ra is the arithmetic roughness average, n the number of height positions along the line profile, Z_i the height at position i and z the average height. The summary of results from AFM measurements is presented in Table 5.3.

Table 5.3 Summary of AFM Measurements Performed on Tantalum Nitride Films Deposited with Different Nitrogen Flow.

Sample no.	Nitrogen Concentration	Roughness Ra (nm)	Description
080102Ta04c	5%	2.64	Rough irregular structure
071702Ta06c_2	14%	1.17	Comparatively smooth
080102Ta05c	18%	1.84	Regular projections
072302Ta04c	21%	1.72	Conical projections
080702Ta05c	28%	3.39	Cylindrical projections
080702Ta06c	33%	2.45	Conical irregular projections

The atomic force images show the change in the morphology of the film with the change in the nitrogen flow. The tantalum nitride film deposited with 5% nitrogen concentration shows rough irregular structure (Figure 5.12a), while, the AFM image of tantalum nitride film deposited with 14% concentration (Figure 5.12b) shows smaller surface features, combined with a reduction in the roughness (Ra) of the film (i.e. 2.64 nm to 1.17 nm). Surface projections at regular intervals of same size and increased roughness are observed in tantalum nitride films deposited with 18% nitrogen concentration. The film deposited with 28% nitrogen concentration also had the regular cylindrical projections that were larger than those observed in the film deposited with

18%, with a corresponding increase in the roughness. The films deposited with 21% and 33% nitrogen concentration showed similar conical projections, though the latter film was rougher.

XRD spectra of the films deposited with the nitrogen flow of 5%, 14%, 18%, 21%, 28% and 33% are presented in Figure 5.14 and 5.15 respectively. A broad peak on the XRD pattern (Figure 5.14a) of the film deposited with 5% nitrogen flow is noted, which indicates the film to be amorphous. This peak may include the peaks of Ta_2N (002) and (101) at $2\theta = 35.9°$ and $38.5°$ respectively [56] but could also correspond to TaN (101) at $2\theta = 36.8°$ [57]. The XRD spectra of the tantalum nitride films deposited with the nitrogen flow of 14% and 18% is shown in Figure 5.15b and 5.15c respectively. The two prominent peaks at a 2θ angles of $34.7°$ and $41.1°$ are identified as corresponding to TaN (110) [57] and TaN (200) [58] respectively. The same two peaks with different intensity ratios are seen in XRD spectra of tantalum nitride films deposited with nitrogen concentration of 21%, 28% and 33%, shown in Figure 5.15 a, b and c respectively. The TaN (200) peak is more prominent in films deposited with 21% nitrogen concentration and TaN (110) is more prominent in XRD spectrum for films deposited with 33% nitrogen concentration. A summary of these results are tabulated in Table 5.4.

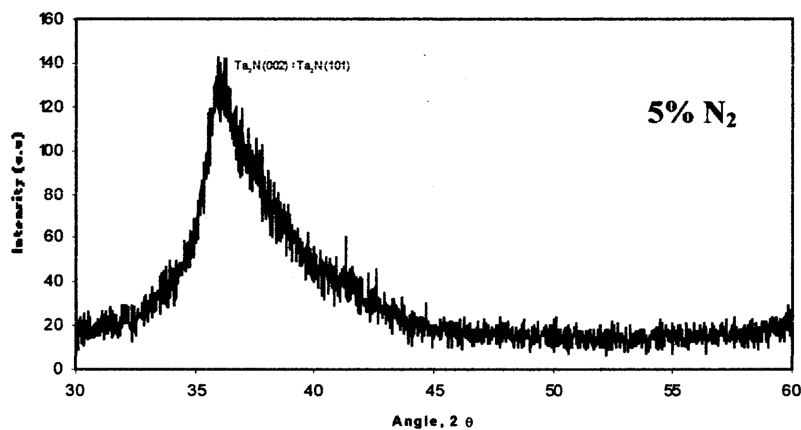

a)

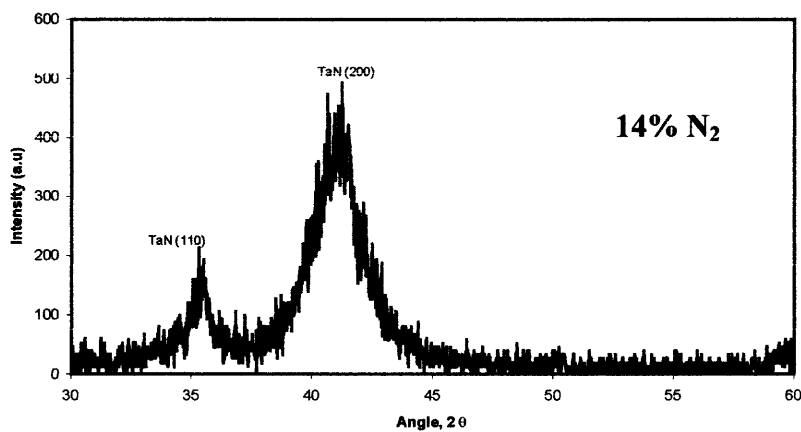

b)

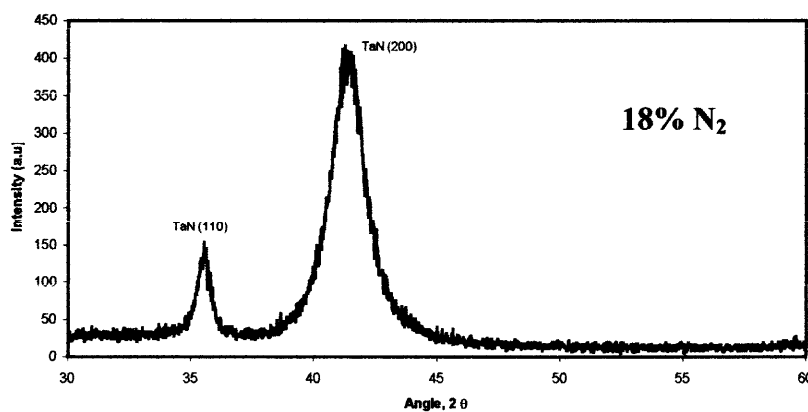

c)

Figure 5.14 X-ray diffraction spectra of tantalum nitride film deposited, on SiO_2 substrate, with a) 5% b) 14% c) 18% nitrogen concentration in the sputtering gas.

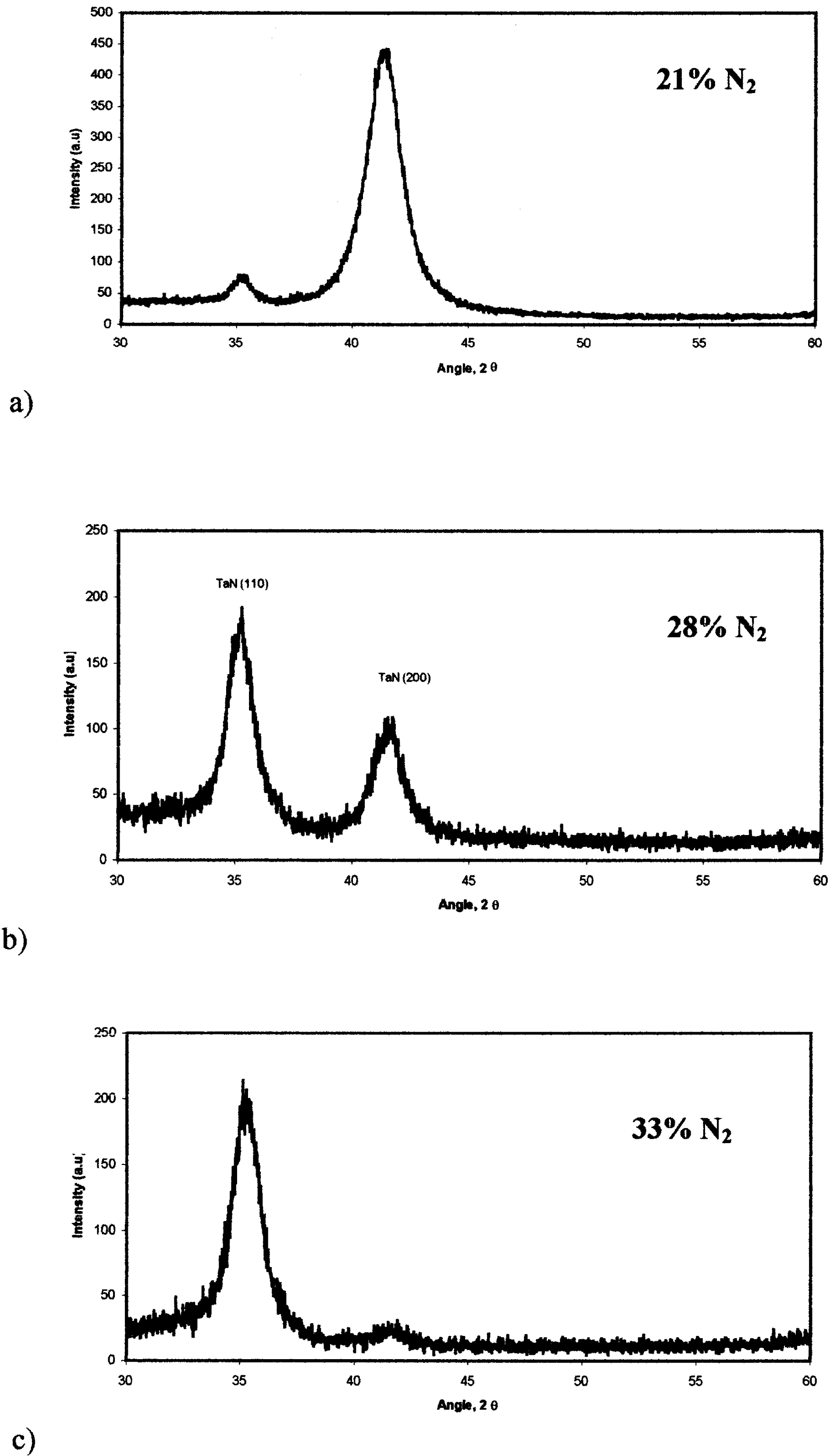

Figure 5.15 X-ray diffraction spectra of tantalum nitride film deposited, on SiO_2 substrate, with a) 21% b) 28% c) 33% nitrogen concentration in the sputtering gas.

Table 5.4 Summary of XRD Results on the Tantalum Nitride Films deposited on SiO_2.

Sample no.	Nitrogen concentration	Structure of the film	Crystallographic orientation
080102Ta04c	5%	Ta_2N	Amorphous
071702Ta06c$_2$	14%	TaN	110,200
080102Ta05c	18%	TaN	110,200
072302Ta04c	21%	TaN	200, trace of 110
080702Ta05c	28%	TaN	110,200
080702Ta06c	33%	TaN	110, trace of 200

X-ray diffraction was also used to study the structure of tantalum nitride films deposited on steel substrates. Comparison of XRD spectra of tantalum nitride layers deposited with different nitrogen concentration on steel substrates are shown in Figure 5.16. A broadened peak evident in the spectra of tantalum nitride film deposited with nitrogen concentrations between 1 to 5% indicates the amorphous nature of the film and was also observed in the film deposited with the same flow on SiO_2 substrates. With an increase in the nitrogen concentration in the sputtering gas mixture, the composition of tantalum nitride films changed from Ta_2N to TaN, which is reflected in the XRD patterns (Figure 5.16). There was a transition from Ta_2N phase to TaN phase as the concentration is increased above 5%. With higher concentrations (28% and 33%) of nitrogen, broader peaks (at $2\theta = 34°$) were observed in the XRD spectrum on steel, which were not observed on SiO_2, indicating the change in the structure as compared to the spectra for 14, 18 and 21 % nitrogen. All the spectra have the peak appearing at 2θ angle of 44.5, which corresponds to the steel, i.e. the substrate. Hence, the tantalum nitrides on SiO_2 and

steel substrates grown under the same conditions were similar. The seed layer promoting the bcc phase in Ta films and coatings appear to be cubic TaN.

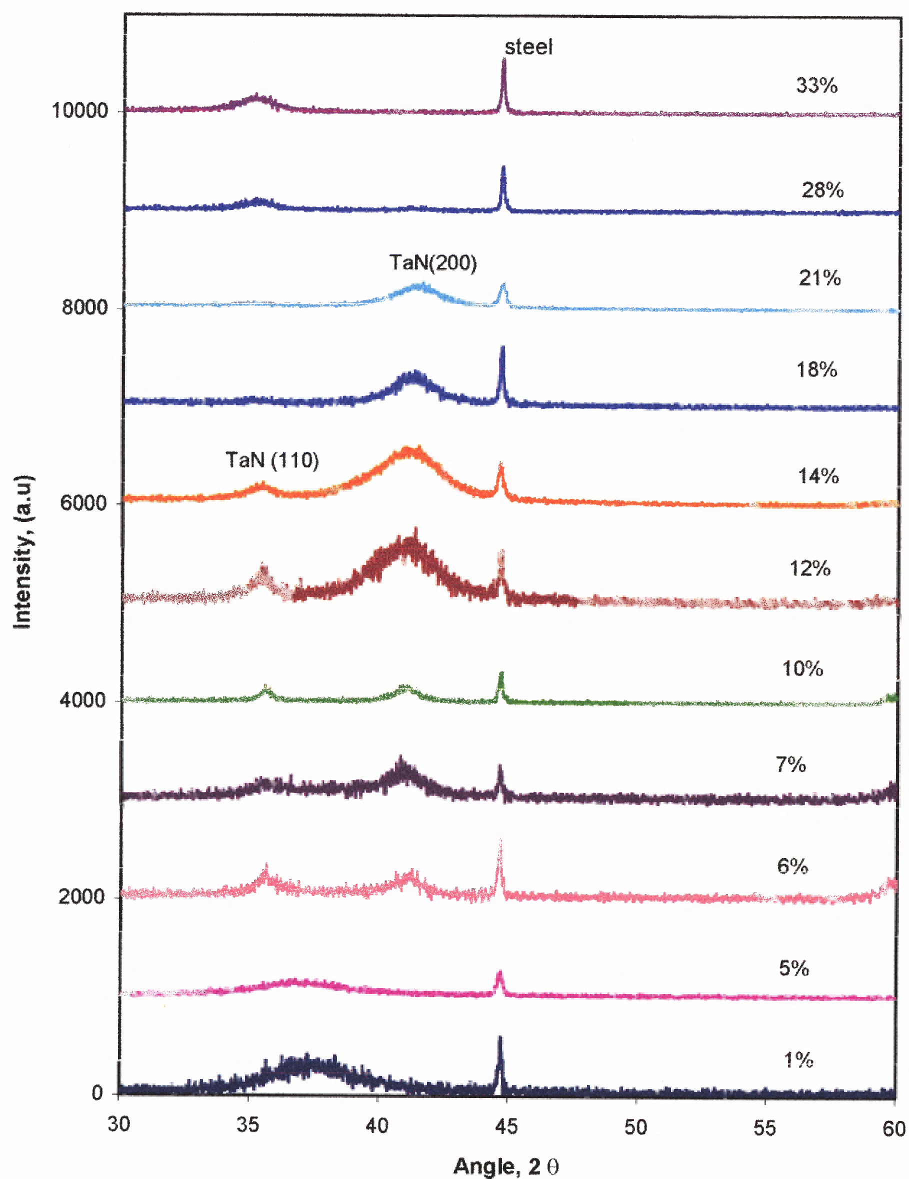

Figure 5.16 Comparison of the XRD patterns measured on tantalum nitride films deposited on steel substrates with varying nitrogen concentration in the sputtering gas mixture of argon and nitrogen.

Depth concentration profiles of nitrogen in selected nitrided layers were measured using a nuclear reaction analysis (NRA) technique using the $^{15}N(p, \alpha\gamma)^{12}C$ reaction at the 898 keV resonance energy. The energy of the proton beam was increased in small steps, so that the intensity of the detected γ radiation from the nuclear reaction was proportional to nitrogen concentration at a depth where the protons passing through the sample were slowed down to the resonance energy. The nitrogen content of selected tantalum nitride films is shown in Figure 5.17. The data were obtained on 1 μm and 0.8 μm thick nitride layers deposited on steel substrate with 5% and 14% nitrogen concentration sputter gas at a pressure of 5 mtorr. The results of NRA show nearly 50% nitrogen content in the nitride film deposited with 14% nitrogen concentration that confirms the formation of stoichiometric TaN at this concentration. In nitride films deposited at 5% nitrogen content, only 30% nitrogen content was found that indicates the Ta_2N phase in these films. These results agree with conclusions from the XRD data.

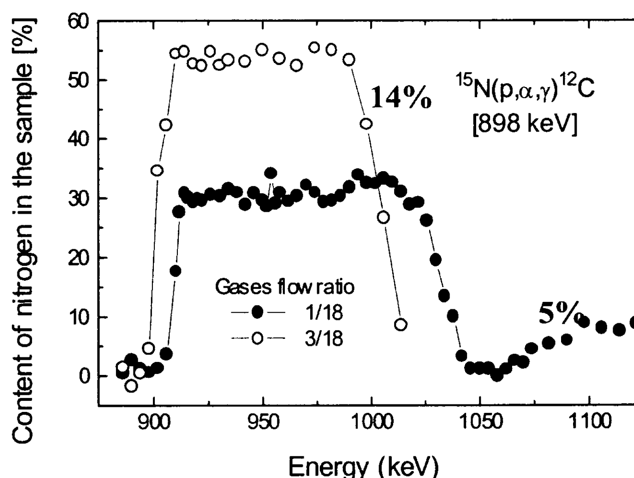

Figure 5.17 The nitrogen content of tantalum nitride films deposited with nitrogen concentrations of 5% and 14% (flow of 1/18 and 3/18 respectively), measured by NRA. Film thicknesses were 1.0 μm and 0.8 μm, respectively.

Scanning electron microscopy was performed on a thin tantalum nitride seed layer deposited on steel. A larger area of the nitride films was exposed by SEM. One such image of a tantalum nitride film is shown in Figure 5.18. The tantalum nitride film deposited on polished steel substrates showed smooth surfaces yet some SEM images indicated discontinuities of a few micron in size in the thin seed layer films.

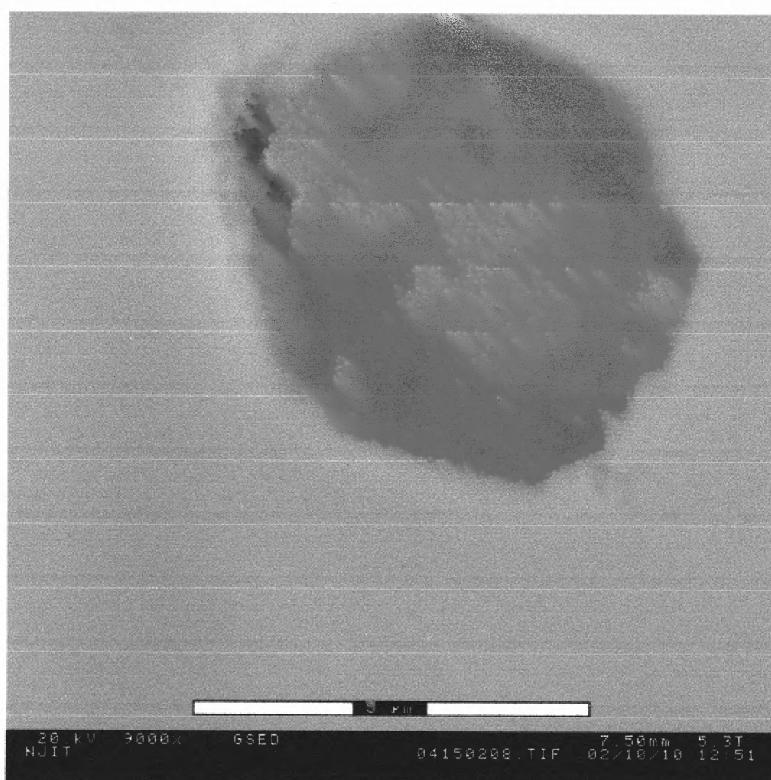

Figure 5.18 Scanning electron micrograph of tantalum nitride film of thickness 10 nm deposited on a sputter etched steel substrate.

5.3 Tantalum Deposited on Heated Substrate

Another method of producing bcc Ta coatings on the steel involved heating of the substrates. Ta deposited on steel at room temperature had always the beta or a mixed phase. To find the critical temperature required for the growth of bcc Ta, a series of experiments were performed with tantalum deposited on steel substrates heated to temperatures from 100 to 450 °C. Figure 5.19 and Figure 5.20 show the XRD spectra of Ta deposited with argon and krypton on steel, heated to 400 °C and 350 °C respectively. As seen from the patterns, the films have the same bcc structure but different crystallographic textures.

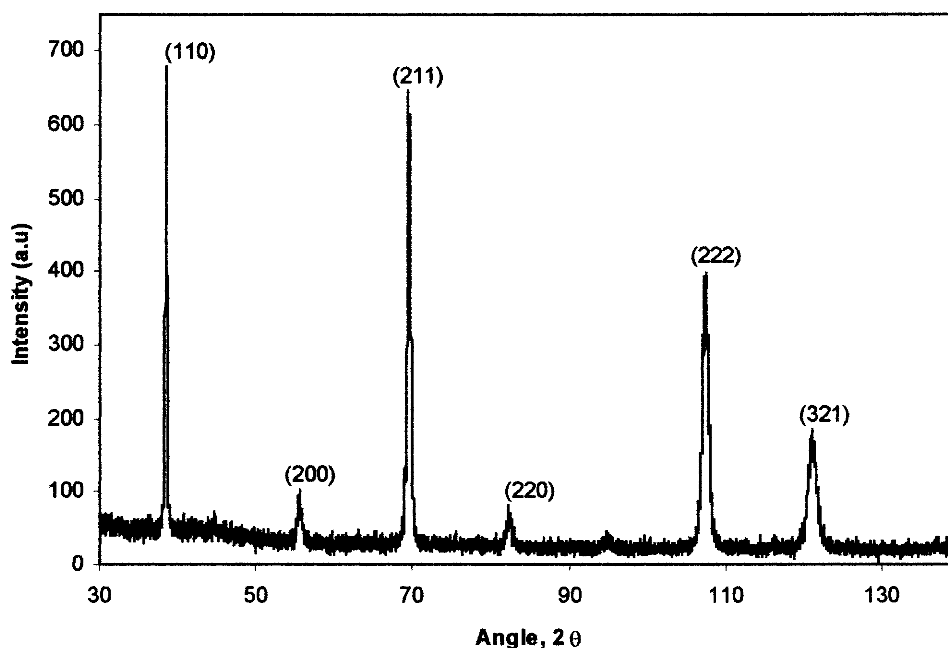

Figure 5.19 XRD pattern of Ta deposited (5 μm) on steel substrate heated to 400 °C in argon, all peaks correspond to the bcc Ta phase.

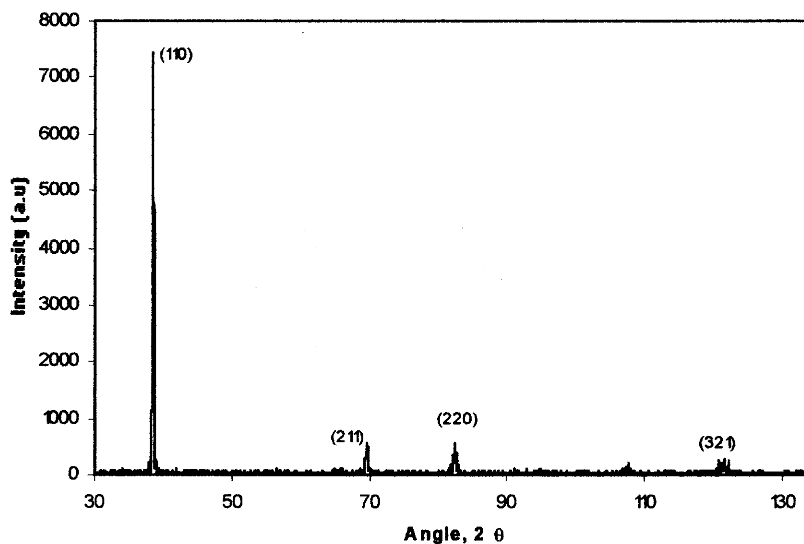

Figure 5.20 XRD spectrum of Ta deposited (3 μm) on heated steel substrate (350 °C) with krypton as the sputtering gas, all peaks correspond to the bcc Ta phase.

Figure 5.21 shows the XRD spectrum of a Ta film deposited on a steel substrate heated to 200 and 250 °C with Ar and Kr respectively. Peaks representing both beta and bcc are present in these spectra. This mixed phase was usually obtained on the Ta films deposited on the steel substrates heated below the critical temperature of 400 °C and 350 °C with argon and krypton respectively. Figure 5.22 shows the XRD pattern of a Ta film (4μm) deposited on a steel substrate heated to 400 °C during deposition with Ar. As seen in the spectrum, a strong peak (222) at 107° is observed. Figure 5.23 shows the comparison of Ta coatings of different thickness deposited with Ar on heated steel substrate (400 °C). The 222 peak of bcc Ta was the only peak detectable in the spectrum of thicker (11 and 50 μm) Ta coating. These results are also tabulated in Table 5.5.

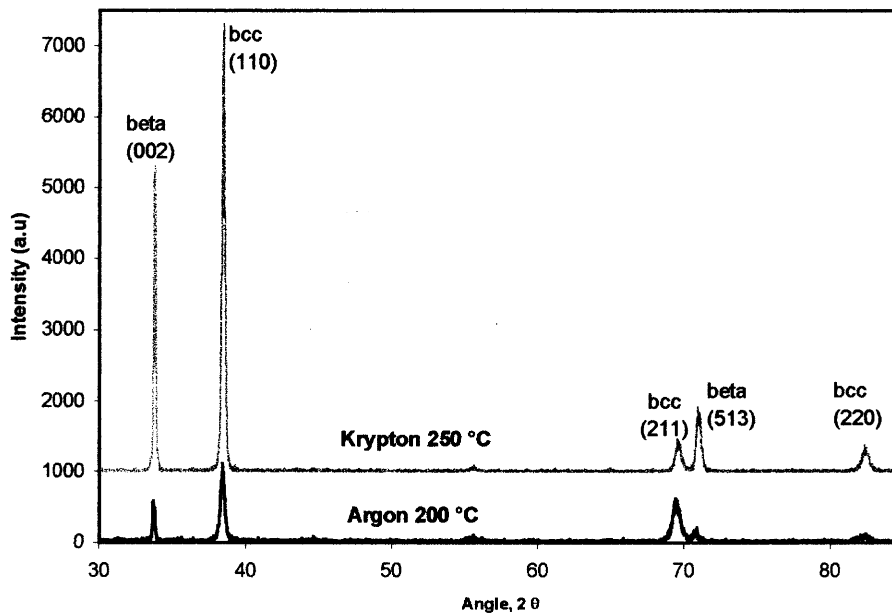

Figure 5.21 XRD spectrum of mixed phase Ta coating deposited on steel substrate at 200 °C with argon sputtering gas and at 250 °C with krypton gas.

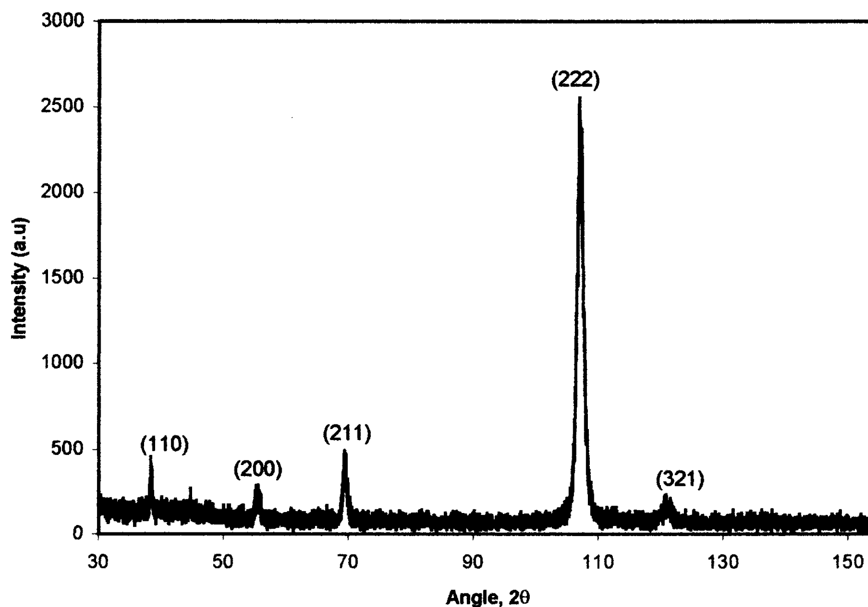

Figure 5.22 XRD pattern of Ta film (4 μm) deposited on steel substrate maintained at 400 °C during deposition using argon.

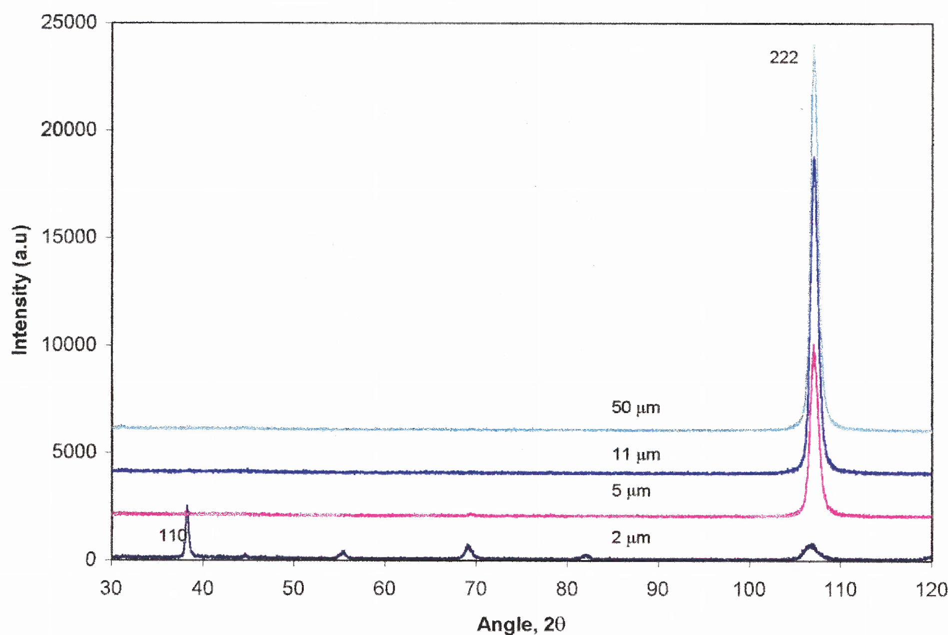

Figure 5.23 XRD spectrum of Ta deposited on heated steel substrate (400 °C) showing the bcc structure with the crystallographic texture changing with the growing thickness of the coating.

Table 5.5 Results Showing the Change in Crystallographic Orientation with Change in the Film Thickness

Sample no.	Substrate temperature	Film thickness (μm)	Crystallographic Orientation of bcc Ta film
082401Ta04a	400 °C	2	110,200,211,220,222
073002Ta07a$_1$	400 °C	5	211,222
092501Ta01a	400 °C	11	222
092501Ta02a1	400 °C	50	222

In a special case as XRD test was performed on both sides of the film (2 μm) that peeled off from the steel substrate. This was done to check the phase at the interface of the bcc Ta film. Figure 5.24 shows the XRD spectra of one such analysis on such a peeled off Ta film. As seen in the spectra (Figure 5.24) both sides of the Ta film had the

identical bcc phase. Photomicrography was performed on the cross-sectioned thick (50 μm) bcc Ta coating produced on heated steel substrate (at NJIT) as shown in Figure 5.25. No beta phase was found at the interface of steel and the coating.

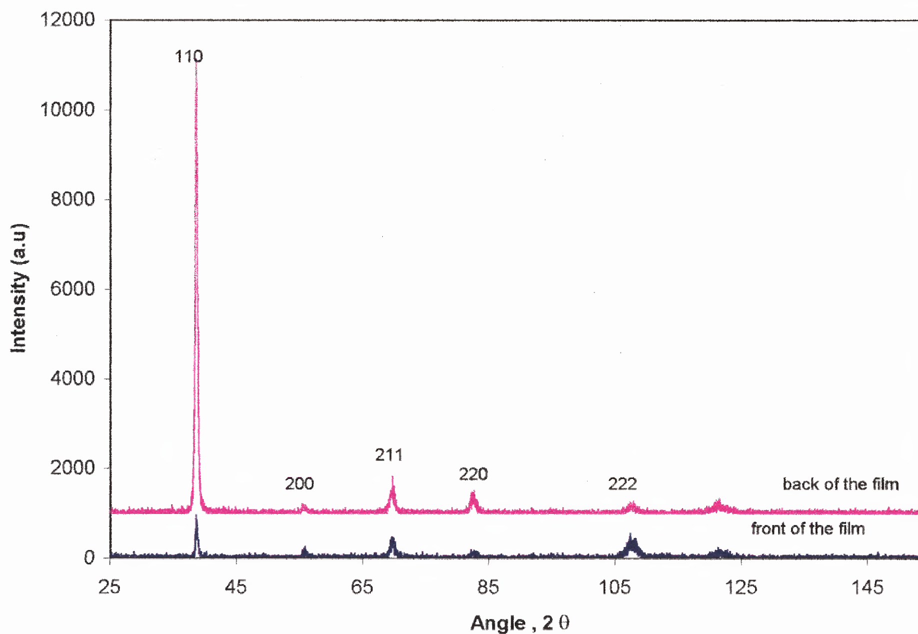

Figure 5.24 XRD spectrums from front and back of bcc Ta (5 μm thick) detached film deposited on heated steel substrate.

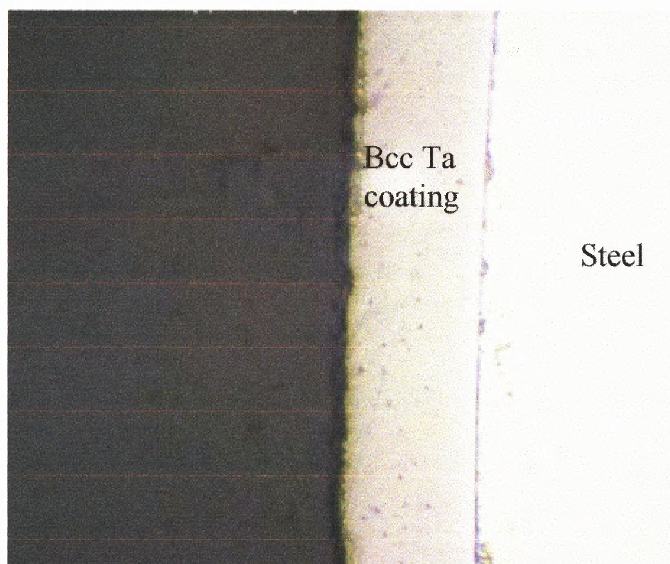

Figure 5.25 Photomicrograph of the bcc Ta coating deposited on heated steel substrate with no trace of beta phase in the coating.

5.4 Adhesion of Ta Coatings

Figure 5.26 and Figure 5.27 shows scanning electron micrographs of Ta coatings, deposited on steel substrate with and without sputter etching (after the groove test performed at Benet Laboratories, with knife edged tungsten carbide tool bit). In Figure 5.26 minor adhesion failure at the edge of the sample was observed which might be due to the irregular coating under the screw that was used to hold the steel to the substrate holder. Figure 5.27 shows a major failure in the Ta coating deposited without prior sputter etching. This adhesion test performed at Benet laboratories on the Ta coatings deposited with tantalum nitride seed layer suggested that sputtering etching prior to deposition improved the adhesion of the coating with the substrate. The overall adhesion of the Ta coatings deposited on sputter-etched substrate was reported by the Benet Laboratories investigators to be excellent. Sputter etching time of steel substrates for 20 minutes with current density of approximately 25 $\mu A/cm^2$ was found to be sufficient.

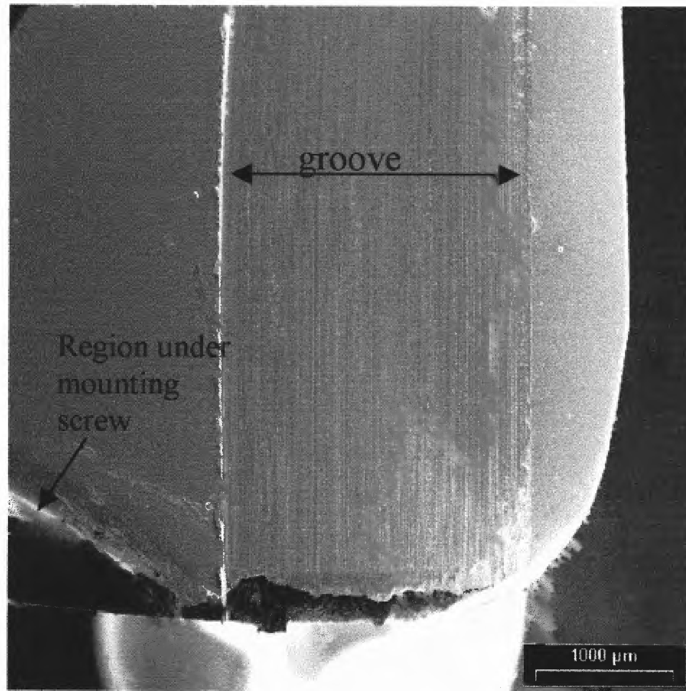

Figure 5.26 SEM image, showing the Ta coating deposited on sputter etched steel sample with an interlayer of tantalum nitride, after the groove test (performed at Benet laboratories).

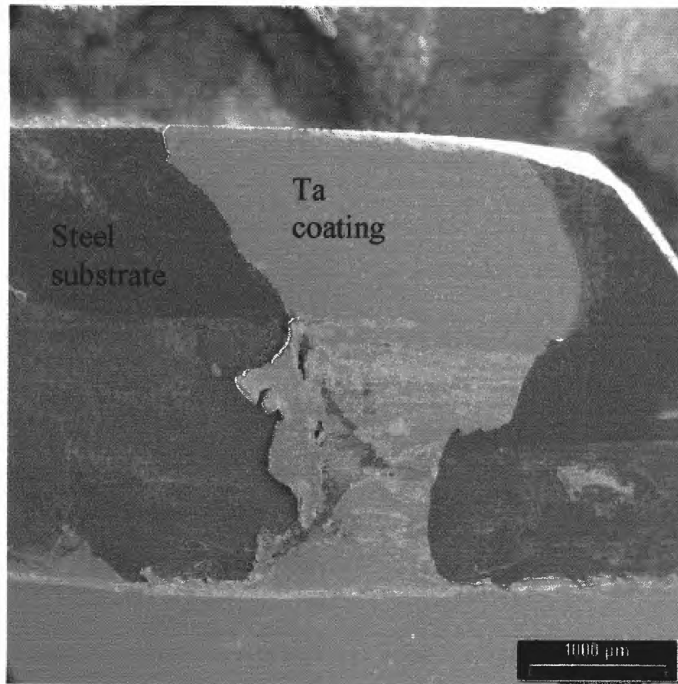

Figure 5.27 Scanning electron micrograph (after groove test) of Ta coating deposited on steel substrate without sputter etching and with an interlayer of tantalum nitride.

Results from the scratch adhesion test performed at NJIT on bcc Ta, and mixed phase coatings with a diamond tip (conical angle, 120°; hemispherical tip of radius 200 μm) are shown in Figure 5.28 and Figure 5.29 respectively. Figure 5.30 and 5.31 shows the results obtained on beta phase Ta coatings. Two distinct modes of failure in the Ta coatings were observed, depending upon the phase composition. Brittle failure was observed with the crack propagating in and around the scratch channel in the beta phase coating. The bcc coating showed ductile behavior, no cracking was observed before complete delamination. No acoustic signals are measured from such failures [59].

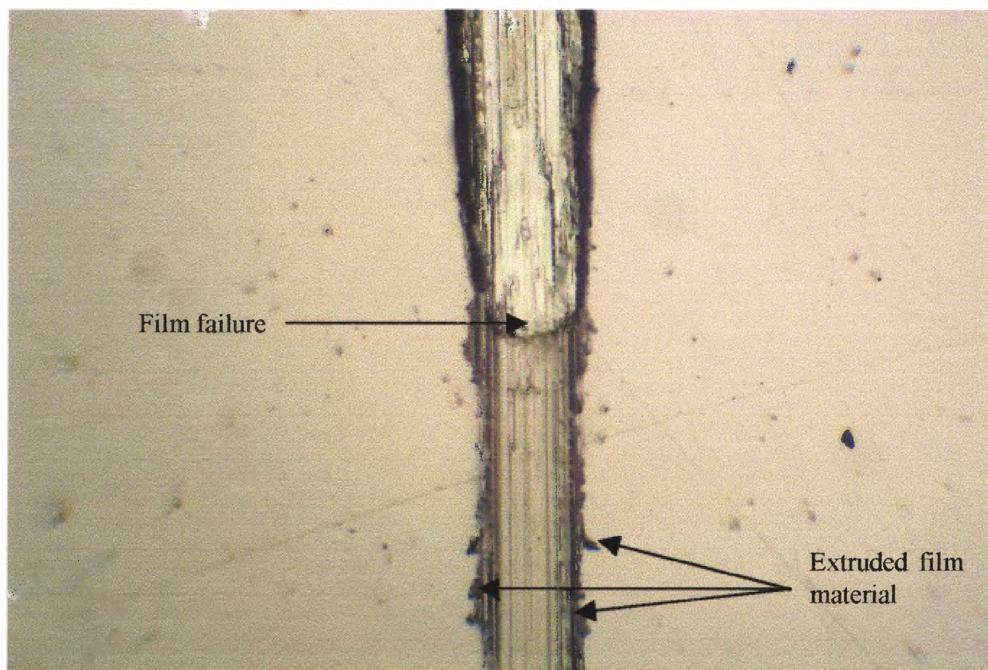

Figure 5.28 Failure pattern of bcc Ta coating deposited on sputter etched steel with 20 nm thick, tantalum nitride interlayer.

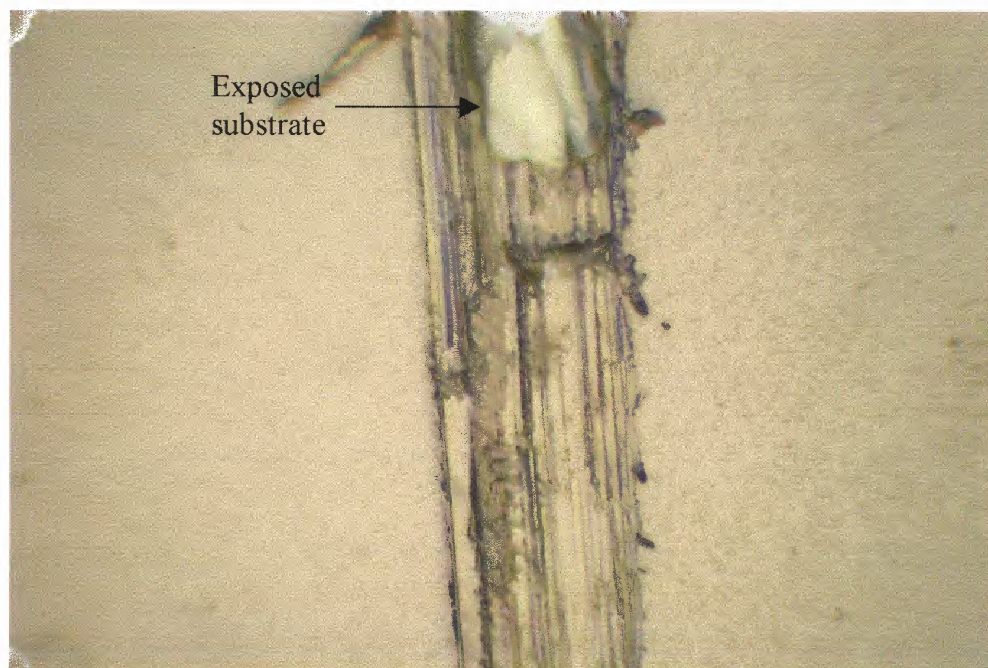

Figure 5.29 Typical scratch pattern obtained on mixed phase tantalum coating deposited on 10 nm thick tantalum nitride interlayer.

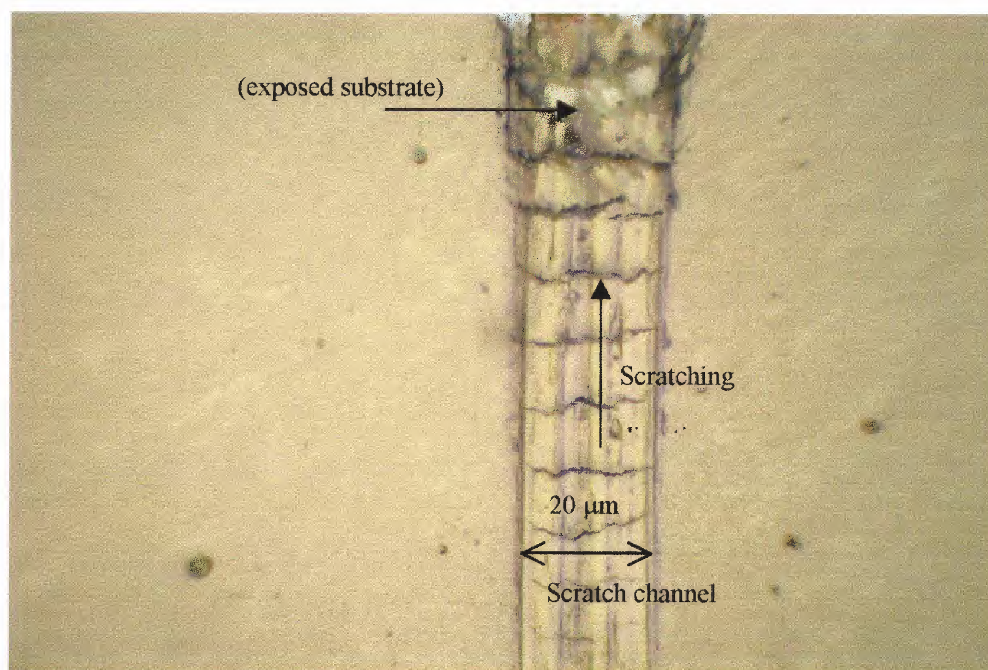

Figure 5.30 Coating failure pattern observed in beta-Ta coating deposited on sputter etched steel substrate.

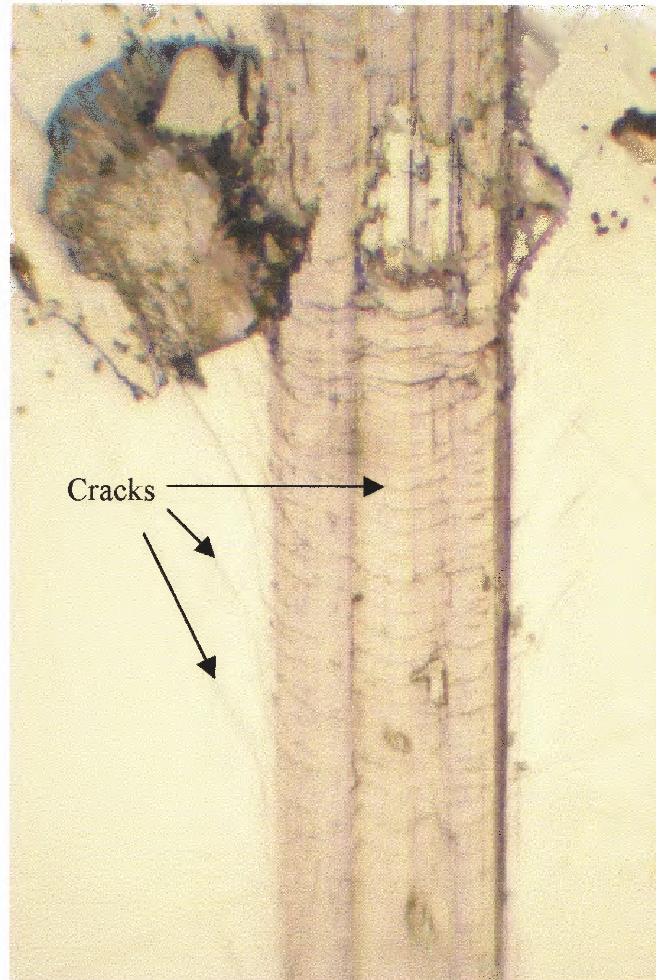

Figure 5.31 Failure observed in the beta Ta coating deposited on steel without the tantalum nitride interlayer.

CHAPTER 6

DISCUSSIONS

6.1 Effect of Tantalum Nitride Interlayer on the Phase of deposited Ta

The results of this research clearly show that the bcc phase of tantalum can be grown by sputter deposition on steel at room temperature, when a seed layer of tantalum nitride is deposited prior to tantalum. Beta Ta or a mixed (beta + bcc) phase is normally formed on steel at room temperature. The results from XRD and resistivity measurements also supported by NRA data as presented in chapter 5 clearly indicate that the stoichiometric tantalum nitride (TaN) interlayer plays an important role in bcc Ta formation.

A critical thickness of 20 nm of TaN is required on steel substrates after sputter etching, while thinner layers (4nm) are needed when sputter etching was not done prior to deposition. Sputter etching however is desired to enhance adhesion of the films. Possible explanation for the requirement of a critical thickness of the interlayer could be, the discontinuity (or the small islands) in thin interlayers of tantalum nitride. Some imperfections in the substrates surface can cause the discontinuity on this nitride interlayer, which could results in the formation of the beta phase of Ta. The fact that the critical thickness of tantalum nitride required for the samples without sputter etching is smaller than the one with sputter etching could be explained by the fact that sputter etching increases the roughness in the steel substrate [43]. Hence, thicker interlayers are required to cover the rougher substrate and to produce a continuous nitride film and subsequent bcc Ta phase in the coating.

A special case of one of the bcc Ta coatings is shown in Figure 6.1, in which beta inclusions were observed in the pure bcc Ta. These results contradict the hypothesis by Collobert and Chouan [30], which states that it is impossible to get beta on bcc Ta. The growth of beta Ta on bcc phase has not been reported in literature to our knowledge. This growth of beta Ta on bcc structure could be due to stresses build up in the growing film.

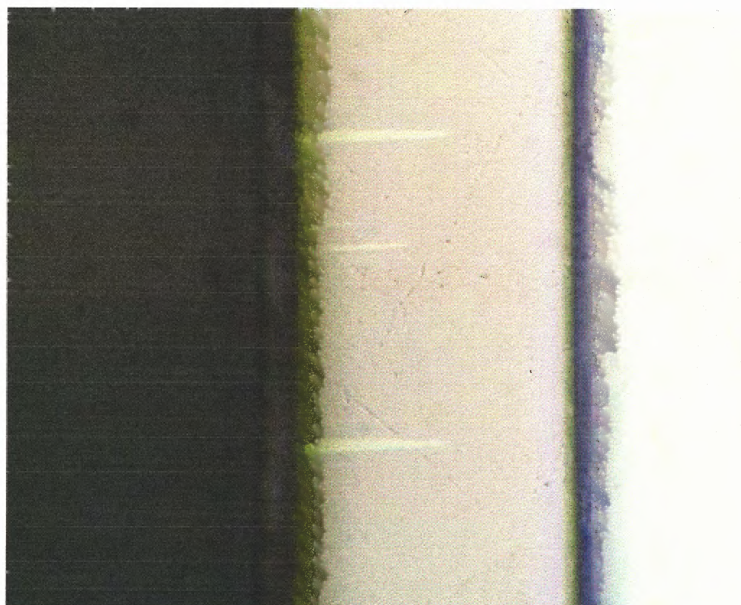

Figure 6.1 Cross section of steel sample with bcc Ta coating grown on tantalum nitride interlayer and beta Ta inclusions are clearly observed as light needles in a grey background of bcc.

6.2 Characteristics of Tantalum Nitride Films

The Ta-N system is extremely rich and complex [60-61] and tantalum nitride film structures have being extensively studied by researchers for a long time. Tantalum nitride has been reported to have a defective structure and its deviations from stoichiometry are common [62].

The results of the work presented in Section 5.2 shows that the electrical resistivity of tantalum nitride film varies with the variation in the nitrogen flow (Figure 5.11). Resistivity values of 200-250 μΩ cm are reported for the Ta_2N phase of tantalum nitride films in the literature [63, 64], which corresponds to the measured resistivity of the films deposited here with 1.6% nitrogen concentration. This indicates that with 1.6% nitrogen concentration in the sputtering gas, the Ta_2N phase is obtained in the films. Resistivity values of 340-370 μΩ cm were measured for films deposited with nitrogen concentrations between 10-14%, indicating a TaN phase. That is in agreement with the resistivity values determined by Krikorian and Chen [65, 66] for this phase. In the films deposited with nitrogen concentrations between 4 to 7 %, resistivity values of 260-300 μΩ was observed which may be due to the mixed phase of Ta_2N and TaN. A dramatic increase was noted in the resistivity of the tantalum nitride film deposited with nitrogen concentrations between 18-33%. A higher percentage of nitrogen in the sputtering gas could result in nitrogen-rich compounds of higher resistivity, like Ta_5N_6, Ta_4N_5 and Ta_3N_5 [67]. This however is not supported by the XRD spectra. Other explanations could be that the film grain boundaries are saturated with nitrogen or that high nitrogen content could also reduce the grain size of the film, as observed by Saha and Barnard [68].

The XRD spectrum of the nitride film, deposited with 5% nitrogen concentration (Figure 5.14a), shows a very broad peak, indicating the amorphous nature of the film. Further, the films deposited with 14%, 18%, 21%, 28%, and 33% nitrogen concentration had the TaN structure indicated by the XRD measurements.

It was observed from the XRD spectra (Figure 5.16) that the structure of tantalum nitride films, deposited with different nitrogen concentration, was similar on steel and on the SiO_2 substrates. However, X-ray diffraction results do not seem to support the formation of nitrogen rich compounds like Ta_5N_6, Ta_4N_5 and Ta_3N_5 as no new peaks indicating these phases were observed. Another possibility could be that the Ta_3N_5 (130) peak [69] overlaps with the TaN (110) peak, at $2\theta = 35°$. The stoichiometry of tantalum nitride films was also confirmed by nuclear reaction analysis. These results show that stoichiometric TaN films were deposited with nitrogen concentration of 14%, while the concentration of 5% resulted in Ta_2N.

It is concluded from this study that an interlayer of TaN on steel favors the formation of bcc Ta. This could be due to the fact that TaN has the same crystal structure and a close lattice match with bcc Ta. The lattice mismatch between TaN (3.35 Å) and bcc Ta (3.34 Å) is approximately only 0.3%. Similar results are reported in literature with the bcc Ta grown by sputtering on Nb, which has also the bcc structure [28]. The lattice mismatch of both bulk Ta and Nb is 0.1%. An advantage of using TaN as an interlayer is that it could be pre-deposited with the same Ta target by the introduction of nitrogen in the sputtering gas without breaking the vacuum.

6.3 Effect of Temperature on Deposited Ta

As is well known the substrate temperature is a very important parameter controlling the structure coatings [70]. In this work, elevated substrate temperatures (T = 400 °C with Ar and 350 °C with Kr) has been found necessary to consistently grow a bcc phase Ta coating directly on steel substrate. The promotion of the bcc phase over the beta phase in the Ta coatings deposited on heated steel substrates can be explained by the increased mobility of Ta atoms in the growing film at the higher temperatures. It is interesting that these substrate temperatures are much lower than required for phase transformation from beta to bcc in bulk and thin film. They are also much lower than the melting point of Ta ($T/T_m = 0.13$). This value of T/T_m in Thornton's zone model Ta coatings corresponds to the starting edge of Zone-T structure [71]. In most commercial applications Zone-T coatings are desired, as they are dense, contain fewer voids and have good adhesion plus lateral strength.

An interesting characteristic was noted in the Ta coatings deposited on heated steel substrates with Ar. These films showed a strong tendency for the alignment of (111) planes with the substrate surface, indicated by a strong peak of bcc Ta at 107° (222) in the XRD spectrum (Figure 5.22). This alignment increases with the increase in the thickness of the Ta film as shown in the XRD patterns presented in Figure 5.23.

Ta coatings produced at Benet Laboratory mainly had the bcc phase with a beta phase interface between the Ta coating and the substrate in a few cases, which reduces the protective quality of the coating. As it was mentioned earlier, the beta phase is more brittle as compared to bcc hence it undergoes failure under stress.

Similar results of beta phase at the interface were obtained for Ta coatings deposited on the heated steel substrate at Pacific Northwest National Laboratories [72]. The beta phase was not observed in bcc Ta coatings produced at NJIT (Figure 5.25). XRD measurement on both sides of the peeled film also showed a mono phase film (Figure 5.24).

CHAPTER 7

SUMMARY AND CONCLUSIONS

In this work, deposition of tantalum on steel by dc magnetron sputtering was studied with the objectives of obtaining high quality bcc phase Ta films/coatings and understanding the process conditions and pertinent mechanisms for their formation. In order to conduct this study, a planar DC magnetron system was first designed, and assembled to allow control of the various process parameters on the crystallographic phase formation and properties of Ta coatings. A cryogenic vacuum pump was used to achieve a base pressure in the high 10^{-8} torr range and a turbo molecular pump was used to pump the system during deposition. The system has the capability of admitting of two different gases at the same time to the chamber through the mass flow controllers. A commercial planar magnetron sputtering source (K.J. Lesker, Torus 2A) with the target diameter of 2 inches was used for all depositions. During experiments in which substrate heating was required, substrates holders were heated with a halogen lamp to achieve the temperature up to 450 °C.

Deposition on unheated steel substrates resulted in formation of the tetragonal phase Ta or a mixed (tetragonal + bcc) phases. This is in agreement with the result reported by other workers in the literature [6,38,40,41]. However, two methods of deposition were found to be successful for consistently achieving the objective of depositing bcc Ta. These are: 1) Deposition of Ta on heated steel substrates and 2) deposition of Ta at room temperature, on a seed layer (interlayer) of tantalum nitride formed by reactive sputtering of Ta in a mixture of Ar and N_2 gases.

It was previously known that bcc Ta can be produced on heated glass substrates [31]. This research proved that it's possible to consistently obtain bcc phase Ta coatings on steel substrates heated above a critical temperature. For argon sputtering gas this critical temperature was found for the first time to be 400 °C. Using krypton, a heavier sputtering gas the critical temperature can be reduced to 350 °C.

The results of the research presented in Section 5.1 also showed for the first time that by using a thin tantalum nitride interlayer, the order of a few tens of nm in thickness, the phase of deposited Ta on steel could be altered. The interlayer was found to promote the formation of bcc phase Ta and to inhibit the formation of beta phase Ta during depositions at room temperature. Thus, the bcc phase of Ta can be reproducibly grown on steel without requiring heating of the substrate. More detailed studies of the influence of the tantalum nitride interlayer on the phase of deposited Ta revealed that the TaN layer could be as thin as 20 nm. This minimum thickness of tantalum nitride interlayer required to promote bcc Ta could be decreased to 4 nm on steel substrate not subjected to sputter etching prior to deposition. It was also found that the stoichiometry of the nitride interlayer defined the phase of tantalum deposited on it. TaN was responsible for the promotion of bcc phase Ta.

A special case of growth of needle-like beta phase inclusions growing in a background of bcc phase is reported for the first time in this dissertation, contrary to the earlier observations reported in the literature that only bcc phase can grow on the tetragonal phase but not the other way around. These inclusions were only observed in a few very thick coatings (> 40 μm) deposited at room temperature on the interlayer, while other coatings, deposited under very similar conditions, consisted only of bcc Ta. This

growth of beta on bcc structure is likely related to the compressive stress built up in the thick film, i.e. phase transformation is a stress release mechanism that may be initiated, for example, by incorporation of an impurity. This is a tentative explanation of this phenomenon. Further experiments with the deposition of thick coating (>5 μm) are suggested to confirm this explanation.

The bcc Ta coatings produced during this research by using both substrate heating and tantalum nitride seed layers had excellent adhesion to steel substrates. This was proved by the scratch adhesion tests performed with a diamond hemispherical tip of radius 200 μm under increasing loads. These adhesion tests revealed high critical load values for failure (>15 N) for these bcc coatings versus low values (< 9 N) for the beta Ta coatings. Sputter etching of steel prior to deposition of the nitride seed layer improved the adhesion of tantalum coatings. This was evident by the groove test, which involves the plowing of coating with the knife edge tool bit. No signs of failure were observed in the coating with sputter-etched steel; however delamination was observed for the coating deposited without sputter etching on steel when tested at a similar load.

The results for this work have demonstrated that by controlling the various process parameters of dc magnetron sputtering, one can produce high quality bcc Ta coatings of multi-micron thickness with excellent adhesion to steel. An important contribution of this dissertation is in the area of understanding methods to sputter bcc Ta. Sputtering is inherently a non-equilibrium process, in which the energy and mobility of adatoms is strongly influenced by energetic ions, atoms, and molecules bombarding the growing film surface, rather than only by the substrate temperature. The non-equilibrium beta phase growth, observed at low substrate temperatures, is enhanced at high sputtering

gas pressure and at a higher sputtering rate. The meta-stable tetragonal beta phase of Ta has been recently found to be highly disordered [73]. It can be concluded from the thesis data that an increase of the surface thermal energy at a moderate deposition rate promote the growth of the equilibrium phase. The adatoms surface mobility is still strongly influenced by the energetic particle bombardment, as evidenced by the difference in the critical temperature of sputtering with argon and krypton. Ions of krypton have a higher mass and thus impart a higher momentum transfer in collisions. The critical temperatures for both sputtering gases are rather low, in comparison with the value of the Ta melting point (2996°C). They are close to the transition temperature between Zone 1 and Zone T at low pressures in the Zone model of sputtering films by Thornton [71]. They are also considerably below the reported transition temperature of 750 °C, from tetragonal to bcc phase. Annealing of the tetragonal phase films deposited at the critical temperature (for Ar) has not resulted in the phase transition.

This work showed that the phase of growing Ta could also be controlled by modification of the steel substrate surface. The dependence of the Ta phase on interlayer stoichiometry is consistent with epitaxial growth, since TaN has the same crystal structure and a close lattice match with bcc Ta. The lattice mismatch between TaN (3.35 Å) and bcc Ta (3.34 Å) is approximately only 0.3%. The epitaxial growth of bcc Ta by sputtering has been also reported on Nb or Ti interlayers [29, 30]. An advantage of using TaN as an interlayer is that it can be deposited with the same Ta target by introduction of nitrogen in the sputtering gas without breaking vacuum thus avoiding possible contamination at the interface. The fact that the critical thickness of tantalum nitride required for the samples without sputter etching is smaller than the one with sputter

etching could be explained by the fact that sputter etching increases the roughness in the steel substrate as reported in the literature [43]. Hence, a thicker interlayer is required to cover the rougher surface and to produce a continuous nitride film resulting in the bcc Ta phase in the coating.

There remain a number of problems that need to be solved before the commercial application of these research findings can be realized. These include issues like defining and controlling the process parameters for the deposition of bcc phase Ta for specific complex commercial systems (like the cylindrical magnetron for deposition in gun barrels). The results of this research have already had an impact on better understanding the deposition process for bcc Ta in ink-jet cartridges (Hewlett Packard, Oregon) and as well as the deposition of protective Ta coatings on gun barrels (at Benet Laboratories) by magnetron sputtering.

APPENDIX

DETAILS OF DEPOSITION CONDITIONS

The films and coating were deposited by DC magnetron sputtering. Noted parameters during the process and after the characterization of the deposited Ta and tantalum nitride films/coatings are listed below in Table A1.

Table A1 Details of Deposition Conditions of Some Samples Referred in Chapter 5

Referred in Fig. no.	Sample no.	S.E	Seed layer thickness (nm)	Substrate temperature	Deposited Ta thickness (μm)	Phase of deposited Ta
5.1	PTa01a053102	yes	20	RT	4	bcc
5.1	PTa03$a_3$53102	yes	-	RT	2	beta
5.2	PTa02a061102	yes	20	RT	2	bcc
5.3	PTa04a070902	yes	5	RT	1	mixed
5.4	PTa01$a_1$021102	yes	15	RT	45	mixed
5.5	PTa01$a_1$021102	yes	15	RT	45	mixed
5.6	PTa01$a_3$021902	no	15	RT	47	bcc
5.7	PTa01$a_3$021902	no	15	RT	47	bcc
5.8	PTa01$a_4$021102	yes	15	RT	45	mixed
5.9	PTa01$a_4$021102	yes	15	RT	45	mixed
5.12/5.14a	PTa04c080102	yes	950	RT	N/A	-
5.12/5.14b	PTa06c071702	yes	840	RT	N/A	-
5.12/5.14c	PTa05c080102	yes	800	RT	N/A	-
5.13/5.15a	PTa04c072302	yes	750	RT	N/A	-
5.13/5.15b	PTa05c080702	yes	700	RT	N/A	-
5.13/5.15c	PTa06c080702	yes	670	RT	N/A	-
5.18	PTa07$a_1$041502	yes	10	RT	N/A	-
5.19	PTa07$a_3$073002	no	N/A	400 °C	5	bcc

Table A1 Details of Deposition Conditions of Some Samples Referred in Chapter 5 (Continued)

5.20	PTa03a081601	no	N/A	350 °C	3	bcc
5.21	PTa02a081601	no	N/A	200 °C	3	mixed
5.21	PTa01a071902	no	N/A	250 °C	5	mixed
5.22	PTa01$a_1$112101	no	N/A	400 °C	5	bcc
5.25	PTa01$a_3$112101	no	N/A	400 °C	50	bcc
5.26	PTa01$a_2$021102	yes	15	RT	45	mixed
5.27	PTa01$a_4$021902	no	15	RT	47	bcc
5.28	PTa03$a_1$012902	yes	15	RT	5	bcc
5.29	PTa02a052202	yes	10	RT	5	mixed
5.30	PTa05$a_2$031202	yes	20	RT	5	beta
5.31	PTa02a100801	no	-	RT	5	beta

REFERENCES

[1] I. Ahmad, and J.P. Picard, "The problem of gun barrel erosion" *Proceedings of the Triservice Technical Meeting on Gun Erosion and Control*, Watervliet Arsenal, Watervliet, NY, 1970.

[2] W. Kock and P. Paschen, "Tantalum-processing, properties and application" *Journ. Of Mat.*, pp. 33-38, October 1989.

[3] F. Brossa, M. Bardy and G. Piatti, "Tantalum protective coatings for fusion reactor application" *Journ. of Nucl. Mat.*, vol.103-104, pp.261-266, 1981.

[4] Y.K. Lee, K. Maung Latt, K. Jaetlyung and L. Lee, "Study of diffusion barrier properties of ionized metal plasma (IMP) deposited tantalum (Ta) between Cu and SiO_2" *Materials Science and Engineering*, B68, pp. 99-103, 1999

[5] G. W. Mellors, Strongsville and et. al., *US Pat. No. 3,444,058*, 1969.

[6] S.L. Lee, M. Cipollo, D. Windover and C. Rickard, "Analysis of magnetron sputtered tantalum coatings versus electrochemically deposited tantalum from molted salt" *Surf. and Coat Techn.*, vol. 120-121, pp. 44-52, 1999.

[7] R.B. Marcus and S. Quigley, "Formation of F.C.C, B.C.C and β-Ta films by Evaporation" *Thin Solid Films*, vol. 2, pp. 467-477, 1968.

[8] S. Wolf and R.N. Taub, *Silicon Processing for VLSI Era Vol. 1- Process Technology*, Lattice Press, 2000.

[9] R.V. Straut and G.K. Wehner, "Sputtering yields at low bombarding energies" *Journ. Appl. Phy.*, vol. 33 (7), pp.2345-2352, 1962.

[10] W. Zou, "Synthesis of Giant Magneto-Resistive Multilayers" *Ph.D dissertation*, University of Virginia, 2000.

[11] D.M. Mattox, Report on *The History of Vacuum Coating Technology*, 2002.

[12] Penning, F. M, "Die glimmenladung bei niedrrigen" *Physica*, vol. III no. 9, pp. 873-875, 1935.

[13] Brian Chapman, *Glow Discharge Processes*, Wiley-Interscience publications, 1980.

[14] S.K. Gandhi, *VLSI Fabrication Principles Silicon and Gallium Arsenide*, Second edition, Wiley-Interscience Publication, 1994.

[15] W. Ensinger, "Corrosion and wear protection of tube inner walls by ion beam sputter coating" *Surf. and Coat. Techn.*, vol. 86-87 (1), pp. 438-442,1936.

[16] V.P. Belevskiy, M.V. Belous, V.G. Permyakov and V.M. Yashnik, "Electro physical properties and phase composition of thin cathode sputtered tantalum film" *Phy. Metal.*, vol. 33 (3), pp. 564-570, 1972.

[17] L. Liu, Hao Gong, Yue wang and Rong Liu, "Annealing effect of tantalum thin films sputtered on [001] Si substrate" *Materials Science and Engineering C*, vol. 16, pp.85-89, 2001.

[18] P.N. Denbigh and R.B. Marcus, "Structure of very thin tantalum and the molybdenum films" *Journ. of Appl. Phys.*, vol. 37 (12), pp. 4325-4330, 1966.

[19] M.H. Read and C. Altman, "A new structure in tantalum thin films" *App. Phys. Let.*, vol. 7(3), pp. 51-52, 1965.

[20] L. Maissel and R. Glang, *Handbook of Thin Film Technology*, McGraw-Hill, pp. 12-18, 1970.

[21] N. Schwartz and E. D. Feit, "Impurity effects in the nucleation of alpha (bcc)-tantalum or beta-tantalum films" *Journ. Electro. Soc.,* vol. 124(1), pp. 123-131, 1977.

[22] W.D. Westwood, "Influence of the conducting under-layer on the properties of sputtered tantalum films" *Thin Solid Films*, vol. 6, pp.307-320, 1970.

[23] D. Mills, "The structure of sputtered tantalum", *Journ. Canad. Ceram. Soc.*, vol. 35, pp.45-52, 1966

[24] L.G. Feinstein and R.D. Hottemann, "Factors controlling the structure of sputtered tantalum films" *Thin Solid Films*, vol. 16, pp. 129-145, 1973.

[25] K. Hieber and N.M. Mayer, "Structural changes of evaporated tantalum during film growth" *Thin Solid Film*, vol. 90, pp. 43-50, 1982.

[26] Sheigehiko Sato, "Nucleation properties of magnetron sputtered tantalum" *Thin Solid Films*, vol. 94, pp.321-329, 1982.

[27] P.N. Baker, "Preparation and properties of tantalum thin films" *Thin Solid Films*, vol. 14, pp. 3-25, 1972.

[28] D.W. Face and D.E. Prober, "Nucleation of body centered cubic tantalum films with a thin niobium underlayer" *Journ. Vac. Sci. Techn.* A, vol. 5(6), pp. 3408-3411, 1987.

[29] G.S. Chen, P.Y. Lee and S.T. Chen, "Phase formation behavior and diffusion barrier property of reactively sputtered tantalum-based thin films used in semiconductor metallization" *Thin Solid Films*, vol. 353, pp. 264-273, 1999.

[30] D. Collobert and Y. Chouan, "A new hypothesis about sputtered tantalum" *Thin Solid Films*, vol. 55, L15-L16, 1978.

[31] Alois Schauer, *US Pat. No. 3,878,079*, 1975.

[32] L.A. Clevenger, A. Mutscheller, J.M.E Harper and K. Barmak "The relationship between deposition conditions, the beta to alpha phase transformation and stress relaxation in tantalum thin films" *Journ. Appl. Phys.*, vol. 72(10), pp.4918-4924, 1992.

[33] Michael Kanellos, "IBM enters the copper age", *Cnetnews.com*, September 1998.

[34] J. Torres, "Advanced copper interconnections for silicon CMOS technologies" *Appl. Surf. Sci.*, vol. 91, pp. 112-123, 1995.

[35] P. Catania et al., " Low resistivity body centered cubic tantalum thin as diffusion barriers between copper and silicon" Journ. Vac. Sci. Techn. A, vol. 10(5), pp.3318- 3321,1992.

[36] E. Colgan and P. Fryer, *US Pat. No. 5,221,449*, 1993.

[37] D. Edelstein, J. Heidenreich, R. Goldblatt, W. Cote, C. Uzod and J. Slattery , "Full copper wiring in sub-0.5/spl mu/m CMOS ULSI technology" *Journ. Elect. Dev. Meeting*, Tech. Dig., pp. 773-776, 1997.

[38] J.F. Cox and E.D. McClanahan, "High rate sputtering of tantalum on gun steel" *Proceedings of the Tri-Service Gun Tube wear and erosion symposium*, pp. 277, 1982.

[39] Dean W. Matson, E.D. McClanahan, S.L. Lee and D. Windover, "Properties of thick sputtered Ta used for protective gun tube coatings" *Surf. and Coat. Techn.*, vol. 146-147, pp. 344-350, 2001.

[40] S.L. Lee and D. Windover, "Phase, residual stress and texture in triode-sputtered tantalum coatings on steel" *Surf. and Coat. Techn.*, vol. 108-109, pp. 65-72, 1998.

[41] S.L. Lee, D. Windover, M. Audino, D.W. Matson, E.D. McClanahan, "High rate sputter deposited tantalum coating on steel for wear and erosion mitigation" *Surf. and Coat. Techn.*, vol. 149, pp.62-69, 2002.

[42] K. Koski, J. Holsa, J. Ernoult and A. Rouzud "The connection between sputter cleaning and adhesion of thin solid films" *Surf. and Coat. Techn.*, vol. 80, pp. 195-199, 1996.

[43] Y. Abbassi, "Determination of Phase Composition of Sputtered Tantalum on Steel Substrates by Resistivity Measurements" *NJIT thesis*, May 2002.

[44] J.L. Vossen, "The prepration of substares for film deposition using glow discharge technique," *Review article*, RCA Laboratories, Princeton NJ, pp. 159-165, 1979.

[45] J.I. Goldstein, D.E. Newbury, P. Echlin, D.C. Joy, A.D. Roming, C.E. Lyman, C. Fiory and E. Lifshin, *Scanning electron microscopy and X-Ray microanalysis a A text for biologist, materials scientists, and geologists*, Second edition, Plenum Press, 1994.

[46] http://www.di.com.

[47] Swanson Tatge, *Natl. Bur. Stand.(U.S.)*, Circ. 539,I,29,1953.

[48] P.T. Moseley, C.J. Seabrook, "The crystal of β-tantalum" *Acta Cryst.*, Sec. B, vol. 29, pp. 1170-1172, 1973.

[49] *Encyclopedia of Materials Characterization*, chapter 11.4, pp. 680-694, Manning publication, 1992.

[50] J.R. Tesmer and M. Nastasi, *Handbook of Modern Ion Beam Materials Analysis,* Materials Research Society, Pittsburg, PA, 1995.

[51] http://www.srim.org.

[52] W. Lee, J. Lin and C. Lee, "Characterization of tantalum nitride films deposited by reactive sputtering of Ta in N_2/Ar gas mixtures," *Mat. Chem. and Phys.*, vol.68, pp. 266-271, 2001.

[53] T. Riekkinen, J. Moarius, T. Laurila, A. Nurmela, I. Suni and J. K. Kivilahti, "Reactive sputter deposition and properties of Ta_xN thin films," *Micro. Engg.,* vol. 64, pp. 289-297, 2002.

[54] C. Chang, J.S. Jeng and J.S. Chen, "Micro structural and electrical characteristics of reactively sputtered Ta-N thin films," *Thin Solid Films*, vol. 413, pp. 46-51, 2002.

[55] J.E. Sundgren, B.O. Johansson and S.E. Karlsson, "Kinetics of nitride formation on titanium targets during reactive sputtering," *Surf. Sci.*, vol. 128, pp.265, 1983.

[56] JCPDS-ICDD File Card No. 26-985.

[57] JCPDS-ICDD File Card No. 39-1485.

[58] JCPDS-ICDD File Card No. 32-1283.

[59] C.S. Paur, "Crystallographic Structure and Mechanical Properties of Tantalum Coatings on Steel Deposited by DC Magnetron Sputtering," *MS Thesis*, NJIT, 2002.

[60] C.S. Chin, Y. W. Kim, D. Gall, J.E. Green and I. Petrov, "Phase composition and microstructure of polycrystalline and epitaxial TaN_x layers grown on oxidized Si(001) and MgO(001) by reactive sputter deposition", *Thin Solid Films*, vol. 402, pp. 172-182, 2002.

[61] T.B. Massalski (Ed.), *Binary Alloy Phase Diagrams*, ASM International, Ohio, pp. 2703, 1990.

[62] L.E. Thod, *Transition Metal Carbides and Nitrides*, academic press, New York, 1971.

[63] M. Ohring, *The Materials Science of Thin Films*, Academic Press, New Jersey, pp. 128, 1992.

[64] S. Nakao, M. Numata and T. Ohmi, "Thin and low resistivity tantalum nitride diffusion barrier and giant-grain copper interconnects for advanced ULSI metallization" *Jap. Journ. of Appl. Phys.*, vol. 38, pp. 2401-2405, 1999.

[65] E. Krikorian and R.J. Sneed, "Deposition of tantalum, tantalum Oxide and tantalum nitride, with controlled electrical characteristics," *Journ. of Appl. Phys.*, vol. 37, No. 10, pp. 3674-3681, 1966.

[66] G. S. Chen, P.Y. Lee, S. T. Chen, "Phase formation behavior and diffusion barrier property of reactively sputtered tantalum-based thin films used in semiconductor metallization" *Thin Solid Films*, vol. 353, pp. 264-273, 1999.

[67] X. Sun, E. Kolawa, J. Chen, J. Reid, M.A Nicolet, "Properties of reactively sputtering deposited Ta-N thin films" *Thin Solid Films,* vol. 236, pp. 347-351, 1993.

[68] R. Saha and J.A. Barnard, "Effect of structure on the mechanical properties of Ta and Ta(N) thin films prepared by reactive DC magnetron sputtering" *Journ. of Crystal Growth*, vol. 174, pp. 495-500, 1997.

[69] JCPDS-ICDD File Card No. 79-1533.

[70] J.A. Thorton, in: G.E. McGuire (Ed), *Semiconductor Materials and Process Technology Handbook*, Noyes, pp.329, 1988.

[71] J.A. Thornton, "High rate thick film growth", *Ann. Rev. Mater. Sci.*, vol. 7, pp. 239-244, 1977.

[72] D.W. Matson, E.D. McClanahan, J.P. Rice, S.L. Lee and D. Windover, "Effect of sputtering parameters on Ta coatings for gun bore applications," *Surf. and Coat. Techn.*, vol. 133-134, pp. 411-416, 2000.